

SPATIAL VARIATION OF STRONG GROUND MOTION

by

Ebru Harmandar

B.S., Civil Engineering, Yıldız Technical University, 1999

M.S., Structural Engineering, Boğaziçi University, 2002

Submitted to the Kandilli Observatory and
Earthquake Research Institute in partial fulfillment of
the requirements for the degree of
Doctor of Philosophy

Graduate Program in Earthquake Engineering

Boğaziçi University

2009

DEDICATION

I dedicate this dissertation to my beloved mom and dad, and my dear sister, Didem; for their continuous encouragement and care that helped me overcome setbacks and stay focused on my doctorate study.

I also dedicate this dissertation to my precious husband, Buğra, whose love and support provided me the strength and perseverance I needed to achieve my goals; and to my sweet daughter, Nil, whose innocence and happiness taught me the beauty of life; and to the memory of my son, Taha, who has taught me the patience to live the life.

Without them I couldn't overcome difficulties during the tough time.

ACKNOWLEDGEMENTS

I would like to express in depth my sincere gratitude to my advisor, Prof. Dr. Mustafa Erdik for his invaluable guidance, interest, and motivation not only during the preparation of this dissertation, but also throughout my doctorate program. I am grateful to him. I would also like to thank my co-supervisor, Prof. Dr. Eser Durukal for her advices, discussions and for encouraging me to study aboard.

I am indebted to Prof. Dr. Nuray Aydınođlu, Prof. Dr. Erdal Şafak, Prof. Dr. Ođuz Özel and Prof. Dr. Hayrullah Karabulut, for their participation in my advisory committee, and for their valued feedbacks.

I would like to express my appreciation to the faculty and Ph. D. candidates of Department of Structural Engineering in Politecnico di Milano, whom I had pleasure to work and share the beauties of Milan. I would like to express my special thanks to research team and administrator staff of NORSAR for providing earthquake strong motion data and for making my stay in Kjeller very homely and very cheerful. This part that I supply data recorded by NORSAR, of the dissertation has been supported by Transnational Access research visit at NORSAR under the NERIES Project, EC 026130.

I am deeply grateful to the Istanbul Earthquake Rapid Response and Early Warning System staff who provided earthquake strong motion data and kindly helped whenever I needed. I also take this opportunity to express my gratitude to the faculty in Department of Earthquake Engineering in Bođaziçi University for expanding my knowledge and vision over the years; and to my colleagues for all the support they have given at my hard times. Especially, I would like to express my heartfelt thanks to Gökçe Tönük for her invaluable friendship, motivation, and support from the beginning of my Kandilli years. I would also like to thank to Hasibe Gül for her friendly help.

Each and everyone listed above and others who have not been named directly, but whose friendship remains important to me, deserve my gratitude and my admiration for supporting me through this portion of my life and career.

ABSTRACT

SPATIAL VARIATION OF STRONG GROUND MOTION

Earthquake ground accelerograms measured at different locations along a large engineered structure could be significantly different. This has led to considerable research in the last decade on the modeling of the spatially varying earthquake ground motion. The spatial variability of strong ground motion incorporates the effects of wave propagation, amplitude variability and phase variability, as well as the local site effects on the motion. This variation of ground motion could have the possibility to cause important effect on the response of linear lifelines such as long bridges, pipelines, communication systems, and should preferably be accounted for in their design.

The objective is to evaluate and improve existing spatial variation quantification relationships by studying data available from different networks; investigate the possibility of employing functional forms for the characterization of spatial variation of ground motion in the assessment of strong ground motion distribution.

This thesis focuses on studying on the spatial variability of ground motion using strong ground motion measurements. A rational and rigorous methodology for the interpolation of measured ground motion from discrete array stations to be used in the bias adjustment of the theoretical shake map assessments with the empirical ground motion measurements is developed. The generation of the estimated maps of shaking after an earthquake is often influenced by the limited number of sensors and/or difficulty of monitoring at inaccessible locations that impacts the collection of desired information. This gap in information can be filled through the estimation of missing information conditional upon the measured records. Methodology is presented for estimating properly-correlated earthquake ground motion parameters; herein peak ground acceleration (PGA), at an arbitrary set of closely-spaced points, compatible with known or prescribed ground motion parameters (PGA) at other locations.

The variation of ground strain due to wave propagation, site response and loss of coherence is investigated. This study concentrates on the stochastic description of the spatial variation, and focuses on spatial coherency. The estimation of coherency from recorded data and its interpretation are presented. Coherency model for Istanbul for the assessment of simulation of spatially variable ground motion needed for the design of extended structures is derived.

In addition to the realistic characterization of spatial variation, simulation of spatially variable earthquake ground motion is another essential part of the examination of the effects of spatial variation, especially for extended lifeline structures. This thesis concludes with the generation of earthquake ground motion compatible with prescribed target-response spectrum and their coherencies are consistent with a given spatial coherency function for a finite array of ground surface stations.

ÖZET

KUVVETLİ YER HAREKETİNİN KONUMSAL DEĞİŞİMİ

Büyük boyutlu yapıların farklı temel noktalarında ölçülen deprem ivme kayıtları belirgin bir şekilde farklılık göstermektedir. Bu gözlem, son on yılda yer hareketlerinin konumsal değişiminin modellenmesinde önemli araştırmalar yapılmasına yol açmıştır. Kuvvetli yer hareketlerinin konumsal değişimi; yer hareketleri üzerindeki yerel zemin etkilerinin yanısıra, dalga yayılım etkilerini, deprem genliğindeki değişimi ve faz değişimini içinde barındırmaktadır. Yer hareketlerindeki bu değişim; uzun köprüler, boru hatları ve iletişim şebekeleri gibi doğrusal altyapı şebekelerinin deprem yükleri altında davranışında önemli etkilere neden olabilmektedir ve bu yapıların tasarımında öncelikli olarak dikkate alınması gerekmektedir.

Bu çalışmada, farklı ağlardan elde edilen verileri kullanarak mevcut konumsal değişim ilişkilerinin değerlendirilmesi ve geliştirilmesi; kuvvetli yer hareketi dağılımının değerlendirilmesinde, yer hareketinin konumsal değişiminin tanımlanması için kullanılacak fonksiyonların araştırılması amaçlanmaktadır.

Bu tezde, kuvvetli yer hareketleri ölçümleri kullanılarak yer hareketlerinin konumsal değişimi ele alınmıştır. Teorik şiddet haritalarındaki Bayes uyarlamaları için ampirik yer hareketi ölçümleriyle birlikte kullanılacak aralıklı ağ istasyonlarında ölçülen yer hareketlerinin enterpolasyonu için rasyonel ve hassas bir metodoloji geliştirilmiştir. Depremden sonra oluşturulan şiddet haritaları; sınırlı sayıda sensörlerden ve/veya istenilen verinin toplanmasında etkili olan erişilmez yerlerde monitörlemenin zorluğundan çoğunlukla etkilenmektedir. Verideki bu boşluk, gerçek kayıtlara bağlı olan eksik verilerin simule edilmesiyle doldurulacaktır. Buradan yola çıkılarak; yakın aralıklı noktalardan oluşan gelişigüzel seçilmiş kümelerde, farklı lokasyonlarda bilinen ve ya öngörülen yer hareketi parametreleri (pik yer ivmesi) ile uyumlu, birbirleriyle tamamen bağlantılı deprem yer hareketleri parametreleri (pik yer ivmesi) tahmini için bir metodoloji geliştirilmiştir.

Zemin birim şekildeğiřtirmesinin de mekansal deęiřimi dalga yayılımına, zemin davranıřına ve uyumluluk kayıplarına baęlı olarak incelenmektedir. Ayrıca, bu alıřma, konumsal deęiřimin stokastik tanımını ve konumsal uyumluluęunu (koherasyon) irdelemektedir. Kayıtlardan elde edilen verilerin birbirleri arasındaki koherasyonu belirlenmiř ve deęerlendirilmiřtir. Yatayda uzun yapıların tasarımında kullanılmak üzere ihtiya duyulan konumsal deęiřen yer hareketlerinin simulasyonu iin İstanbul'a ait koherasyon modeli geliřtirilmiřtir.

Konumsal deęiřimin realistik tanımlanmasına ek olarak konumsal olarak deęiřen deprem yer kayıtlarının simulasyonu; altyapı řebekeleri üzerinde konumsal deęiřimin etkilerinin arařtırılmasında önemli rol oynamaktadır. Bu tez, sonlu sıralı yer istasyonu aęı iin, uyumluluk deęerlerinin verilen koherasyon modeliyle örtüřtüęü, önceden tanımlı tasarım ivme spektrumuyla baędařan kuvvetli yer hareketlerinin üretilmesiyle neticelendirilmiřtir.

TABLE OF CONTENTS

DEDICATION.....	iii
ACKNOWLEDGEMENTS.....	iv
ABSTRACT.....	v
ÖZET	vii
TABLE OF CONTENTS.....	ix
LIST OF FIGURES	xii
LIST OF TABLES.....	xxi
LIST OF SYMBOLS / ABBREVIATIONS	xxii
1. INTRODUCTION	1
1.1. Background	1
1.2. Objectives and Scope of the Thesis	5
2. ARRAY AND DATA DESCRIPTION.....	8
2.1. Istanbul Earthquake Rapid Response System.....	8
2.1.1. Array Configuration and Instrumentation	8
2.1.2. Geology and Soil Properties.....	11
2.1.3. Earthquake Data	11
2.2. The Norwegian Seismic Array (NORSAR).....	13
2.2.1. Array Configuration and Instrumentation	13
2.2.2. Earthquake Data	14
2.3. The Strong Motion Array in Taiwan (SMART-1).....	16
2.3.1. Array Configuration and Data	16
3. ESTIMATION OF PEAK GROUND ACCELERATIONS AND ANALYZING SPATIAL VARIABILITY OF GROUND MOTION	19
3.1. Introduction.....	19
3.2. Estimation of Peak Ground Acceleration based on Modified Kriging Method..	19
3.2.1. Kriging Method	24
3.2.2. Modified Kriging Method	26
3.2.3. Comparison of Results with the Values Obtained from Attenuation Relationships.....	30

3.2.4. Comparison of Results and the Values Obtained from Spline Interpolation	41
3.3. Statistical Spatial Variability of Ground Motion	49
3.3.1. Methodology.....	50
3.3.2. Spatial Variability of Peak Ground Acceleration	52
3.4. Conclusions	54
4. ASSESSMENT OF EARTHQUAKE INDUCED GROUND STRAINS IN THE DÜZCE EARTHQUAKE	56
4.1. Introduction	56
4.2. Domain Reduction Method	57
4.3. Results and Conclusions	64
5. STOCHASTIC DESCRIPTION OF THE SPATIAL VARIATION OF SEISMIC GROUND MOTION.....	70
5.1. Definition of Coherency.....	70
5.2. Data Processing.....	73
5.3. Evaluation of Coherency.....	75
5.3.1. Cross Spectral Density	77
5.3.2. Power Spectral Density	77
5.3.3. Coherency.....	78
5.4. Spatial Variability Models	93
5.4.1. Introduction	93
5.4.2. Empirical Coherency Models.....	93
5.4.3. Semi-empirical Models	94
5.4.4. Development of the Coherency Model for Istanbul.....	96
5.4.5. Regression Results.....	98
6. SIMULATION OF SPATIALLY VARIABLE GROUND MOTION	101
6.1. Introduction.....	101
6.2. Methodology to Simulate Target Spectrum Compatible Ground Motion	104
6.3. Methodology to Simulate Ground Motion Consistent with the Target Coherency Model	107
6.3.1. Estimation of the Power Spectrum.....	108
6.3.2. Adaptation of Coherency Model	110
6.3.3. Coherency Phase	111

6.3.4. Numerical Illustration.....	112
7. CONCLUSIONS AND RECOMENDATIONS.....	119
REFERENCES	124

LIST OF FIGURES

Figure 2.1.	Configuration of urban stations in IERRS	10
Figure 2.2.	İstanbul site classification map	11
Figure 2.3.	Locations of the events recorded by IERREWS	13
Figure 2.4.	The locations of the Norwegian seismic array stations (Ringdal, 2005)	15
Figure 2.5.	Schematic plot of Norway's IMS seismic arrays (Ringdal, 2005)	15
Figure 2.6.	The configuration of the SMART-1 array	17
Figure 3.1.	Peak ground accelerations for the geometric mean of the horizontal components at each Rapid Response System station triggered during the September 19, 2003 earthquake	20
Figure 3.2.	Peak ground accelerations for the geometric mean of the horizontal components at each Rapid Response System station triggered during the May 16, 2004 earthquake	21
Figure 3.3.	Peak ground accelerations for the geometric mean of the horizontal components at each Rapid Response System station triggered during the June 24, 2004 earthquake	21
Figure 3.4.	Peak ground accelerations for the geometric mean of the horizontal components at each Rapid Response System station triggered during the September 29, 2004 earthquake	22
Figure 3.5.	Peak ground accelerations for the geometric mean of the horizontal components at each Rapid Response System station triggered during the October 20, 2006 earthquake	22
Figure 3.6.	Peak ground accelerations for the geometric mean of the horizontal components at each Rapid Response System station triggered during the October 24, 2006 earthquake	23

Figure 3.7.	Peak ground accelerations for the geometric mean of the horizontal components at each Rapid Response System station triggered during the March 12, 2008 earthquake	23
Figure 3.8.	Selection of the observed data to predict PGA at unknown point (left) and diagram for the calculation of the weights w.r.t. Equation (3.8) (right).....	27
Figure 3.9.	Configuration of the estimated data and surrounding observed data	28
Figure 3.10.	Procedure of the modified kriging method	29
Figure 3.11.	Residuals (y-axis) between the observed and estimated data at each Rapid Response System station (x-axis) triggered during the September 19, 2003 earthquake	30
Figure 3.12.	Residuals (y-axis) between the observed and estimated data at each Rapid Response System station (x-axis) triggered during the May 16, 2004 earthquake	31
Figure 3.13.	Residuals (y-axis) between the observed and estimated data at each Rapid Response System station (x-axis) triggered during the June 24, 2004 earthquake	32
Figure 3.14.	Residuals (y-axis) between the observed and estimated data at each Rapid Response System station (x-axis) triggered during the September 29, 2004 earthquake	33
Figure 3.15.	Residuals (y-axis) between the observed and estimated data at each Rapid Response System station (x-axis) triggered during the October 10, 2006 earthquake	34
Figure 3.16.	Residuals (y-axis) between the observed and estimated data at each Rapid Response System station (x-axis) triggered during the October 24, 2006 earthquake	35
Figure 3.17.	Residuals (y-axis) between the observed and estimated data at each Rapid Response System station (x-axis) triggered during the March 12, 2008 earthquake	36

Figure 3.18. Comparison of PGA of the observed data (red circles) with PGA obtained by this study (short black lines) and PGA obtained by Akkar and Bommer (2007) attenuation relationship (blue circles) at each Rapid Response System station (x-axis) triggered during the September 19, 2003 earthquake. The shaded yellow regions for each Rapid Response System station are the \pm one geometric standard deviations of the data based on this study 37

Figure 3.19. Comparison of PGA of the observed data (red circles) with PGA obtained by this study (short black lines) and PGA obtained by Akkar and Bommer (2007) attenuation relationship (blue circles) at each Rapid Response System station (x-axis) triggered during the May 16, 2004 earthquake. The shaded yellow regions for each Rapid Response System station are the \pm one geometric standard deviations of the data based on this study 38

Figure 3.20. Comparison of PGA of the observed data (red circles) with PGA obtained by this study (short black lines) and PGA obtained by Akkar and Bommer (2007) attenuation relationship (blue circles) at each Rapid Response System station (x-axis) triggered during the June 24, 2004 earthquake. The shaded yellow regions for each Rapid Response System station are the \pm one geometric standard deviations of the data based on this study 38

Figure 3.21. Comparison of PGA of the observed data (red circles) with PGA obtained by this study (short black lines) and PGA obtained by Akkar and Bommer (2007) attenuation relationship (blue circles) at each Rapid Response System station (x-axis) triggered during the September 29, 2004 earthquake. The shaded yellow regions for each Rapid Response System station are the \pm one geometric standard deviations of the data based on this study 39

Figure 3.22. Comparison of PGA of the observed data (red circles) with PGA obtained by this study (short black lines) and PGA obtained by Akkar and Bommer (2007) attenuation relationship (blue circles) at each Rapid Response System station (x-axis) triggered during the October

20, 2006 earthquake. The shaded yellow regions for each Rapid Response System station are the \pm one geometric standard deviations of the data based on this study 39

Figure 3.23. Comparison of PGA of the observed data (red circles) with PGA obtained by this study (short black lines) and PGA obtained by Akkar and Bommer (2007) attenuation relationship (blue circles) at each Rapid Response System station (x-axis) triggered during the October 24, 2006 earthquake. The shaded yellow regions for each Rapid Response System station are the \pm one geometric standard deviations of the data based on this study 40

Figure 3.24. Comparison of PGA of the observed data (red circles) with PGA obtained by this study (short black lines) and PGA obtained by Akkar and Bommer (2007) attenuation relationship (blue circles) at each Rapid Response System station (x-axis) triggered during the March 12, 2008 earthquake. The shaded yellow regions for each Rapid Response System station are the \pm one geometric standard deviations of the data based on this study 40

Figure 3.26. Comparison of PGA of the observed data (black stars) with PGA obtained by this study (pink circles) and PGA obtained by RRMap software (blue circles) at each phantom station using the data triggered during the September 19, 2003 earthquake..... 42

Figure 3.27. Comparison of PGA of the observed data (black stars) with PGA obtained by this study (pink circles) and PGA obtained by RRMap software (blue circles) at each phantom station using the data triggered during the May 16, 2004 earthquake..... 42

Figure 3.28. Comparison of PGA of the observed data (black stars) with PGA obtained by this study (pink circles) and PGA obtained by RRMap software (blue circles) at each phantom station using the data triggered during the June 24, 2004 earthquake..... 43

Figure 3.29. Comparison of PGA of the observed data (black stars) with PGA obtained by this study (pink circles) and PGA obtained by RRMap

software (blue circles) at each phantom station using the data triggered during the September 29, 2004 earthquake..... 43

Figure 3.30. Comparison of PGA of the observed data (black stars) with PGA obtained by this study (pink circles) at each phantom station using the data triggered during the October 20, 2006 earthquake..... 44

Figure 3.31. Comparison of PGA of the observed data (black stars) with PGA obtained by this study (pink circles) and PGA obtained by RRMap software (blue circles) at each phantom station using the data triggered during the October 24, 2006 earthquake..... 44

Figure 3.32. Comparison of PGA of the observed data (black stars) with PGA obtained by this study (pink circles) at each phantom station using the data triggered during the March 12, 2008 earthquake 45

Figure 3.33. Distribution of PGA obtained by this study (left), by RRMap software (right), and by Akkar and Bommer (2007) attenuation relationship (center) at each phantom station using the data triggered during the September 19, 2003 earthquake 46

Figure 3.34. Distribution of PGA obtained by this study (left), by RRMap software (right), and by Akkar and Bommer (2007) attenuation relationship (center) at each phantom station using the data triggered during the May 16, 2004 earthquake..... 46

Figure 3.35. Distribution of PGA obtained by this study (left), by RRMap software (right), and by Akkar and Bommer (2007) attenuation relationship (center) at each phantom station using the data triggered during the June 24, 2004 earthquake..... 47

Figure 3.36. Distribution of PGA obtained by this study (left), by RRMap software (right), and by Akkar and Bommer (2007) attenuation relationship (center) at each phantom station using the data triggered during the September 29, 2004 earthquake 47

Figure 3.37. Distribution of PGA obtained by this study (left) and by Akkar and Bommer (2007) attenuation relationship (right) at each phantom

	station using the data triggered during the October 20, 2006 earthquake	48
Figure 3.38.	Distribution of PGA obtained by this study (left), by RRMap software (right), and by Akkar and Bommer (2007) attenuation relationship (center) at each phantom station using the data triggered during the October 24, 2006 earthquake	48
Figure 3.39.	Distribution of PGA obtained by this study (left) and by Akkar and Bommer (2007) attenuation relationship (right) at each phantom station using the data triggered during the March 12, 2008 earthquake .	49
Figure 3.40.	Number of stations per group for the May 16, 2004 earthquake and the September 29, 2004 earthquake	51
Figure 3.41.	Logarithmic standard deviations of PSV ratios as a function of station separation	52
Figure 3.42.	PGA ratios of earthquakes recorded by SPITZBERGEN array.....	53
Figure 3.43.	Mean values of the PGA ratios of earthquakes recorded by SPITZBERGEN array.....	53
Figure 3.44.	Logarithmic standard deviations of PGA ratios as a function of station separation	54
Figure 4.1.	The scheme of the DRM procedure applied to the Düzce urban area (Scandella <i>et al.</i> , 2007).....	58
Figure 4.2.	Location of available Borehole and shallow ground studies and soil profile of the NS cross-section of Düzce	60
Figure 4.3.	V_s profile used in Step I.....	60
Figure 4.4.	Observed and simulated velocity and displacement time histories of EW, NS, and UD components at Bolu station	61
Figure 4.5.	Fourier Amplitude Spectra of EW, NS, and UD components at Bolu station.....	62
Figure 4.6.	Observed and simulated velocity and displacement time histories of EW and NS components at Karadere station	62

Figure 4.7.	Fourier Amplitude Spectra of EW and NS components at Karadere station	63
Figure 4.8.	V_s profile used in Step II.....	63
Figure 4.9.	Mesh model of Düzce basin	64
Figure 4.10.	Observed and simulated displacement time histories (left) and Fourier amplitude spectra of NS component at Düzce station	65
Figure 4.11.	Observed and simulated displacement time histories (left) and Fourier amplitude spectra of UD component at Düzce station.....	65
Figure 4.12.	Variation of displacement time histories and displacement amplitude spectra w.r.t. depth at cross section I along the NS cross-section.....	66
Figure 4.13.	Variation of displacement time histories and displacement amplitude spectra w.r.t. depth at cross section II along the NS cross-section	66
Figure 4.14.	Variation of displacement time histories and displacement amplitude spectra w.r.t. depth at cross section III along the NS cross-section	67
Figure 4.15.	Variation of displacement time histories and displacement amplitude spectra w.r.t. depth at cross section IV along the NS cross-section.....	67
Figure 4.16.	Variation of displacement time histories and displacement amplitude spectra w.r.t. depth at cross section V along the NS cross-section	68
Figure 4.17.	Variation of peak ground displacement, velocity and acceleration along the NS cross-section at the basin surface	69
Figure 4.18.	Variation of peak ground strains in the horizontal and vertical directions along the NS cross-section at the basin surface	69
Figure 5.1.	Comparison of the number of data points for Hamming window for the pair R31-R44 (September 19, 2003 earthquake).....	74
Figure 5.2.	Fourier Amplitude Spectrum of the noise and signal part of the station R51 for the September 19, 2003 earthquake; and the signal to noise ratio	75
Figure 5.3.	Acceleration time history (m/s^2) for ten records taken from the September, 19 2003 earthquake	75

Figure 5.4.	The lagged coherency between stations I06 and I12 recorded by SMART-1 (this study).....	78
Figure 5.5.	The lagged coherency between stations I06 and I12 recorded by SMART-1 (Zerva and Zervas, 2002).....	79
Figure 5.6.	Coherency values for each distance bins and average coherency values for EW direction (11-point) –September 29, 2004 earthquake.....	80
Figure 5.7.	Average coherency values of each distance bins with respect to direction and smoothing window length –September 29, 2004 earthquake	81
Figure 5.8.	Coherency values for each distance bins and average coherency values for EW direction (11-point) – September 19, 2003 earthquake.....	82
Figure 5.9.	Average coherency values of each distance bins with respect to direction and smoothing window length – September 19, 2003 earthquake	83
Figure 5.10.	Coherency values for each distance bins and average coherency values for EW direction (11-point) – May 16, 2004 earthquake.....	84
Figure 5.11.	Average coherency values of each distance bins with respect to direction and smoothing window length – May 16, 2004 earthquake	85
Figure 5.12.	Coherency values for each distance bins and average coherency values for EW direction (11-point) – October 20, 2006 earthquake	86
Figure 5.13.	Average coherency values of each distance bins with respect to direction and smoothing window length – October 20, 2006 earthquake	87
Figure 5.14.	Coherency values for each distance bins and average coherency values for EW direction (11-point) – October 24, 2006 earthquake	88
Figure 5.15.	Average coherency values of each distance bins with respect to direction and smoothing window length – October 24, 2006 earthquake	89

Figure 5.16.	Coherency values for each distance bins and average coherency values for EW direction (11-point) – March 12, 2008 earthquake	90
Figure 5.17.	Average coherency values of each distance bins with respect to direction and smoothing window length – March 12, 2008 earthquake.	91
Figure 5.18.	Average coherency values of six earthquakes recorded by IERRS with respect to separation distance and frequency	92
Figure 5.19.	The derived coherency model for each distance bins using all earthquake data.....	99
Figure 5.20.	Residuals of the coherency model (Eq. (5.17)) for each distance bins ...	100
Figure 6.1.	Methodology of RspMatch2005 (Hancock <i>et al.</i> , 2006).....	106
Figure 6.2.	The August 17, 1999 Kocaeli earthquake recorded at MSK station: Acceleration (g), velocity (cm/s) and displacement (cm)	113
Figure 6.3.	Comparison of target spectrum and the matched response spectrum	113
Figure 6.4.	Target spectrum compatible time histories: Acceleration (g), velocity (cm/s) and displacement (cm)	114
Figure 6.5.	Decay of coherencies with respect to frequency for different separation distances.....	115
Figure 6.6.	Acceleration time history of reference station and simulated data at d=100 m at the left column. Relative acceleration time history with respect to reference station at the right column	115
Figure 6.7.	Velocity time history of reference station and simulated data at d=100 m at the left column. Relative velocity time history with respect to reference station at the right column.....	116
Figure 6.8.	Displacement time history of reference station and simulated data at d=100 m at the left column. Relative displacement time history with respect to reference station at the right column	116
Figure 6.9.	Comparison of Fourier amplitude of reference station and simulated data at d=100 m at the left column. Comparison of target, spectrum at reference station and spectrum at d=100 m at the right column	117

LIST OF TABLES

Table 2.1.	Site-class information of IERRS stations.....	12
Table 2.2.	Source properties of the events recorded by IERREWS.....	13
Table 2.3.	Station properties of the Spitsbergen array (SPITS).....	16
Table 2.4.	Earthquake properties triggered by the Spitsbergen array (SPITS).....	18
Table 4.1.	Source parameters of the rupture model for the November 12, 1999 earthquake	59
Table 4.2.	Site properties of the auxiliary problem.....	59
Table 4.3.	Dynamic soil properties for the reduced model	64
Table 5.1.	Regression coefficients based on Equation (5.15) for East-West direction of the earthquakes data recorded by IERRS (11-point).....	96
Table 5.2.	Regression coefficients based on Equation (5.16) for East-West directions of the earthquakes data recorded by IERRS (11-point)	97
Table 5.3.	Regression coefficients based on Equation (5.17) for East-West directions of the earthquakes data recorded by IERRS (11-point)	98

LIST OF SYMBOLS / ABBREVIATIONS

A_i	Amplitude of the ground acceleration
$a(t)$	Ground acceleration at time t
a, b	Coefficients of proposed method based on modified kriging method
a_1, a_2, a_3, a_4, a_5	Coefficients of coherency model
d	Station separation distance
$F(\Delta)$	Function that accounts for the spatial correlation of the motion
L_f	Fault length
M_o	Slip moment
M_W	Moment magnitude
m	Window length for coherency
N	Number of recordings/data sample
N_f	Number of frequency intervals
Q_s	Quality factor
r_0	Scale length of random inhomogeneities along the path
S_{xx}	Power spectral density at station x
S_{yy}	Power spectral density at station y
S_{xy}	Cross spectral density at stations x and y
S_g	One-sided local power spectrum
u^*	Ground motion parameter
V	Apparent seismic wave velocity
V_S	Shear wave velocity
V_P	P-wave velocity
v_R	Rupture velocity
W	Spectral smoothing window
W_f	Fault width
w_i	Modified kriging weights
w'	Semivariogram

β	Function used to locate the coherency phase angle
Δ	Average separation distance between the stations
$\Delta\omega$	Frequency step
ϕ_i	Independent random phases
γ_{xy}	Coherency between stations x and y
ξ	Distance between two stations
λ	kriging weight
μ	Arithmetic Mean
μ_g	Geometric mean
$\mu_{i,j}$	Coherency phase for the i^{th} frequency at station j
μ_R	Mean value by Kawakami and Mogi (2003)
μ_2	A measure of the relative variation of the elastic properties in the medium
ρ	Density
σ_E^2	Variance
σ_g	Geometric standard deviation
$\sigma_{\Delta\log Y}$	Standard deviation of differences in the logarithm of the peak motion Y
σ_{indobs}	Standard deviation of an individual observation about a regression
σ_P'	Standard deviation
θ_{xy}	Phase angle
τ_j	Time lag between two stations
v_{rm}	Elastic shear wave velocity in the random medium
ω_u	Cut-off frequency (Nyquist frequency)
AR	Autoregressive
ARCESS	Regional Seismic Array
ARMA	Autoregressive moving average
CWT	Continuous Wavelet Transform
DRM	Domain Reduction Method

GeoELSE	GeoELasticity by Spectral Elements
IERREWS	Istanbul Earthquake Rapid Response and Early Warning System
IMS	International Monitoring System
MA	Moving average
NOA	NORSAR Array
NORESS	Norwegian Experimental Seismic System
NORSAR	Norwegian Seismic Array
PGA	Peak ground acceleration
PGA_{est}	Estimated peak ground acceleration
PGA_{GM}	Peak ground acceleration for the geometric mean of two horizontal components
PGA_{obs}	Observed peak ground acceleration
PGD	Peak ground displacement
PGS_{xx}	Peak ground strain at the longitudinal direction
PGS_{yy}	Peak ground strain at the vertical direction
PGV	Peak ground velocity
PSV	Pseudo spectral velocity
RF	Random Field
RRMap	Rapid Response Mapping Application
SDOF	Single Degree of Freedom
SMART-1	Strong Motion ARray in Taiwan, Phase (1)
SPITS	Spitsbergen
w.r.t.	with respect to

1. INTRODUCTION

1.1. Background

The spatial variation of seismic ground motion indicates the discrepancy in amplitude and phase of ground motion recorded over extended areas. This variability has an important effect on the response of linear lifelines such as bridges, pipelines, communication systems, and should preferably be accounted for in their design. The spatial variation of earthquake ground motion can occur as a consequence of source properties, wave propagation through different earth strata, soil media and topographic features and serves to quantify the amplitude and phase differences of ground motion over distance or area.

A large number of field studies of earthquake damage indicated that the degree of damage suffered by similar and nearby structures varies significantly from one location to another for any earthquake event. It has been seen that the differences in ground motion cause this variation. It may produce additional loads in the structures like linear lifelines than the loads produced if the spatial variation was not considered, and should preferably be taken into account in their design. Especially, for the structures with rigid extended foundations, the spatial variation may lead to a reduction of the translation response at foundation level and an increase in the rocking and torsional response. For the structures with flexible foundations and/ or with multiple supports (such as suspension bridges), the spatial variation may cause increased localized deformations and strains (Luco and Wong, 1986).

Variation in waveform (phase) and variation in amplitude are two components that explain the spatial variation of strong ground motion. The variation in waveform can be explained by spatial coherency. The amplitude variation describes variation in scaling. In other words, the similarity between ground motions at different locations can be described in the time domain or in the frequency domain. The cross covariance represents this similarity of the motion in the time domain. Conversely, the coherency explains the similarity in the frequency domain. The coherency describes the degree of correlation

between the amplitudes and phase angles of two time histories in the frequency domain. A value of one indicates full coherence (or perfect correlation), while value of zero indicates full incoherence (or no correlation). The mathematical form of the coherency function $\gamma_{xy}(\omega)$ between two accelerograms recorded at two stations x and y is given as :

$$\gamma_{xy}(\omega) = \frac{S_{xy}(\omega)}{\sqrt{S_{xx}(\omega)S_{yy}(\omega)}} \quad (1.1)$$

in which $S_{xx}(\omega)$ is the power spectral density at station x, $S_{xy}(\omega)$ is the cross-power spectral density between stations x and y. The coherency will be explained in details in Chapter 5.

A number of factors cause the spatial incoherence. One is traveling-wave or wave-passage effect, in which nonvertically propagating waves reach different points on the ground surface at different times, producing a time shift between the motions at those points. Another cause of incoherence in the nearfield is the extended source effect, in which differences in the relative geometry of the source and sites produce different time shifts, and consequently different motion, at the sites. Finally, ray-path effects caused by scattering (reflection, refraction, *etc.*) of waves by inhomogeneities along the travel path can cause incoherence. Furthermore, the spatial variability in seismic ground motion can result from relative surface fault motion for recording stations located on either side of a causative fault; soil liquefaction; landslides; and from the general transmission of the waves from the source through the different earth strata to the ground surface (Zerva, 2009).

The installation of dense instrument arrays initiated the comprehensive analyses of the spatial variation of seismic ground motion. Before the installation of these arrays, the spatial variation of the motion was attributed to the apparent propagation of the waveforms on the ground surface, *i.e.*, it was considered, at least in engineering applications, that the difference in the motion between two stations was caused solely by a time delay in the arrival of the time history at the further away station (Zerva and Zervas, 2002). The data recorded at dense seismograph arrays have provided valuable information on additional causes and more detailed descriptions for the spatial variation of the motion.

The analysis of the spatial variation of the seismic ground motion and its effect on a variety of structural systems was extensively studied after the installation of the first dense seismograph arrays in the late 1970's- early 1980's. One of the first arrays installed was the El Centro differential array that recorded the 1979 Imperial Valley earthquake. After the event triggered by the array, the spatial variability studies based on array data started appearing in the literature. These data provided valuable information on the physical causes underlying the variation of the motion over extended areas and the means for its modeling.

A large number of studies confirmed that the correlation of the motion decreases as the frequency and the separation distance between the stations increase. Signal processing techniques were developed to describe the spatial variability of the seismic data, generally, during the strong motion shear-wave window, by means of the coherency. In the literature, coherency models fitted to the decay of the recorded data with frequency and separation distance has been published. The modeling of the spatial variability of the ground motion has an important effect on the evaluation of the response of a wide range of above-ground and buried structural systems. An extensive number of publications analyzed the effects of the spatial variation of the seismic ground motion on the response of pipelines, tunnels, dams, suspensions, bridges, nuclear power plants, as well as on conventional building structures. Spatial variability of the strong ground motion can significantly influence internal forces induced in abovementioned structures with multiple supports. Currently, the topic actively investigated and considerations of its effects have appeared, in various forms, in design recommendations. Recently, a book, Zerva (2009), is published that specifically deals with the spatial variability of ground motion.

Alternatively, the generation of estimated maps of shaking after an earthquake provides an important seismological tool to guide emergency response. Estimation of the variation of ground motion between stations is important in characterizing the uncertainty inherent in the interpolations necessary to produce these maps. Hence, the statistical properties of the spatial variability in terms of separation distance between the stations over extended areas have been studied by the researchers.

For the quantification of the variability of seismic ground motion, Schneider *et al.* (1990) used Fourier amplitude spectra; Abrahamson and Sykora (1993) relied on the acceleration response spectra; Joyner and Boore (1981) examined the dependence of peak horizontal acceleration and velocity on moment magnitude, distance and recording-site-geology. Abrahamson (1988) studied the relationship between the intra-event variation of peak ground acceleration (PGA) and earthquake magnitude. Kawakami and Mogi (2003) analyzed the spatial intra-event variability of PGA's as a function of separation distance. The study of Field *et al.* (1997) addressed the variability of pseudo-velocity response spectra. Evans *et al.* (2003) repeated the analysis by using pseudo-spectral velocity (PSV) response spectra as a function of inter-station distance. On the other hand, coherency is commonly used to describe the spatial variation, since previous studies have shown that the spatial variation of strong ground motion is strongly dependent on frequency (Loh *et al.*, 1982; Smith *et al.*, 1982; McLaughlin, 1983; Harada, 1984; Abrahamson, 1985). Coherency models have been developed by several researchers: Abrahamson, (1993), Harichandran and Vanmarcke (1986), Harichandran (1988), Harichandran (1991), Loh (1985), Loh and Yeh (1988), Loh and Lin (1990), Novak (1987), Oliveira *et al.* (1991), Ramadan and Novak (1993a), Vernon *et al.* (1991), and Zerva and Zhang (1997). An overview of the spatial variation of ground motion is given by Zerva and Zervas (2002). The influence of ground motion variability in earthquake loss modeling is examined by Bommer and Crowley (2006). Song *et al.* (2009) explored the spatial coherence between earthquake source parameters.

In addition, random vibration analyses can directly use spatially variable seismic ground motion as input motion for the linear response of the structures. For complex long structures and for the evaluation of the nonlinear seismic response, the deterministic solution is essential with the effect of the spatial variation of the seismic event considered in terms of multiple-support excitation. The determination of ground motion requires numerical simulation techniques to account for the spatial correlation of earthquake ground motion. Spectral representation method (Rice, 1944; Shinozuka, 1972); AR (auto-regressive), MA (moving-average), and ARMA (auto-regressive-moving-average) (Conte *et al.* 1992; Ellis and Cakmak, 1991; Mignolet and Spanos, 1992; Spanos and Mignolet 1992; Shama, 2007); local average subdivision method (Fenton and Vanmarcke, 1990); based on wavelet transforms (Gurley and Kareem, 1994; Zeldin and Spanos, 1996);

covariance matrix decomposition (Hao *et al.*, 1989, Zerva and Katafygiotis, 2000); envelope functions containing random phase variability (Abrahamson, 1992); coherency function approximation by a Fourier series (Ramadan and Novak, 1993b; Ramadan and Novak, 1994) are some of the methods used for the simulation of spatially variable strong ground motion.

1.2. Objectives and Scope of the Thesis

The spatial variation of ground motion can have significant effects on the dynamic response of engineered structures due to the wave-passage effect; the extended source effect; and ray-path effects. Furthermore, the spatial variability in seismic ground motion can result from relative surface fault motion for recording stations located on either side of a causative fault; soil liquefaction; landslides; and from the general transmission of the waves from the source through the different earth strata to the ground surface.

The aim of this study is to evaluate and improve existing spatial variation quantification relationships by studying the data available from different networks; to investigate the possibility of employing functional forms for the modeling of spatial variation of ground motion; to development of a methodology for the assessment of strong ground motion distribution in urban context; and to simulate the spatially incoherent earthquake ground motion.

This study focuses on 1) studying the spatial variability of the ground motion using strong ground motion measurements, 2) developing a rational and rigorous methodology for the interpolation of measured ground motion of discrete array stations to be used in the bias adjustment of the theoretical shake map assessments with the empirical ground motion measurements, 3) studying the variation of ground strain due to wave propagation, site response and loss of coherence, 4) deriving coherency model for Istanbul for the assessment of simulation of spatially variable ground motion needed for the design of extended structures, 5) constituting a simulation scheme that generates ground motion compatible with prescribed design response spectrum and consistent with prescribed coherency function.

Spatial variation of ground motion has been reviewed with these objectives throughout this study. Chapter 2 gives the information about the arrays and the data used for the analyzing of spatial variation of ground motion. The events recorded by Istanbul Earthquake Rapid Response and Early Warning System (IERREWS) are used for the development of the methodology to estimate the ground parameters over a distance or an area. Also, the observed data from the same events are utilized to obtain the statistical spatial variation with respect to separation distance. The data recorded by Norwegian Seismic array are also used representing the shorter distances for the estimation of statistical spatial variation. During the calculation of the coherency values, a code is generated. For the validation of this code, data from SMART -1 (Strong Motion Array in Taiwan) array are used. Location and the configuration of the arrays are illustrated and properties of corresponding events are explained.

Chapter 3 highlights the estimation of the ground motion parameters, *i.e.* peak ground acceleration (PGA), at unsampled sites within the area covered by existing observations. Hereby, a new methodology originated from kriging scheme is proposed. A brief description of kriging method based on the assumption of spatially correlation of spatially distributed parameters (*i.e.* values are close together tend to have similar characteristics) was made. In addition, the variability of peak ground motion parameters based on data from Istanbul Earthquake Rapid Response System and Norwegian Seismic array is analyzed. The analysis is essentially done for the standard deviations of the logarithmic differences of PGA values considering all station pairs for each event. These PGA ratios are defined as spatial intraevent variations of PGA's and their statistical characteristics are examined. The relation between the standard deviations and the separation distances is presented. The local site effects are discussed. The comparison of the results based on the new methodology with the results obtained from attenuation relationships and spline interpolation method is demonstrated.

Chapter 4 presents the topic of ground-surface strains. A procedure, termed Domain Reduction Method (DRM) is utilized to estimate ground strains, involving the simultaneous effects of the seismic source, the propagation path, complex geological site conditions, such as strong lateral variations of soil properties, and topographic

amplification. This approach is applied to Düzce Basin with reference to the November 1999 event.

Chapter 5 addresses the general properties of coherency function and the coherency estimation procedure based on conventional spectral analysis. Data processing procedures are highlighted. The coherency values derived from the data of the seven events recorded by Istanbul Earthquake Rapid Response stations are shown. Semi-empirical and empirical coherency models are reviewed. Regression procedure for the evaluation of coherency model for Istanbul is explained. Residuals are shown for the generated coherency model.

In Chapter 6, the concept of the simulation of target spectrum and coherency function compatible spatially variable ground motion is described. It begins with the explanation of the software for the generation of ground motion related to the prescribed target spectrum, and then continues with the explanation of the method used for the simulation of spatially variable ground motion consistent with a coherency function. The chapter proceeds with comparison of the simulated ground motion with observed data.

Finally, Chapter 7 presents the conclusions, future possible studies and the improvements.

2. ARRAY AND DATA DESCRIPTION

The installation of the dense arrays provides to analyze the spatial variation of strong ground motion. El Centro Differential array consisted of seven stations installed linearly was the one of the first arrays with a total length of 312.6 m and recorded the 1979 Imperial Valley earthquake. Minimum separation distance between the stations is 7.6 m. Another array, located in Lotung, in the north-east corner of Taiwan, which has provided a large quantity of data for small and large magnitude events that have been extensively studied by engineers and seismologists, is the SMART-1 array (Strong Motion ARray in Taiwan). The LSST (ground surface and down-hole instrumentation) array was constructed in 1985 within the SMART-1 array close to station M08. Permanent and temporary additional arrays have been and are being deployed around the world for analysis of the properties of strong ground motion, eg, EPRI Parkfield, USGS Parkfield, Hollister, Stanford, Coalinga, USGS ZAYA, Pinyon Flat, Tarzana, San Fernando Valley, Sunnyvale, Imperial Valley Differential, Hollister Differential all in California, USA; Chiba Experiment Station, Tokyo, Japan, Nice, France; Thessaloniki, Greece; L'Aquila, Italy (Zerva and Zervas, 2002).

In this study, the spatial variation of seismic ground motion in terms of strong motion parameters are utilized by using data recorded by the Istanbul Earthquake Rapid Response and Early Warning System (IERREWS) and the Norwegian Seismic Array NORSAR array. The data triggered by SMART-1 Array are used in the stage of generation of coherency model.

2.1. Istanbul Earthquake Rapid Response System

2.1.1. Array Configuration and Instrumentation

The Istanbul Earthquake Rapid Response and Early Warning System (IERREWS) is operated by the Department of Earthquake Engineering of Bogazici University Kandilli Observatory and Earthquake Research Institute. 100 strong motion recorders are installed in dial-up mode throughout the city to form a building damage map immediately after an

earthquake for rapid response purposes. Ten of the strong motion stations are sited at locations as close as possible to the Great Marmara Fault in on-line data transmission mode to enable Earthquake Early Warning. The stations consist of external, tri-axial (three orthogonal axis), force-balance (servo) type accelerometers, recorders, timing and communication modules. The distribution of strong motion stations of the rapid response system in Istanbul is shown in Figure 2.1 (Erdik *et al.*, 2003). Their inter-station distances vary between 0.67 km and 56 km.

The objective of the Istanbul Earthquake Rapid Response System (IERRS) is to provide reliable information for accurate, effective characterization of the shake- and damage maps for rapid response; recorded motion for analysis of structures; long-term improvements in seismic microzonation, seismic provisions of building codes; and seismological data for the estimation of the source and seismic wave propagation (Erdik, 2006).

The strong motion accelerograms utilized in the IERREW System have the following basic specifications (Erdik *et al.*, 2003):

- Overall recording range: The strong motion instrumentation utilized in the IERREW system can record an acceleration range of +/-2.0 g full scale with industry accepted specifications.
- Recorder dynamic range: The instrumentation has 18-bit (dial-up stations) or 24-bit (on-line) resolution. The least significant bit (LSB) resolution is 0.015 mg.
- Noise floor: The noise level is less than 0.02 mg RMS in the frequency range of 0-40 Hz. The instruments provide on-site recording for two hours or more of strong motion recording. Timing accuracy: Within 1/10th of a sampling interval of GPS absolute time (UTC).
- Sample rate: 200 samples per second (5.0 ms sampling interval) with adequate antialias filtering (filter corner at 80 per cent of the nyquist frequency, and down by 100 dB at the nyquist).

- Triggering: Nominal trigger level is 1.0-5.0 mg within a pass band of 0.1 to 12 Hz. The actual trigger levels are established by site conditions. Once triggered, the recorder shall stay triggered for at least 30 seconds after the last occurrence of acceleration over 5.0 mg.

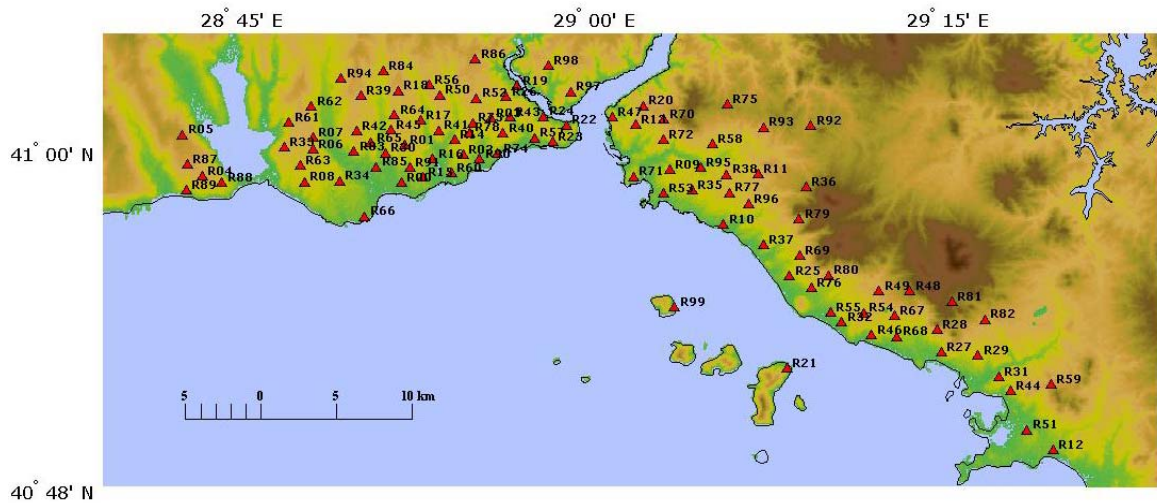


Figure 2.1. Configuration of urban stations in IERRS

All of the instruments were calibrated in the laboratory using an air-bed electro-magnetic shaker for calibration of the sensitivity constants of the sensors. Additional bi-directional tilt tests at site were conducted for confirmation. In normal times the rapid response stations are interrogated (for health monitoring and instrument monitoring) on regular basis (Erdik, 2006). After triggered by an earthquake, each station processes the streaming three-channel strong motion data to yield the spectral accelerations at specific periods, 12 Hz filtered peak ground acceleration and peak ground velocity and sends these parameters (in the form of SMS messages) at every 20s directly to the main data center through the GSM communication system. The main data processing center is located at the Department of Earthquake Engineering and Kandilli Observatory and Earthquake Research Institute of Bogazici University. A secondary center located at the Seismological Laboratory of the same Institute serves as a redundant secondary center that can function in case of failure in the main center. Shake and damage distribution maps will be automatically generated at the data centers after the earthquake and communicated to the

end users within 5 minutes. Full-recorded waveforms at each station can be retrieved using GSM and GPRS modems subsequent to an earthquake (Erdik *et al.*, 2003).

2.1.2. Geology and Soil Properties

The site classification map for Istanbul is prepared by OYO International Cooperation within the microzonation project of the İstanbul Metropolitan Municipality for the European and Asian parts of Istanbul. The distribution of average shear wave velocity for the top 30 m of soil (V_{s30}) distribution map is presented in Figure 2.2. This map shows that most part of the south part of the European side have low V_{s30} values. The Asian region has stiffer soil conditions and has comparatively high shear wave velocities. The detailed site-class information of the stations is provided in Table 2.1.

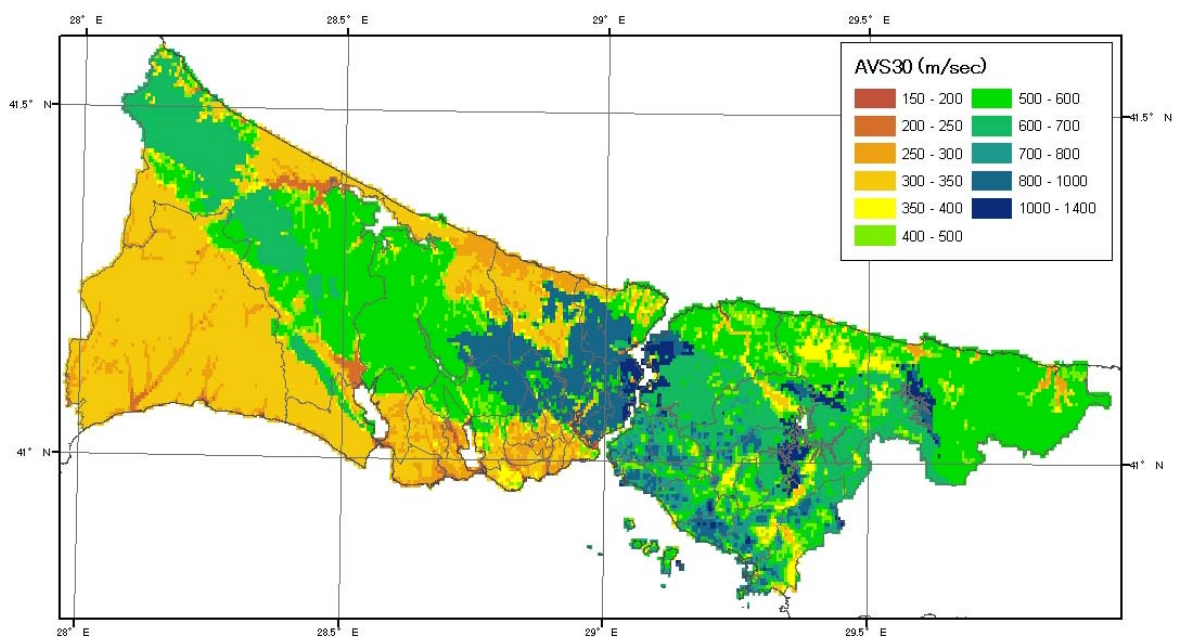


Figure 2.2. İstanbul site classification map

2.1.3. Earthquake Data

Since the development of the IERRS in 2001, many large and small earthquakes have been recorded by a large number of stations. In this study, seven of them are used. The locations of events are shown in Figure 2.3. Their source properties are summarized in Table 2.2. The local magnitudes range from 3.1 to 5.2. Minimum epicentral distances

for each earthquake are approximately 1, 14, 1, 14, 101, 52, and 30 km; and maximum epicentral distances are 22, 58, 23, 34, 130, 70, and 50 km with respect to earthquake numbers from 1 to 7, defined in Table 2.2. Fault mechanisms are strike-slip for the first six earthquakes; for the seventh earthquake, it is determined as normal mechanism.

Table 2.1. Site-class information of IERRS stations

Station Name	Vs30 (m/sec)	Site Class	Station Name	Vs30 (m/sec)	Site Class	Station Name	Vs30 (m/sec)	Site Class	Station Name	Vs30 (m/sec)	Site Class
R00	349	D	R25	561	C	R50	307	D	R75	800	B
R01	332	D	R26	293	D	R51	739	C	R76	513	C
R02	301	D	R27	795	B	R52	304	D	R77	855	B
R03	316	D	R28	714	C	R53	917	B	R78	329	D
R04	302	D	R29	951	B	R54	865	B	R79	733	C
R05	307	D	R30	289	D	R55	655	C	R80	572	C
R06	320	D	R31	785	B	R56	295	D	R81	738	C
R07	300	D	R32	838	B	R57	322	D	R82	620	C
R08	332	D	R33	323	D	R58	1082	B	R83	306	D
R09	565	C	R34	344	D	R59	575	C	R84	405	C
R10	897	B	R35	778	B	R60	296	D	R85	341	D
R11	570	C	R36	574	C	R61	346	D	R86	526	C
R12	425	C	R37	806	B	R62	331	D	R87	296	D
R13	789	B	R38	463	C	R63	333	D	R88	277	D
R14	285	D	R39	297	D	R64	321	D	R89	237	D
R15	328	D	R40	327	D	R65	300	D	R90	272	D
R16	305	D	R41	306	D	R66	396	C	R91	340	D
R17	277	D	R42	329	D	R67	899	B	R92	573	C
R18	325	D	R43	313	D	R68	744	C	R93	891	B
R19	176	D	R44	686	C	R69	768	B	R94	276	D
R20	643	C	R45	270	D	R70	806	B	R95	564	C
R21	590	C	R46	795	B	R71	721	C	R96	702	C
R22	358	D	R47	725	C	R72	866	B	R97	817	B
R23	364	C	R48	722	C	R73	327	D	R98	817	B
R24	294	D	R49	877	B	R74	301	D	R99	557	C

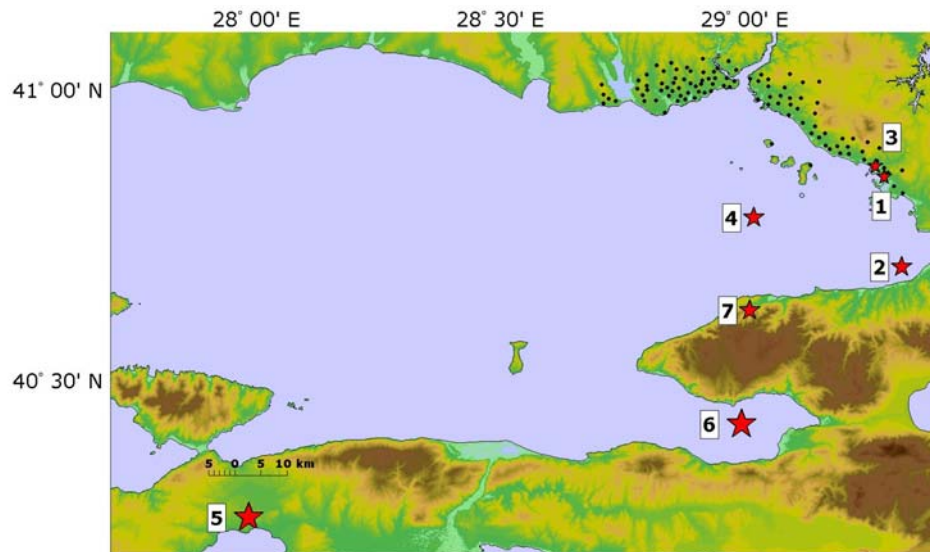


Figure 2.3. Locations of the events recorded by IERREWS

Table 2.2. Source properties of the events recorded by IERREWS

Eq. No	Earthquake	Date	Latitude	Longitude	GMT	M_L	M_d	Recorded data number
1	Güzelyalı	19/09/2003	40.8498	29.2867	00:51	3.1	3.2	16
2	Yalova	16/05/2004	40.6957	29.3222	03:30	4.3	4.2	72
3	Güzelyalı	24/06/2004	40.8676	29.2683	13:28	3.2	3.2	14
4	Marmara Sea	29/09/2004	40.7797	29.0200	15:42	4.0	-	86
5	Kuşgözü	20/10/2006	40.2635	27.9843	21:15	-	5.2	43
6	Gemlik	24/10/2006	40.4240	28.9947	17:00	-	5.2	47
7	Çınarcık	12/03/2008	40.6210	29.0110	20:52	4.8	-	54

2.2. The Norwegian Seismic Array (NORSAR)

2.2.1. Array Configuration and Instrumentation

Ever since NORSAR was established in 1968, the focus of research has been upon developing advanced array processing techniques. Originally, NORSAR was constructed as a large aperture array, with an initial diameter of 100 km, and 22 subarrays comprising a total of 132 short period and 22 three-component long-period seismometers. NORSAR was reduced in size to 7 subarrays (diameter 60 km) in 1976. From the beginning, the

research at NORSAR focused on processing techniques for large, so-called teleseismic arrays (<http://www.norsar.no/c-71-Station-Network.aspx>).

In the 1980's, emphasis shifted to smaller arrays, since the prospects of in-country stations for CTBT (Comprehensive Nuclear-Test-Ban Treaty) monitoring were emerging. This resulted in the first regional array, Norwegian Experimental Seismic System (NORESS), which was constructed in southern Norway in 1984, and had 25 seismometer sites within an area of only three km in diameter (Ringdal, 1990; Kværna, 1990). A sister array, the Arctic Regional Seismic Array (ARCESS), was established in northern Norway in 1987 (Mykkeltveit *et al.*, 1990). NORESS and ARCESS have since become the standard for arrays in the International Monitoring System.

In brief, the large teleseismic arrays are the NORSAR array (NOA PS27) with a diameter of 60 km, the regional ARCESS array (ARCES PS28) with a diameter of three km and the small Spitsbergen array (SPITS AS72) with a diameter of one km. The NOA array consists of 42 different sites with a total of 63 instruments. These are organized in seven different subarrays. This is the largest array in the IMS network. The ARCES array has 25 sites with 36 instruments and the SPITS array has 9 sites with 12 instruments. SPITS array represents minimum requirements for the size of an International Monitoring System (IMS) array (Ringdal, 2005). Figure 2.4 demonstrates the locations of the Norwegian seismic array stations. Figure 2.5 shows the approximate design of the three arrays and their relative size. On the left, the ARCES array in Karasjok and the SPITS array on the island of Spitsbergen. On the right the NOA array with its group of seven subarrays near the town of Hamar.

2.2.2. Earthquake Data

The data recorded by the ARCESS and NOA array is eliminated due to the fact that the magnitude of the earthquakes is not higher than 3.0 and most stations triggers vertical motion. The six of the nine stations of SPITS array records all components of the strong ground motion. Therefore, the earthquake data with higher magnitude recorded by these six stations are considered in this study. The latitude, longitude, elevation, and instrument

information are listed in Table 2.1. The magnitude ranges from 3.0 to 4.16. The detailed information about the events is represented in Table 2.4.



Figure 2.4. The locations of the Norwegian seismic array stations (Ringdal, 2005)

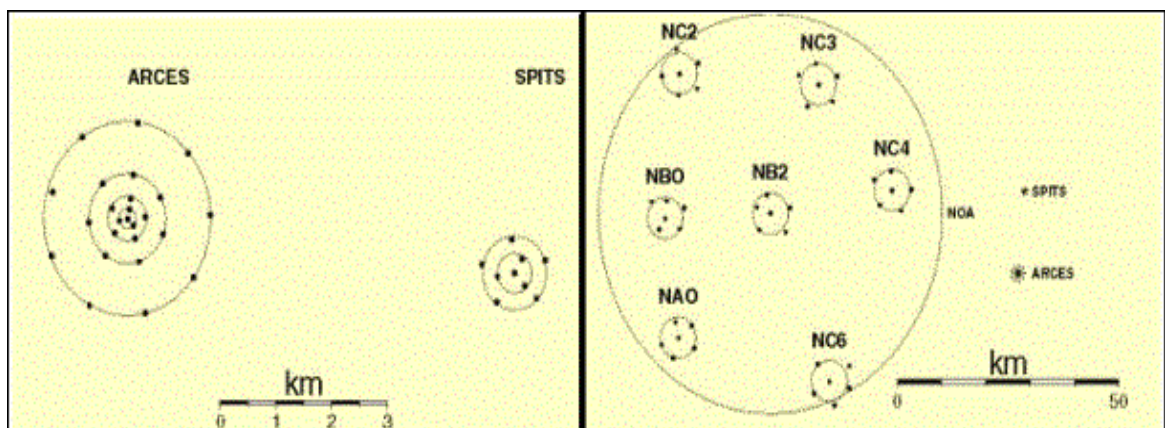


Figure 2.5. Schematic plot of Norway's IMS seismic arrays (Ringdal, 2005)

2.3. The Strong Motion Array in Taiwan (SMART-1)

2.3.1. Array Configuration and Data

SMART-1 array (Strong Motion ARray in Taiwan, Phase (1)), located in Lotung, in the north-east corner of Taiwan, which started being operative in 1980, consists of 37 force-balanced triaxial accelerometers arranged on three concentric circles, the inner denoted by I, the middle by M, and the outer by O (Figure 2.6). Twelve equispaced stations, numbered 1-12, were located on each ring, and station C00 was located at the centre of the array. Two additional stations, E01 and E02, were added to the array in 1983, at distances of 2.8 and 4.8 km, respectively, south of C00. The array was located in a recent alluvial valley except for station E02 that was located on a slate outcrop (Shin *et al.*, 2003).

Table 2.3. Station properties of the Spitsbergen array (SPITS)

Station	Latitude	Longitude	Elevation (km)	Instrument	Component
SPA0	78.1777	16.3700	0.320	CMG-3TB	BB3C
SPA1	78.1797	16.3755	0.320	CMG-3TB	BBZ
SPA2	78.1759	16.3766	0.250	CMG-3TB	BBZ
SPA3	78.1773	16.3588	0.339	CMG-3TB	BBZ
SPB1	78.1796	16.3906	0.301	CMG-3TB	BB3C
SPB2	78.1742	16.3846	0.200	CMG-3TB	BB3C
SPB3	78.1737	16.3584	0.234	CMG-3TB	BB3C
SPB4	78.1789	16.3482	0.340	CMG-3TB	BB3C
SPB5	78.1823	16.3683	0.295	CMG-3TB	BB3C

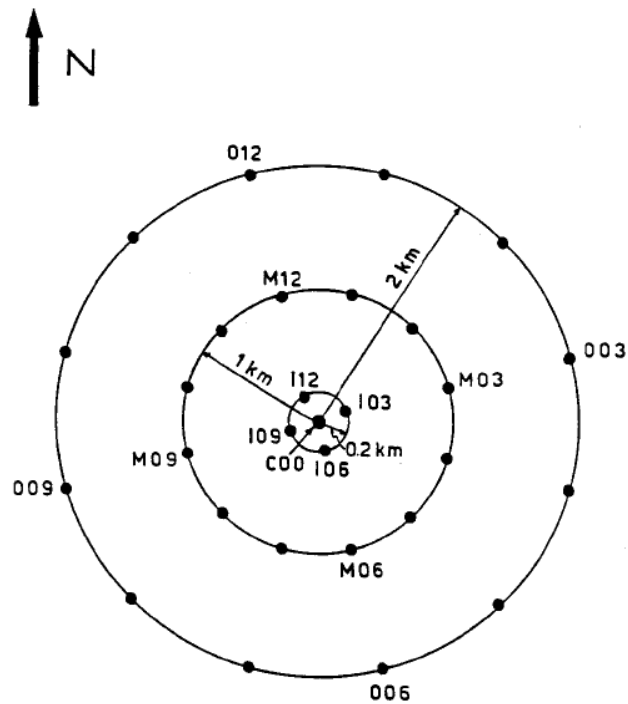


Figure 2.6. The configuration of the SMART-1 array

In Chapter 6, the generation of coherency model is presented. Prior to the constitution of the model, a code is written to derive the coherency values. At this stage, SMART-1 data is used for the verification of the code. The results are compared with Zerva and Zervas, (2002). Comparison is done using the same event, which is Event 5. S-wave window of the data recorded at stations I06 and I12 (separation distance of 400 m) in N-S direction is used for the evaluation of coherency.

Table 2.4. Earthquake properties triggered by the Spitsbergen array (SPITS)

Time	Latitude	Longitude	Magnitude	Distance	Azimuth	Location
19/11/2006	76.232	22.415	3.11	263.98	142.49	WESTERN BARENTS SEA
28/10/2006	76.539	22.347	4.16	234.40	138.45	WESTERN BARENTS SEA
26/10/2006	76.357	20.242	3.26	224.84	152.98	WESTERN BARENTS SEA
06/10/2006	80.863	1.417	3.04	425.32	321.82	NORTH OF SVALBARD
18/09/2006	79.914	20.930	3.71	217.05	24.30	NORDAUSTLANDET SVALBARD
09/08/2006	78.315	8.537	3.90	179.14	278.73	KNIPOVICH REGION
12/08/2006	79.852	20.632	3.14	208.16	23.80	NORDAUSTLANDET SVALBARD
16/08/2006	77.107	19.787	3.02	145.00	143.99	STORFJORDEN SVALBARD
21/08/2006	75.566	13.285	3.31	302.45	196.53	KNIPOVICH REGION
04/07/2006	79.884	4.766	3.50	311.35	313.29	GREENLAND SEA
28/05/2006	74.084	14.255	3.94	461.35	188.09	MOHNS RIDGE
29/04/2006	75.994	23.312	3.00	299.34	141.18	WESTERN BARENTS SEA
10/02/2006	79.672	19.118	3.30	177.36	18.11	NORDAUSTLANDET SVALBARD
20/11/2005	78.031	14.230	3.01	52.04	252.71	WEST SPITSBERGEN SVALBARD
18/10/2005	79.716	19.721	3.45	186.47	21.04	NORDAUSTLANDET SVALBARD
25/09/2005	79.415	5.084	3.23	281.10	304.89	SVALBARD, NORWAY, REGION
13/08/2005	79.446	5.531	4.07	274.21	306.32	SVALBARD, NORWAY, REGION
14/07/2005	76.031	24.102	3.24	307.68	137.38	WESTERN BARENTS SEA
18/07/2005	80.270	32.250	3.02	404.42	47.20	SVALBARD, NORWAY, REGION
18/07/2005	80.186	32.026	3.79	396.41	48.13	SVALBARD, NORWAY, REGION
02/04/2005	78.445	7.917	4.29	193.81	283.01	KNIPOVICH REGION
02/04/2005	78.378	8.416	3.60	182.14	280.95	KNIPOVICH REGION
02/04/2005	78.362	8.134	4.41	188.36	280.31	KNIPOVICH REGION
02/04/2005	78.542	7.396	3.21	206.49	285.73	KNIPOVICH REGION
02/04/2005	78.360	8.362	3.15	183.25	280.29	KNIPOVICH REGION
24/04/2005	78.442	8.665	3.23	177.02	283.36	KNIPOVICH REGION
01/03/2005	77.257	29.080	3.55	318.91	102.52	SVALBARD, NORWAY, REGION
20/01/2005	80.127	32.885	3.67	408.42	49.98	SVALBARD, NORWAY, REGION
27/11/2004	76.087	9.768	3.37	285.55	218.38	KNIPOVICH REGION
04/10/2004	78.439	7.761	3.43	197.26	282.73	KNIPOVICH REGION
08/10/2004	80.481	6.963	3.92	322.35	327.46	SVALBARD, NORWAY, REGION
09/10/2004	75.914	8.019	3.02	328.14	223.71	KNIPOVICH REGION
09/10/2004	78.645	8.000	3.21	195.15	289.60	KNIPOVICH REGION
10/10/2004	75.883	9.817	3.03	304.56	215.88	KNIPOVICH REGION
10/10/2004	77.494	9.208	3.61	185.25	249.15	KNIPOVICH REGION
11/10/2004	75.960	10.747	3.09	284.99	212.34	KNIPOVICH REGION
14/10/2004	81.619	-1.930	3.88	522.06	325.75	NORTH OF SVALBARD
22/10/2004	79.164	19.398	3.15	128.88	29.61	NEW FRIESLAND SVALBARD
24/10/2004	80.021	4.881	3.00	317.91	315.85	NORTH OF SVALBARD
11/10/2004	75.898	9.645	3.53	305.45	216.81	KNIPOVICH REGION
22/09/2004	77.577	8.803	3.42	189.92	253.02	KNIPOVICH REGION
06/12/2006	76.702	19.217	3.07	179.02	155.85	STORFJORDEN SVALBARD

3. ESTIMATION OF PEAK GROUND ACCELERATIONS AND ANALYZING SPATIAL VARIABILITY OF GROUND MOTION

3.1. Introduction

The generation of the estimated maps of shaking after an earthquake is often influenced by the limited number of sensors or difficulty of monitoring at inaccessible locations that impacts the collection of desired information. This gap in information can be filled through the estimation of missing information conditional upon the measured records. A methodology is developed for estimating properly-correlated earthquake ground motion parameters; herein peak ground acceleration (PGA), at an arbitrary set of closely-spaced points, compatible with known or prescribed ground motion parameters (PGA) at other locations.

In addition, estimation of the statistical variation of ground motion between stations is important in characterizing the uncertainty inherent in the interpolations necessary to produce ground motion distribution maps: The so-called ShakeMap. In this study, standard deviations of the logarithmic differences of the ground motion parameters are considered for the quantification of the variability of earthquake ground motion.

3.2. Estimation of Peak Ground Acceleration based on Modified Kriging Method

In earthquake engineering, stochastic approaches are often used to simulate seismic ground motion. Recently, conditional simulation of random processes and fields has been studied in connection with its application to urban earthquake monitoring (Wang *et al.*, 2003). The conditional nature of the simulation stems from the fact that the realizations of the random processes or fields have been recorded at only some locations. One needs to simulate the full random field from the recorded information given (Wang *et al.*, 2003). Generally, the conditional simulation can be performed utilizing Kriging method. The Kriging method was developed by Krige (1966) in solving the ore evaluation problem. So far, the conditional simulation can be carried out by using the Kriging method (Krige, 1966, Journel and Huijbregts, 1978). Kriging methodology provides the best linear

unbiased estimate built on data of a stochastic field. Vanmarcke and Fenton (1991), Vanmarcke *et al.* (1993) directly applied the Kriging method to conditional simulation problems in earthquake engineering. Kriging method was used for conditional simulation in relation to earthquake engineering applications (Hoshiya 1994, Hoshiya and Marugama 1994, Hoshiya 1995, Shinozuka and Zhang 1996).

In this study, Kriging method has been modified and used for the estimation of missing peak ground accelerations conditional upon the measured records recorded by IERRS. For this purpose, first the peak ground accelerations are computed for the geometric mean of the horizontal components for seven earthquakes. Before the computation of PGA, the filter range is detected using Fourier amplitude spectrum and signal to noise ratio for each data recorded during each earthquake. The geometric means of PGA in terms of m/s^2 are shown in Figure 3.1 to Figure 3.7. As it is seen from Figure 3.1 to Figure 3.7, all 100 stations of IERRS were not triggered during each earthquake. PGA ranges from 0.3 m/s^2 to 0.1 m/s^2 . The analyses are done for four cases: PGA without site and distance correction, PGA corrected with respect to distance, PGA corrected with respect to site class, PGA corrected with respect to distance and site class.

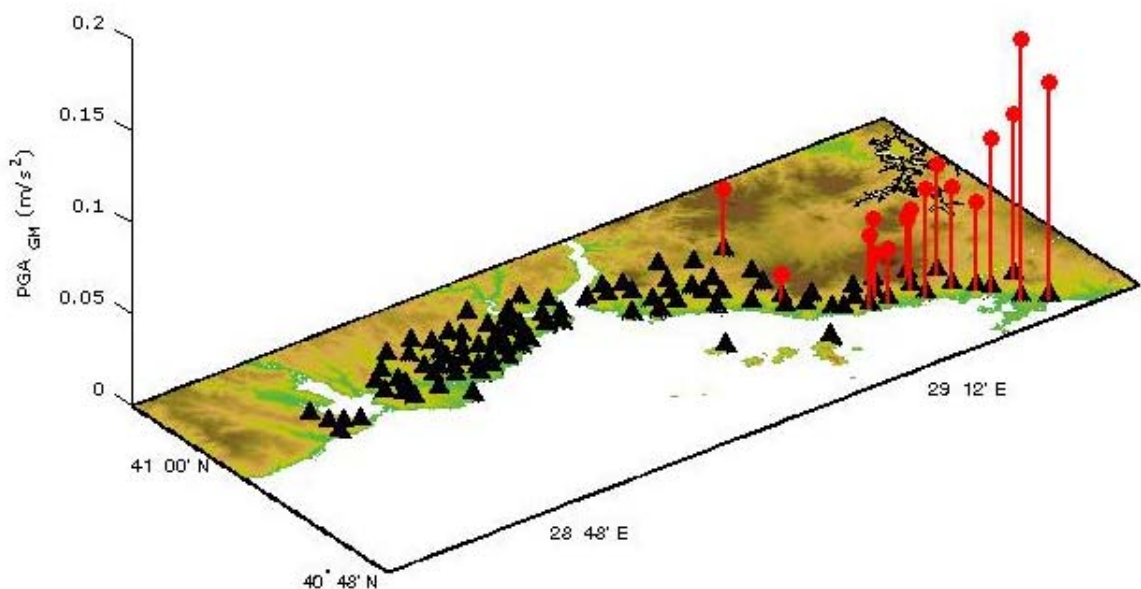


Figure 3.1. Peak ground accelerations for the geometric mean of the horizontal components at each Rapid Response System station triggered during the September 19, 2003 earthquake

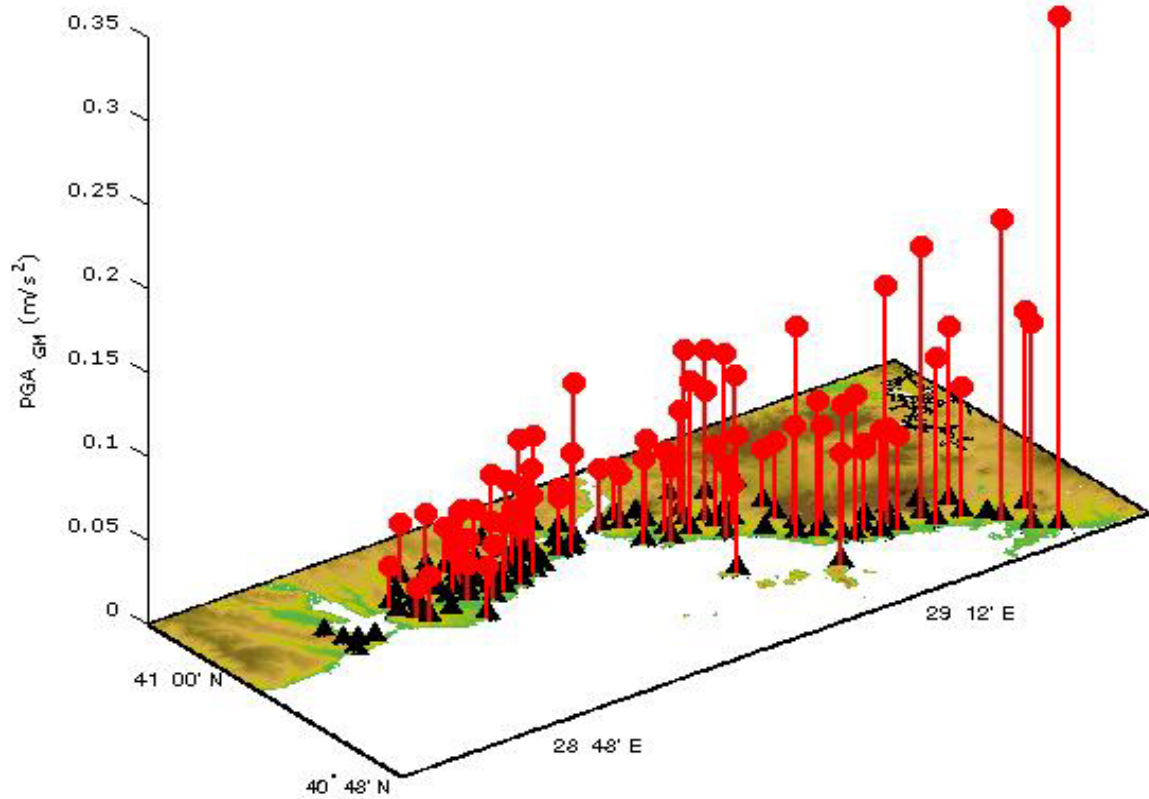


Figure 3.2. Peak ground accelerations for the geometric mean of the horizontal components at each Rapid Response System station triggered during the May 16, 2004 earthquake

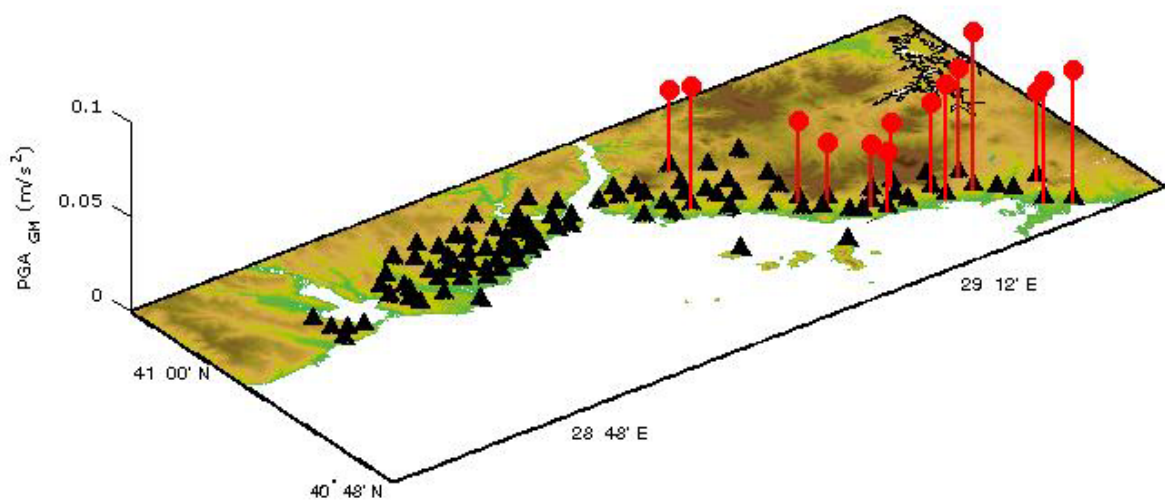


Figure 3.3. Peak ground accelerations for the geometric mean of the horizontal components at each Rapid Response System station triggered during the June 24, 2004 earthquake

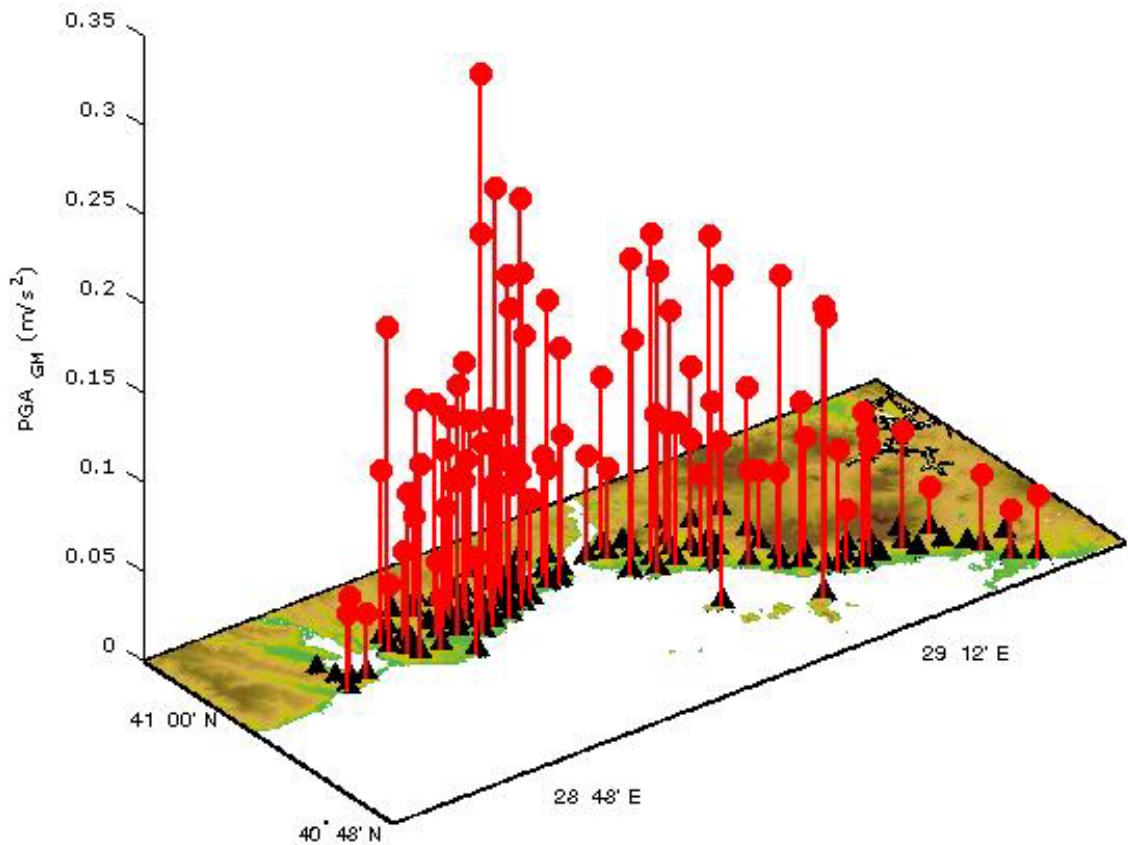


Figure 3.4. Peak ground accelerations for the geometric mean of the horizontal components at each Rapid Response System station triggered during the September 29, 2004 earthquake

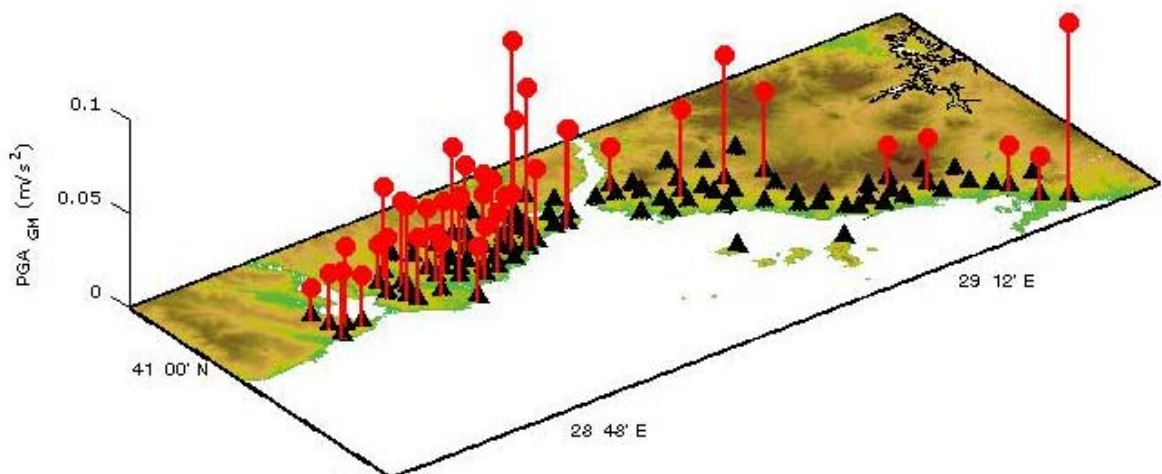


Figure 3.5. Peak ground accelerations for the geometric mean of the horizontal components at each Rapid Response System station triggered during the October 20, 2006 earthquake

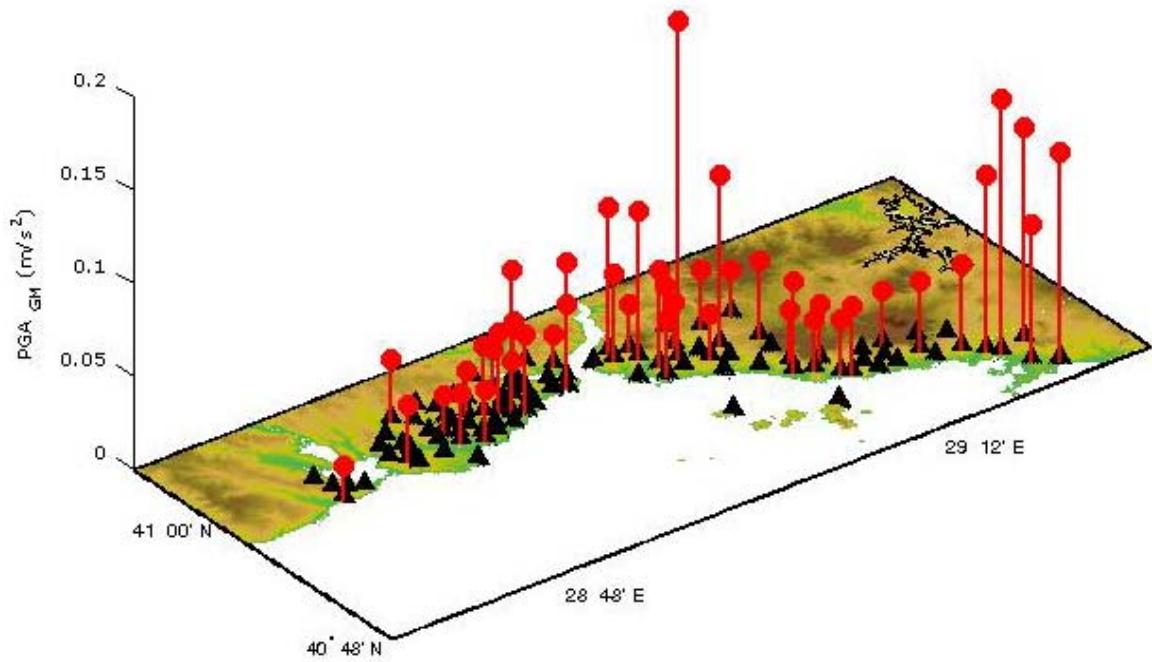


Figure 3.6. Peak ground accelerations for the geometric mean of the horizontal components at each Rapid Response System station triggered during the October 24, 2006 earthquake

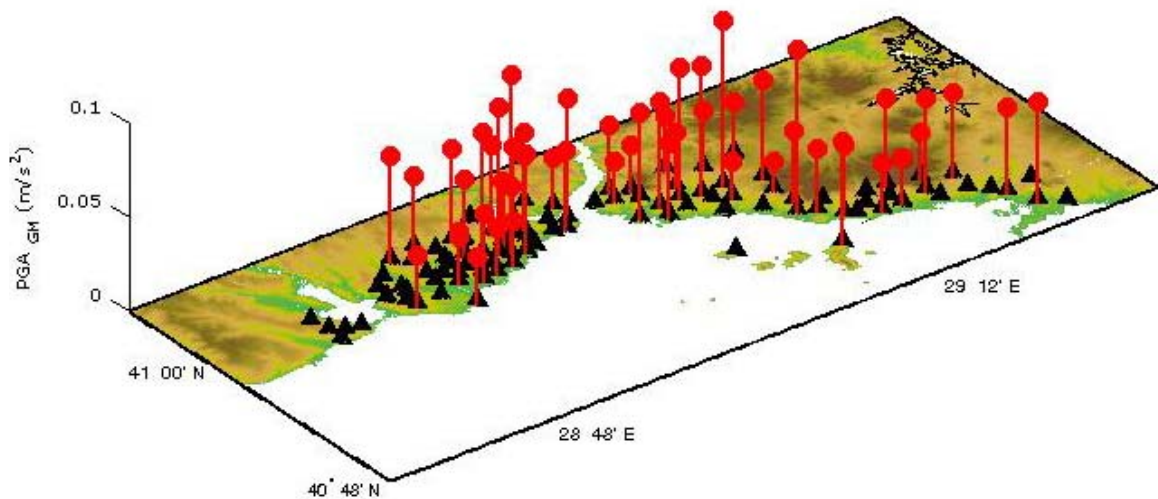


Figure 3.7. Peak ground accelerations for the geometric mean of the horizontal components at each Rapid Response System station triggered during the March 12, 2008 earthquake

3.2.1. Kriging Method

Kriging is a procedure for constructing a minimum error variance linear estimate at a location where the value is unknown. The method is optimal interpolation based on regression against observed data, weighted according to spatial covariance values.

All interpolation algorithms (inverse distance squared, spline, radial basis functions, triangulation, *etc.*) estimate the value at a given location as a weighted sum of data values at surrounding locations. Almost all assign weights according to functions that give a decreasing weight with increasing separation distance. Kriging assigns weights according to a (moderately) data-driven weighting function, rather than an arbitrary function (Bohling, 2005).

The basic form of the kriging estimator is

$$\mathbf{u}^*(\mathbf{x}) - \mu(\mathbf{x}) = \sum_{i=1}^n \lambda_i [\mathbf{u}(\mathbf{x}_i) - \mu(\mathbf{x}_i)] \quad (3.1)$$

where \mathbf{x} is the location vectors for estimation point, $\mu(\mathbf{x})$ is mean values of \mathbf{u} , n is the number of data points in local neighborhood used for the estimation of $\mathbf{u}^*(\mathbf{x})$, λ is the kriging weight assigned to datum $\mathbf{u}(\mathbf{x}_i)$ for estimation location \mathbf{x} .

Kriging estimates residual at \mathbf{u} as weighted sum of residuals at surrounding data points. Kriging weights, λ , are derived from covariance function or semivariogram, which should characterize residual component. Distinction between trend and residual somewhat arbitrary; varies with scale.

The goal is to determine weights, λ , that minimize the variance of the estimator

$$\sigma_E^2(\mathbf{x}) = \text{Var} \left\{ \mathbf{u}^*(\mathbf{x}) - \mathbf{u}(\mathbf{x}) \right\} \quad (3.2)$$

Under the unbiasedness constraint $E \left\{ \mathbf{u}^*(\mathbf{x}) - \mathbf{u}(\mathbf{x}) \right\} = 0$.

The random field (RF) $u(x)$ is decomposed into residual and trend components, $u(x) = R(x) + \mu(x)$, with the residual component treated as an RF with a stationary mean of zero and a stationary covariance (a function of lag, h , but not of position, x) as

$$\text{Cov}\{R(x), R(x+h)\} = E\{R(x)R(x+h)\} = C_R(h) \quad (3.3)$$

where $E\{R(x)\} = 0$. The residual covariance function is generally derived from the input semivariogram model, $C_R(h) = C_R(0) - w'(h)$. Thus the semivariogram feed to a kriging program should represent the residual component of the variable.

The three main kriging variants, simple, ordinary, and kriging with a trend, differ in their treatments of the trend component, $\mu(x)$.

For simple kriging, the trend component is a constant and known mean, $m(x) = m$, so that

$$u^*(x) = \mu + \sum_{i=1}^n \lambda_i [u(x_i) - \mu] \quad (3.4)$$

Using the rules for the variance of a linear combination of random variables the error variance is then given by

$$\sigma_E^2(x) = \sum_{i=1}^n \sum_{j=1}^n \lambda_i(x) \lambda_j(x) C_R(x_i - x_j) + C_R(0) - 2 \sum_{i=1}^n \lambda_i(x) C_R(x_i - x) \quad (3.5)$$

To minimize the error variance, the derivative of the above expression with respect to each of the kriging weights is taken and each derivative is set to zero. This leads to the following system of equations

$$\sum_{j=1}^n \lambda_j(x) C_R(x_i - x_j) = C_R(x_i - x) \quad (3.6)$$

where $i=1, \dots, n$.

Once the kriging weights are obtained, both the kriging estimate and the kriging variance are computed. The main controls on the kriging weights are closeness of the data to the location being estimated, redundancy between the data, and the variogram.

Simple kriging does not constrain the weights and works with residual from the mean. For ordinary kriging, rather than assuming that the mean is constant over the entire domain, the mean does not to be known, since ordinary kriging constrains the sum of weights to be equal to one. Kriging with a trend (the method formerly known as universal kriging) is much like ordinary kriging, except that instead of fitting just a local mean in the neighborhood of the estimation point, a linear or higher-order trend in the (x,y) coordinates of the data points is fitted.

3.2.2. Modified Kriging Method

In kriging, the weights are based not only on the distance between the measured points and the prediction location, but also on the overall spatial arrangement among the measured points and their values. To use the spatial arrangement in the weights, the spatial autocorrelation must be quantified. Hence, semivariogram depicts the spatial autocorrelation.

$$w'_i = \frac{(PGA_j - PGA_k)^2}{2} \quad (3.7)$$

In this study, a new formula is generated for the calculation of the weights to estimate the ground motion:

$$w_i = \sqrt{PGA_j \times PGA_k} \times d \quad (3.8)$$

where d is the distance between the stations j and k. The computation of the weights based on Equation (3.8) in terms of separation distance, demonstrated at the right column of Figure 3.8.

For the estimation of peak ground parameter at a point, minimum four observed data around this point are considered. The upper limit of the distance between the unknown point and the observed data will be 3 km, if the number of observed data supply the minimum data number. Otherwise, the separation distance between the stations can be increase. The selection of data is shown at the left column of Figure 3.8. The selected data is used to calculate the weights using Equation (3.8). Then, the weight values are grouped with respect to station separation distance with 0.1 km intervals to generate a regression curve fit. Gaussian, rational linear and rational quadratic fit and different exponential formula are applied to find the best fit with minimum error. The best fit catch with

$$w_i = a \times d^b \quad (3.9)$$

where a and b are the variables that varies for each estimated station/point. The weights and the curve fit for the estimation of PGA at station R01, recorded during September 29, 2003 earthquake are shown in Figure 3.8, exemplarily.

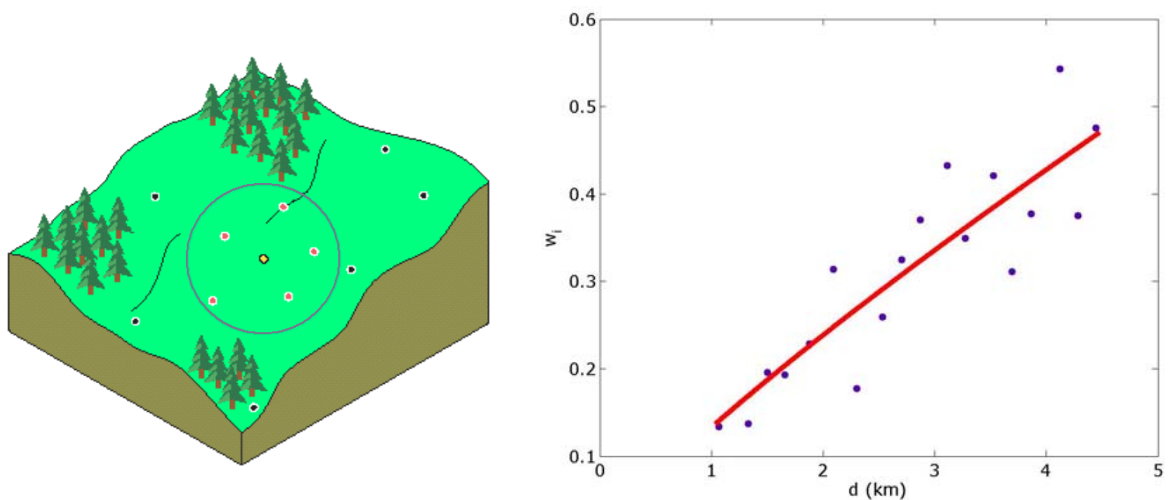


Figure 3.8. Selection of the observed data to predict PGA at unknown point (left) and diagram for the calculation of the weights w.r.t. Equation (3.8) (right)

Then, a mathematical expression is developed to compute PGA using a number of observed PGA including the effect of the weights of each observed data to the estimated station:

$$PGA^{est} = \frac{1}{\sqrt[n]{\prod_{i=1}^n PGA_i^{obs}}} \prod_{i=1}^n \left(\frac{w_i}{d_i} \right)^{\frac{2}{n}} \quad (3.10)$$

where PGA^{est} is the estimated peak ground acceleration, PGA^{obs} is the observed peak ground acceleration, n is the number of observed data used to obtain estimated peak ground acceleration, w_i is the weight of the observed data at i^{th} station, calculated by Equation (3.9), and d_i is the separation distance between the observed and estimated data.

The configuration of the relation between the observed and the estimated PGA is shown in Figure 3.9.

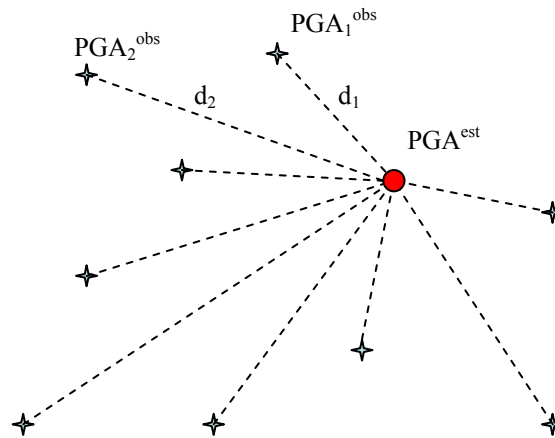


Figure 3.9. Configuration of the estimated data and surrounding observed data

The proposed method for the estimation of ground motion parameters is outlined in Figure 3.10.

In the following section, the developed method is used to compute PGA for each station using the data recorded during the seven earthquakes described before. Estimated values are compared with the observed data for each IERRS station. After this section, the method is used to generate PGA for phantom stations that have no observe value.

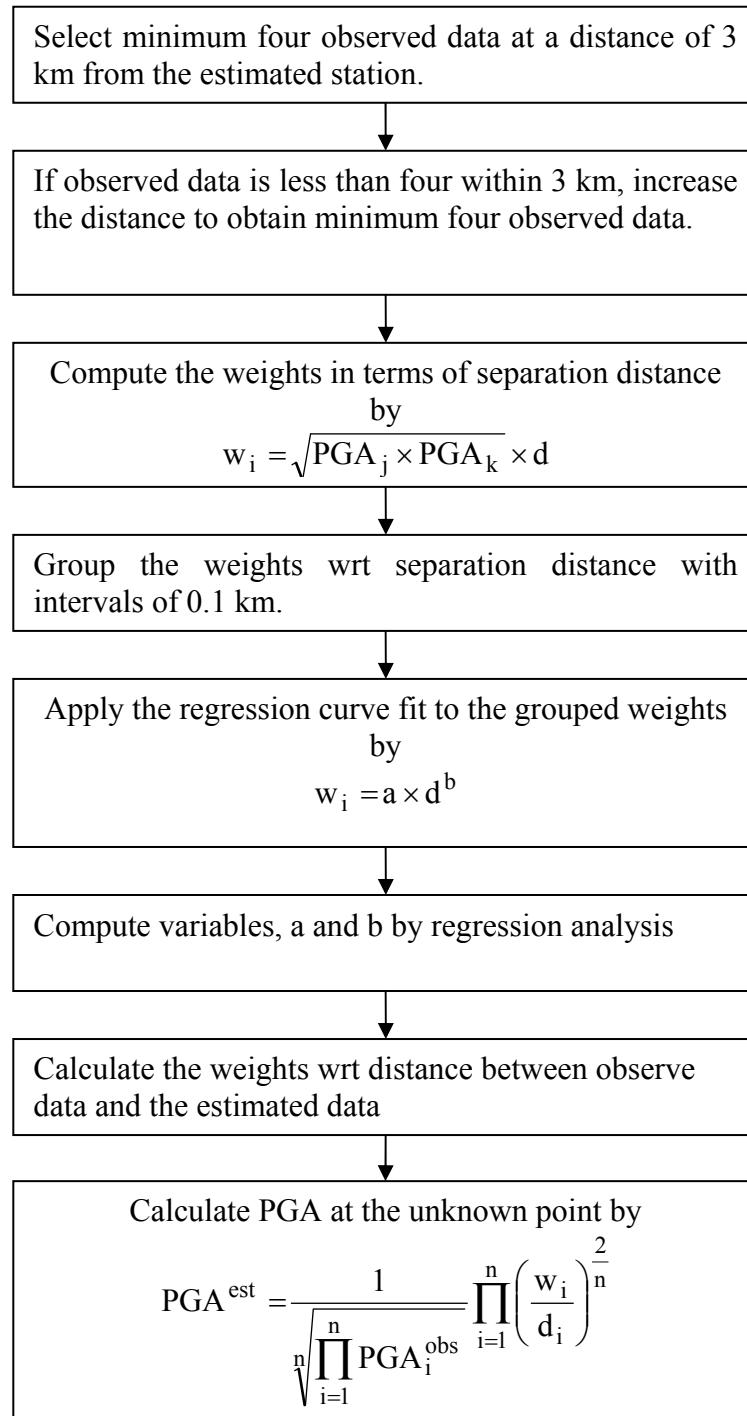


Figure 3.10. Procedure of the modified kriging method

3.2.3. Comparison of Results with the Values Obtained from Attenuation Relationships

The peak ground motion parameter, PGA, is estimated for each IERRS station that has triggered data from each earthquake, using the method outlined in Figure 3.10. The estimation is done for four cases: using observed PGA with no site and distance correction, using observed PGA corrected w.r.t. distance, using observed PGA corrected w.r.t. site class, and using observed PGA corrected w.r.t. distance and site class. The residuals between the estimated PGA and observed PGA for four cases for each earthquake are plotted in Figure 3.11 to Figure 3.17. The residuals for the September 19, 2003 earthquake vary between ± 0.1 . The residuals for the case of PGA corrected w.r.t. site class are smaller than the residual for the other cases.

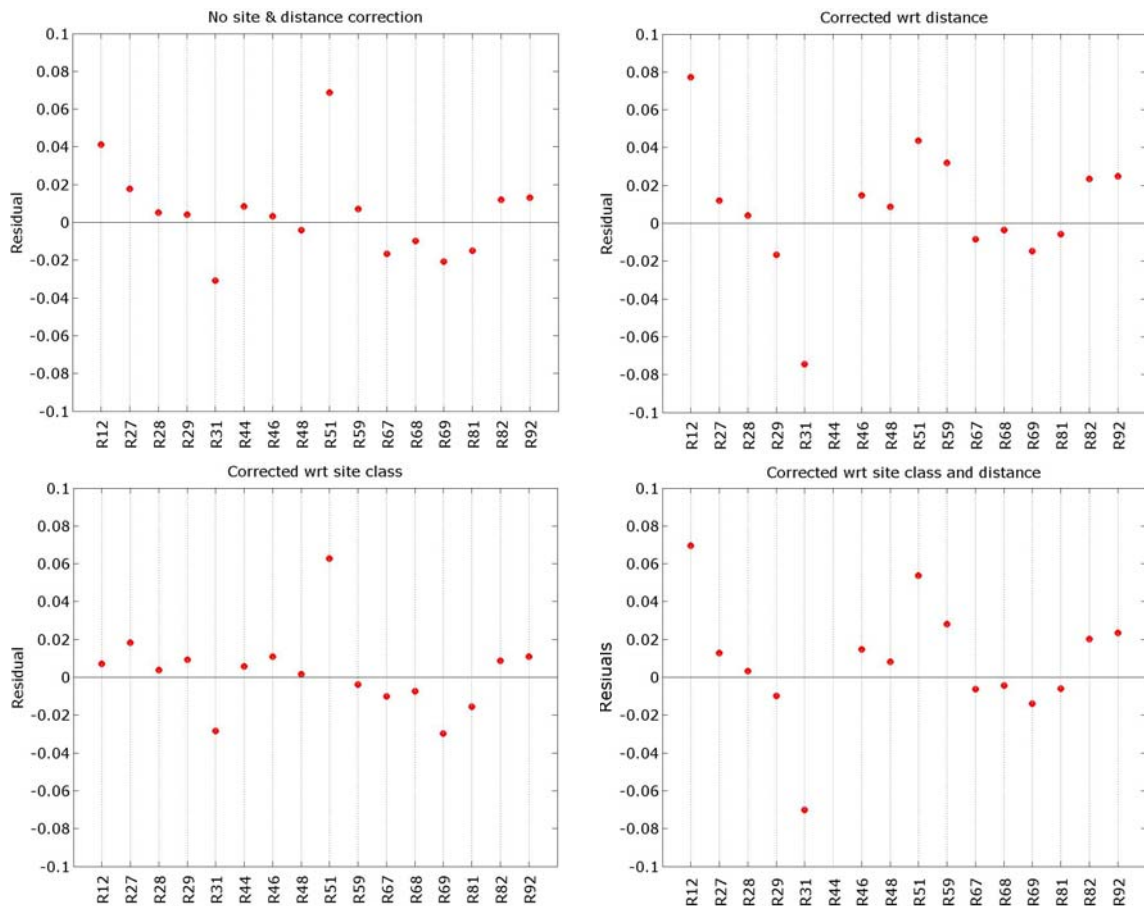


Figure 3.11. Residuals (y-axis) between the observed and estimated data at each Rapid Response System station (x-axis) triggered during the September 19, 2003 earthquake

The proposed method is used to compute PGA at the stations that have observed data recorded during the May 16, 2004 earthquake. The residual at 72 stations are in range of -0.25 and +0.25. There is no significant difference between the residuals computed considering whether site and/or distance correction.

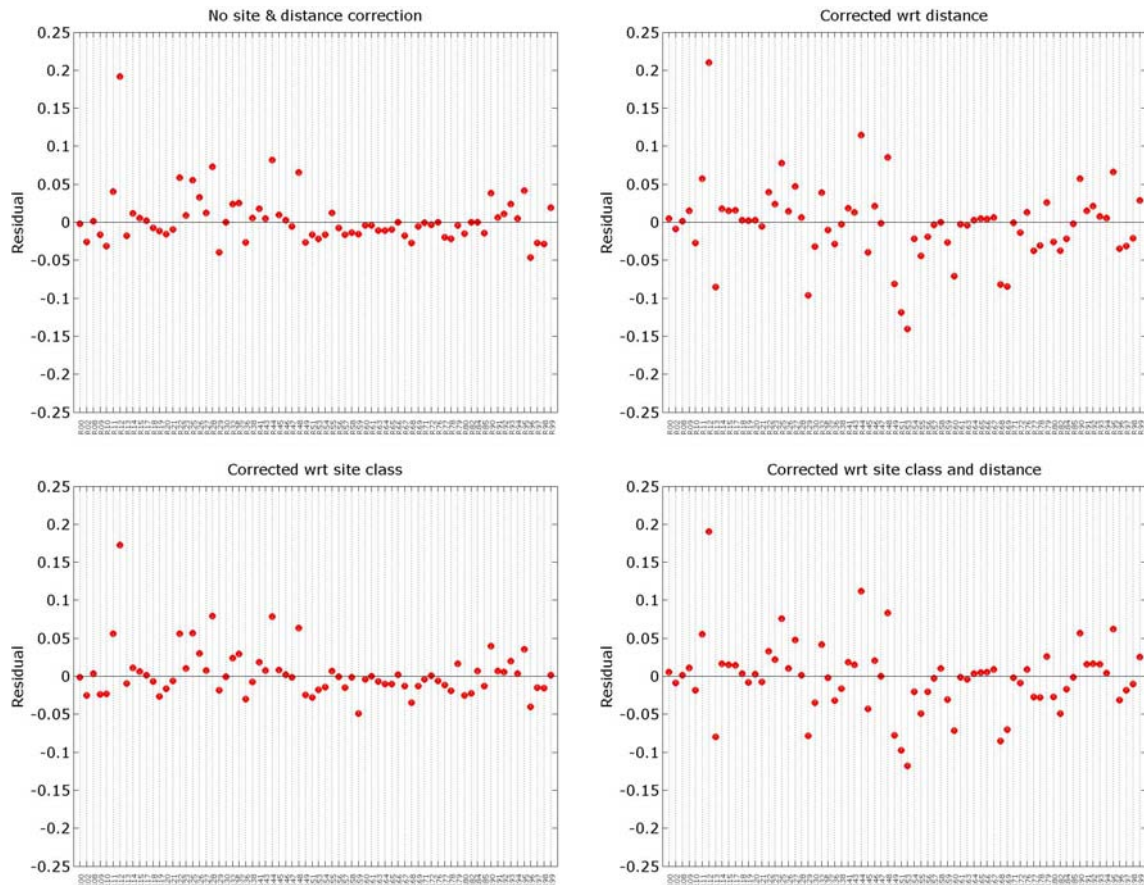


Figure 3.12. Residuals (y-axis) between the observed and estimated data at each Rapid Response System station (x-axis) triggered during the May 16, 2004 earthquake

The residuals between the observed and estimated data at each Rapid Response System station triggered during the June 24, 2004 earthquake shown in Figure 3.13. As it is seen that the results from the case of without site class and distance correction, and from the case of correction with site class, show minimalist and similar values.

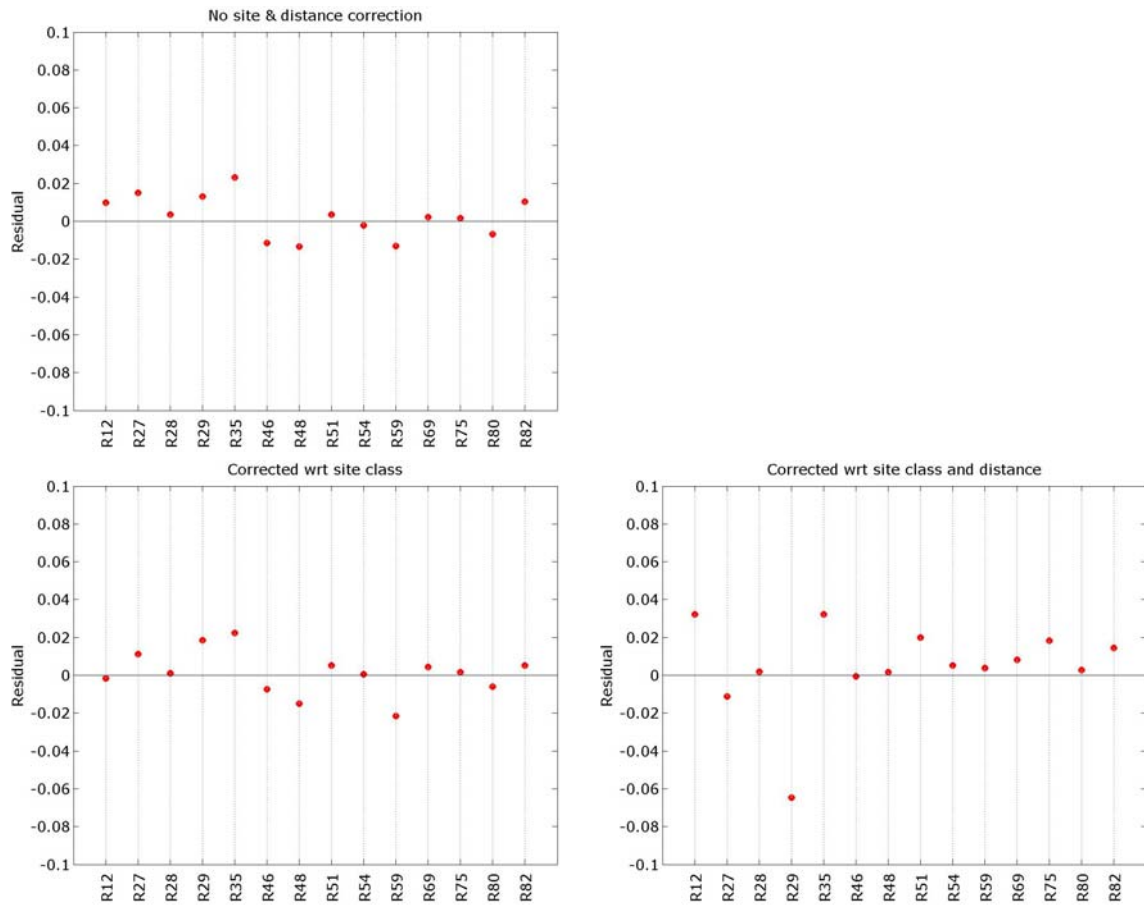


Figure 3.13. Residuals (y-axis) between the observed and estimated data at each Rapid Response System station (x-axis) triggered during the June 24, 2004 earthquake

In Figure 3.14, the differences between the estimated and observed PGA have almost common quantities for each case for the September 29, 2004 earthquake. The reason for the highest residual in Figure 3.14 can be explained with the lack observed data of nearest the estimated station.

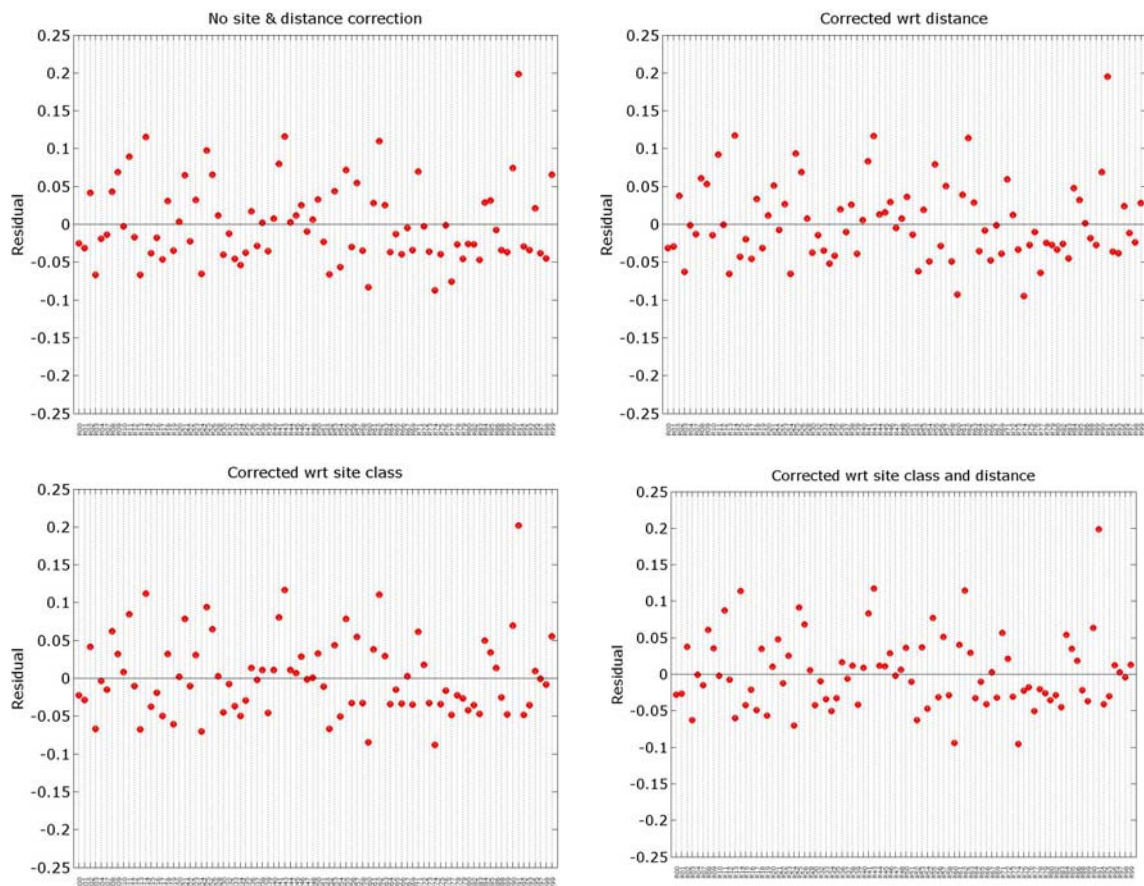


Figure 3.14. Residuals (y-axis) between the observed and estimated data at each Rapid Response System station (x-axis) triggered during the September 29, 2004 earthquake

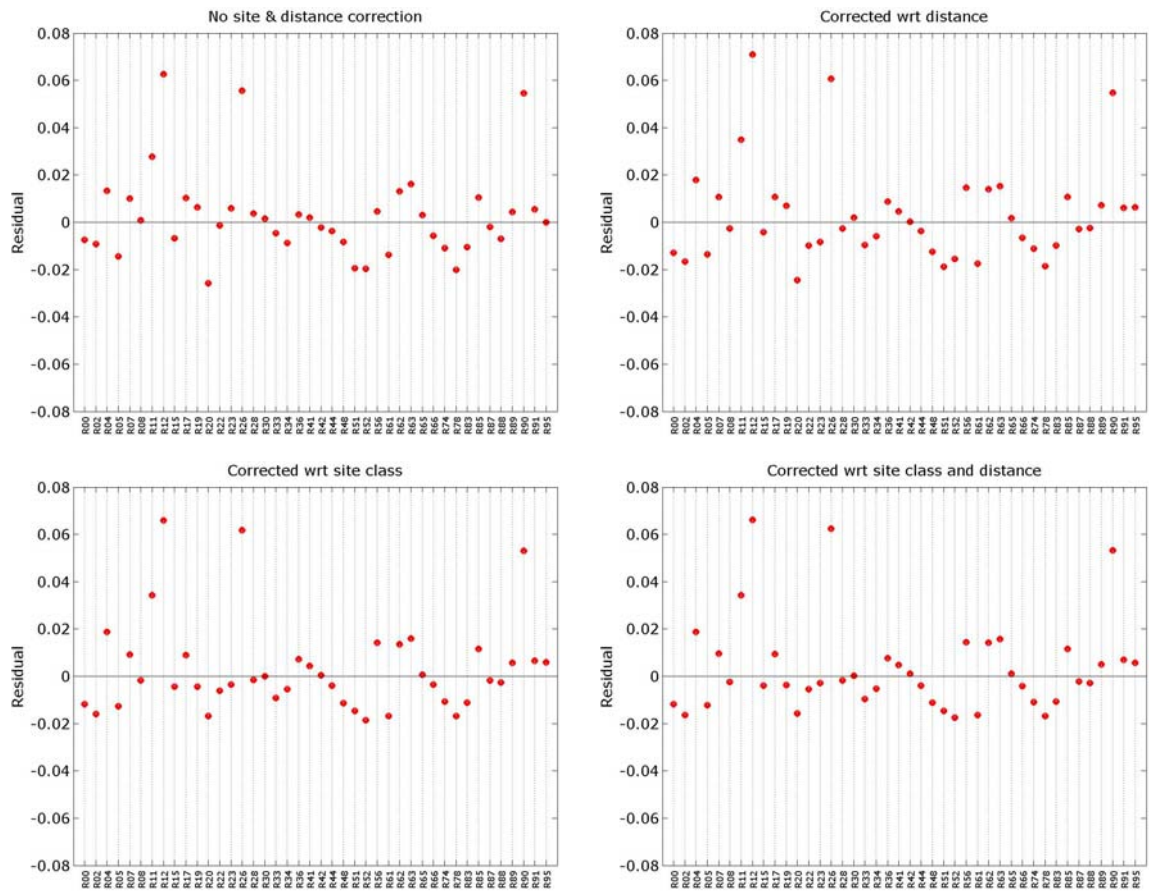


Figure 3.15. Residuals (y-axis) between the observed and estimated data at each Rapid Response System station (x-axis) triggered during the October 10, 2006 earthquake

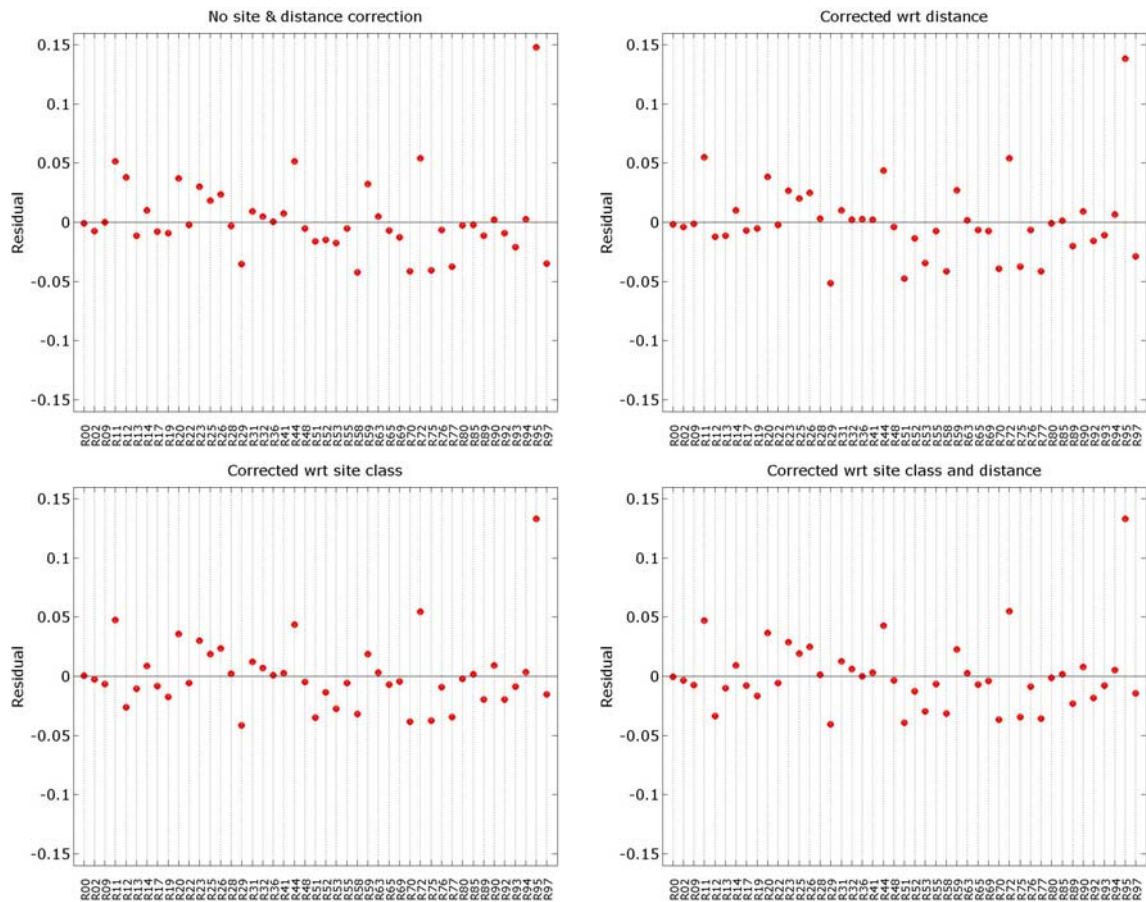


Figure 3.16. Residuals (y-axis) between the observed and estimated data at each Rapid Response System station (x-axis) triggered during the October 24, 2006 earthquake

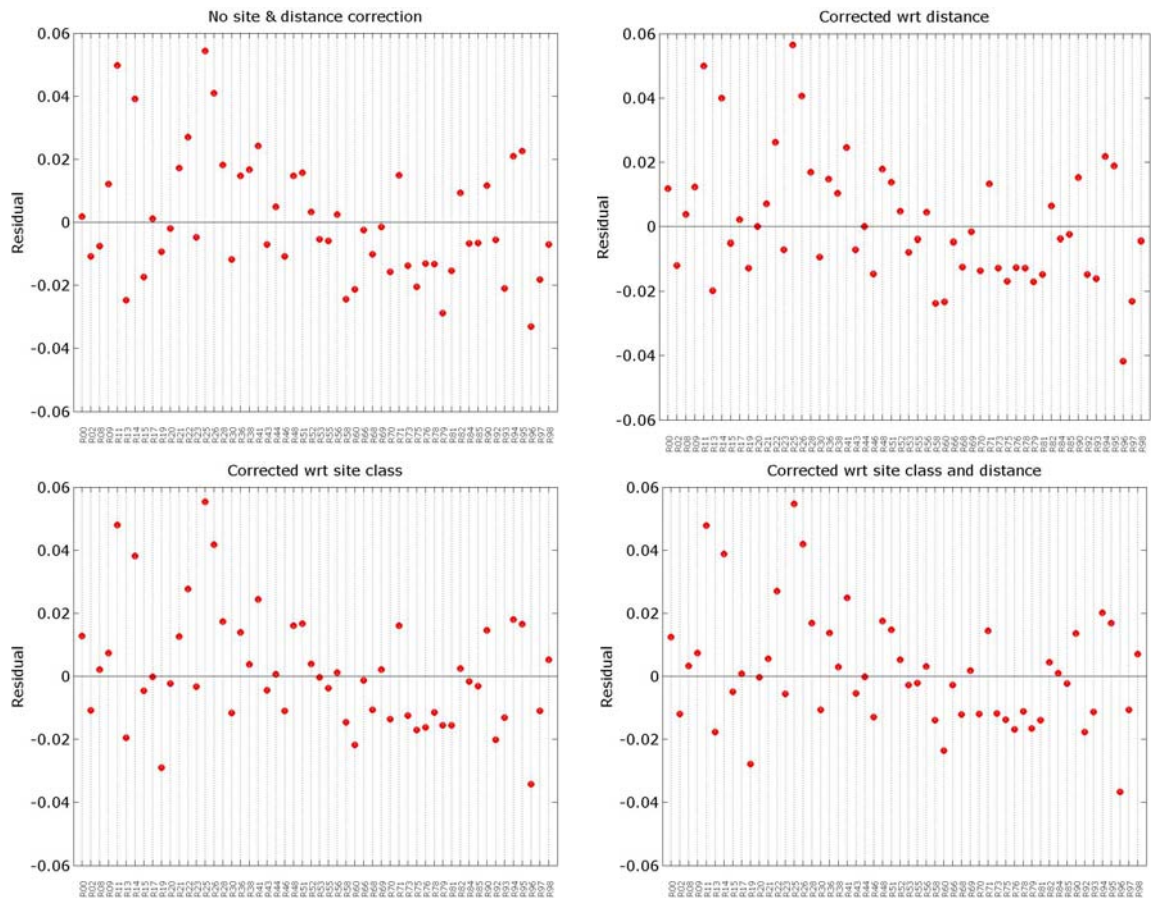


Figure 3.17. Residuals (y-axis) between the observed and estimated data at each Rapid Response System station (x-axis) triggered during the March 12, 2008 earthquake

The residual between the observed and the estimated data for each earthquake are shown in Figure 3.11 to Figure 3.17. The residuals slightly differ from one case to another case for each earthquake. The correction with respect to distance may not be effective, because the epicenters are far away from the stations. The residuals based on the data corrected with respect to site class also do not change, extremely. All in all, the correction with respect to site class and/or distance does not affect the results. Hereafter, PGA values without site class and distance correction is considered for the application of the proposed method. Henceforth, the estimated and observed values are compared with the values generated by Akkar and Bommer (2007) equations for each Rapid Response station considering the properties of each earthquake. Also, geometric standard deviations of the estimated values are included to the comparison. The geometric standard deviation is calculated by

$$\sigma_g = e^{\sqrt{\frac{\sum_{i=1}^n [\ln(\text{PGA}_i) - \ln(\mu_g)]^2}{n}}} \quad (3.11)$$

where μ_g is the geometric mean.

The comparison of the estimated PGA considering $\pm \sigma_g$, the observed PGA, and PGA from Akkar and Bommer (2007) relationship are shown in Figure 3.18 to Figure 3.24. The blue circles are PGA calculated by Akkar and Bommer (2007) equation, red circles are the observed PGA, short black lines are PGA computed by Equation (3.10) proposed in this study, and shaded yellow regions are the geometric standard deviations for the estimated PGA. Akkar and Bommer (2007) equation gives extremely high results for the earthquakes with small magnitude. The reason is that the equation generated from the earthquakes with magnitudes ranging from 5.0 to 7.6. Generally, the results obtained by the proposed method are in good agreement with the observed values.

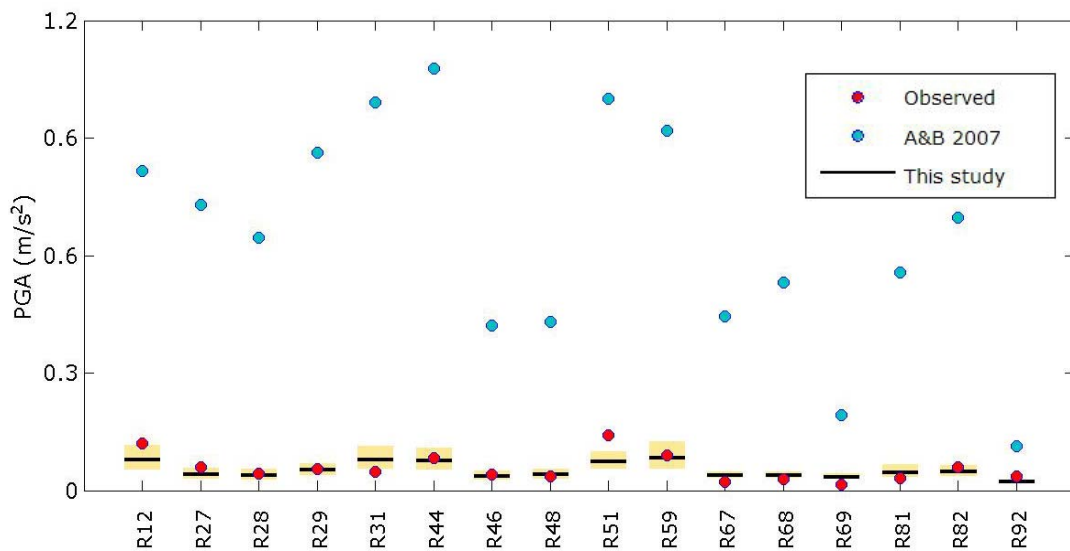


Figure 3.18. Comparison of PGA of the observed data (red circles) with PGA obtained by this study (short black lines) and PGA obtained by Akkar and Bommer (2007) attenuation relationship (blue circles) at each Rapid Response System station (x-axis) triggered during the September 19, 2003 earthquake. The shaded yellow regions for each Rapid Response System station are the \pm one geometric standard deviations of the data based on this study

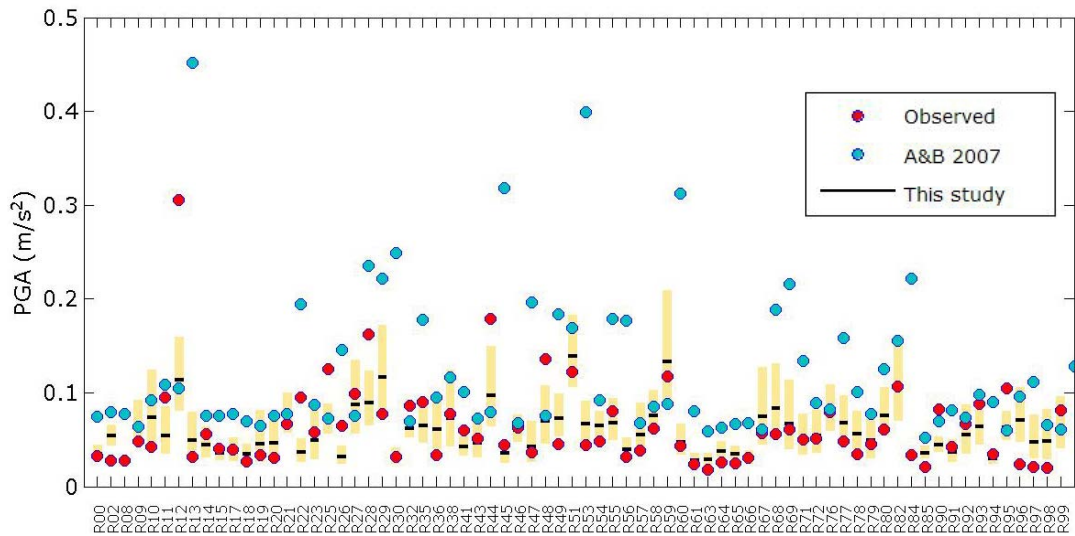


Figure 3.19. Comparison of PGA of the observed data (red circles) with PGA obtained by this study (short black lines) and PGA obtained by Akkar and Bommer (2007) attenuation relationship (blue circles) at each Rapid Response System station (x-axis) triggered during the May 16, 2004 earthquake. The shaded yellow regions for each Rapid Response System station are the \pm one geometric standard deviations of the data based on this study

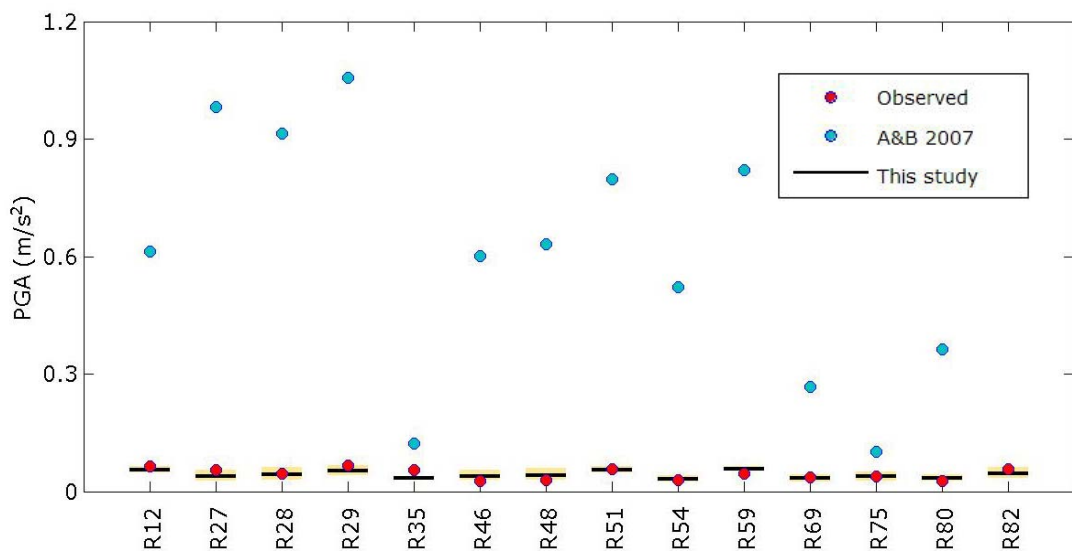


Figure 3.20. Comparison of PGA of the observed data (red circles) with PGA obtained by this study (short black lines) and PGA obtained by Akkar and Bommer (2007) attenuation relationship (blue circles) at each Rapid Response System station (x-axis) triggered during the June 24, 2004 earthquake. The shaded yellow regions for each Rapid Response System station are the \pm one geometric standard deviations of the data based on this study

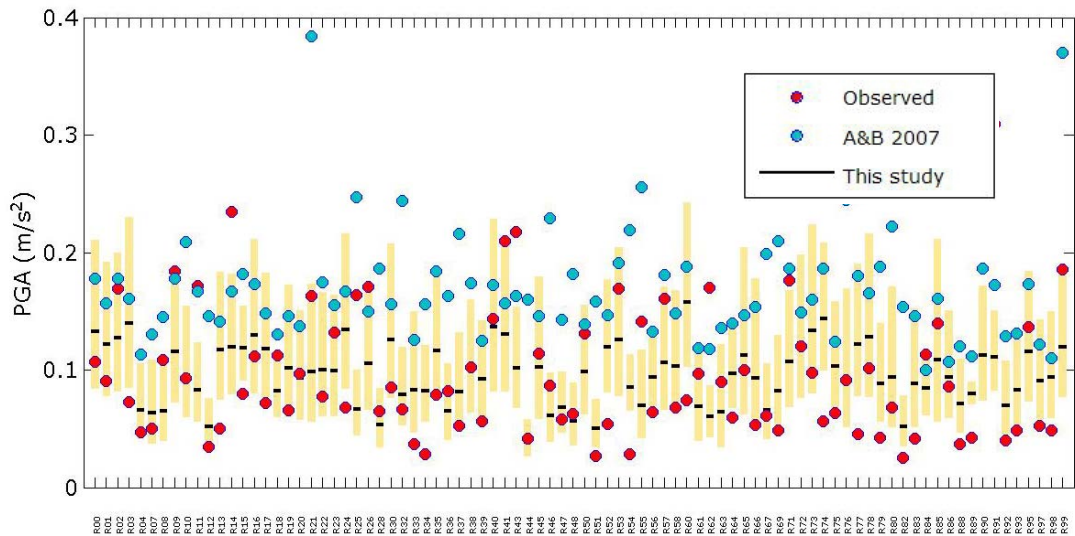


Figure 3.21. Comparison of PGA of the observed data (red circles) with PGA obtained by this study (short black lines) and PGA obtained by Akkar and Bommer (2007) attenuation relationship (blue circles) at each Rapid Response System station (x-axis) triggered during the September 29, 2004 earthquake. The shaded yellow regions for each Rapid Response System station are the \pm one geometric standard deviations of the data based on this study

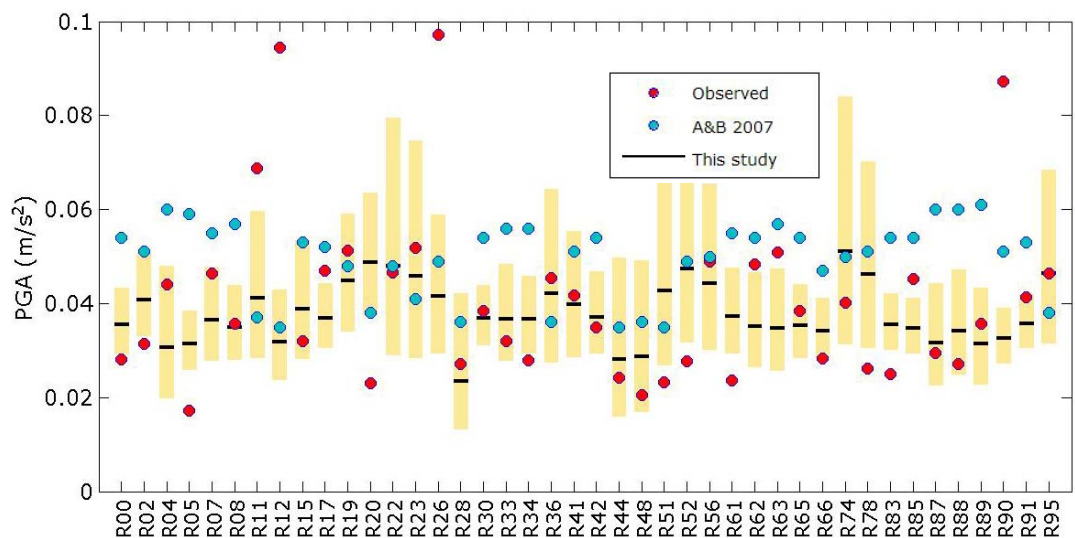


Figure 3.22. Comparison of PGA of the observed data (red circles) with PGA obtained by this study (short black lines) and PGA obtained by Akkar and Bommer (2007) attenuation relationship (blue circles) at each Rapid Response System station (x-axis) triggered during the October 20, 2006 earthquake. The shaded yellow regions for each Rapid Response System station are the \pm one geometric standard deviations of the data based on this study

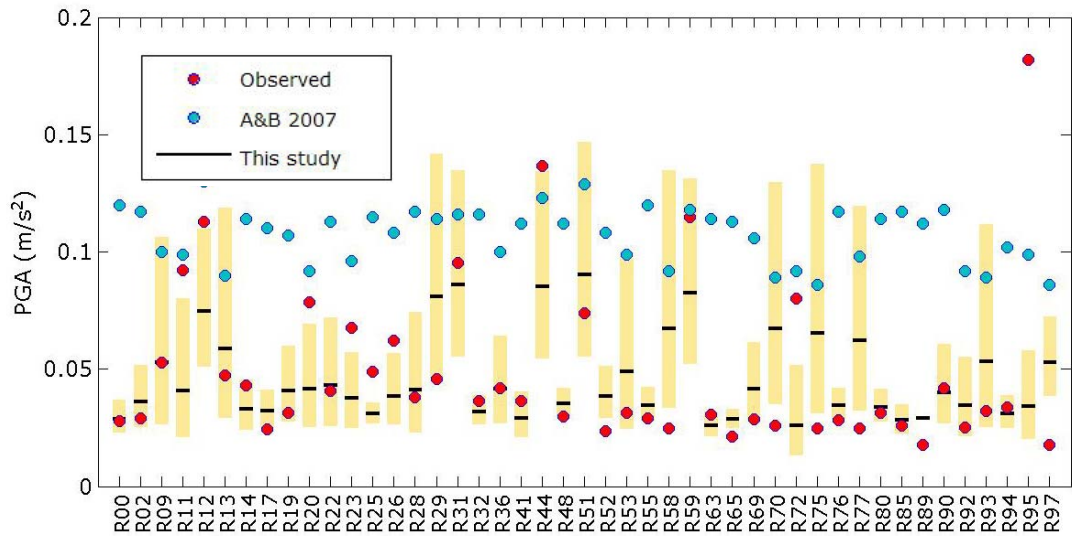


Figure 3.23. Comparison of PGA of the observed data (red circles) with PGA obtained by this study (short black lines) and PGA obtained by Akkar and Bommer (2007) attenuation relationship (blue circles) at each Rapid Response System station (x-axis) triggered during the October 24, 2006 earthquake. The shaded yellow regions for each Rapid Response System station are the \pm one geometric standard deviations of the data based on this study

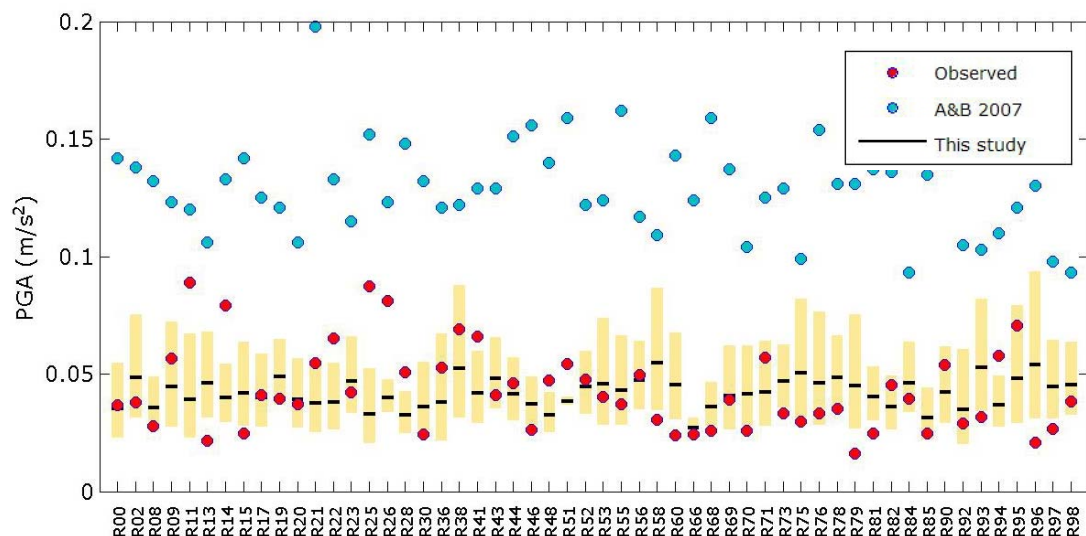


Figure 3.24. Comparison of PGA of the observed data (red circles) with PGA obtained by this study (short black lines) and PGA obtained by Akkar and Bommer (2007) attenuation relationship (blue circles) at each Rapid Response System station (x-axis) triggered during the March 12, 2008 earthquake. The shaded yellow regions for each Rapid Response System station are the \pm one geometric standard deviations of the data based on this study

3.2.4. Comparison of Results and the Values Obtained from Spline Interpolation

The proposed method is used to compute PGA at the phantom stations shown in Figure 3.25. The computed PGA values are compared with the values computed by RRMap (Rapid Response Mapping Application) software based on the spline interpolation.

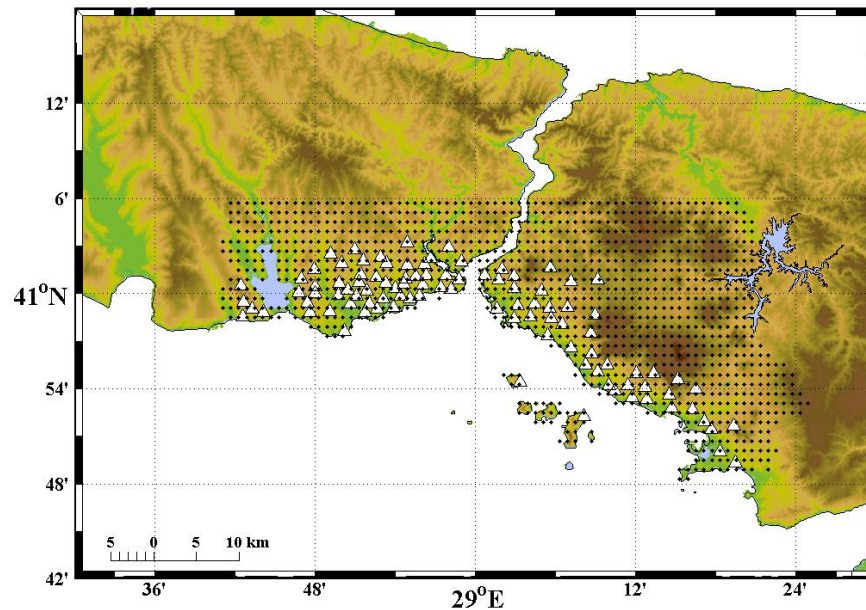


Figure 3.25. Configuration of the phantom stations

The comparisons of the results for each earthquake are represented in Figure 3.26 to Figure 3.32. Black stars are the observed data, red circles are PGA from this study, and blue circles are PGA from RRMap software. The results are shown in longitudinal point of view and in units of g. The results from the proposed method are in good agreement with the observed PGA values. Especially, for the smallest PGA values, the results are much compatible with the observed ones than PGA generated by RRMap.

As a result, the method can be reliably used for the estimation of peak ground motion parameters at the gaps where the observed data is less.

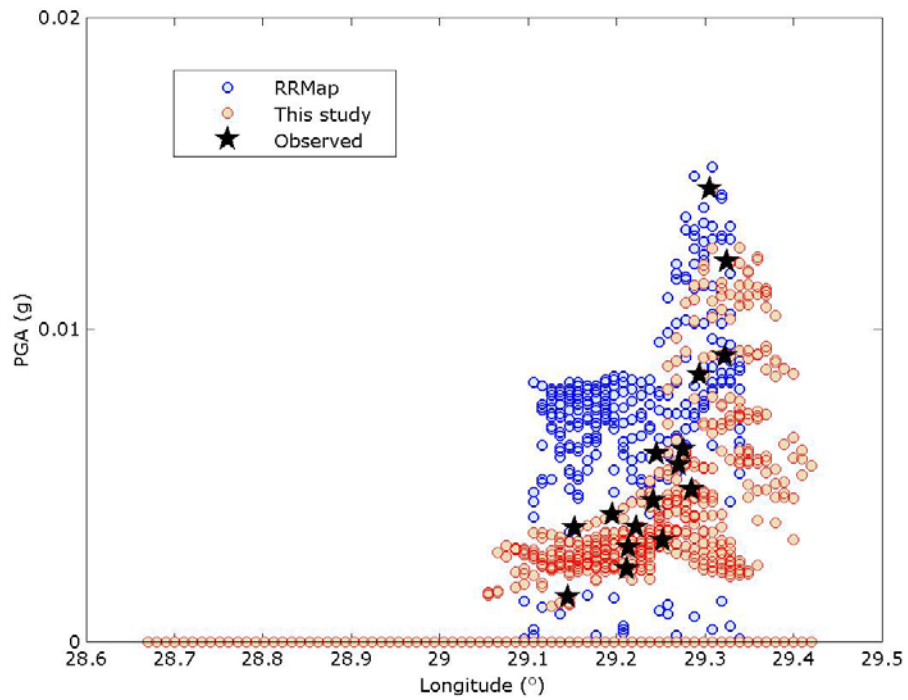


Figure 3.26. Comparison of PGA of the observed data (black stars) with PGA obtained by this study (pink circles) and PGA obtained by RRMap software (blue circles) at each phantom station using the data triggered during the September 19, 2003 earthquake

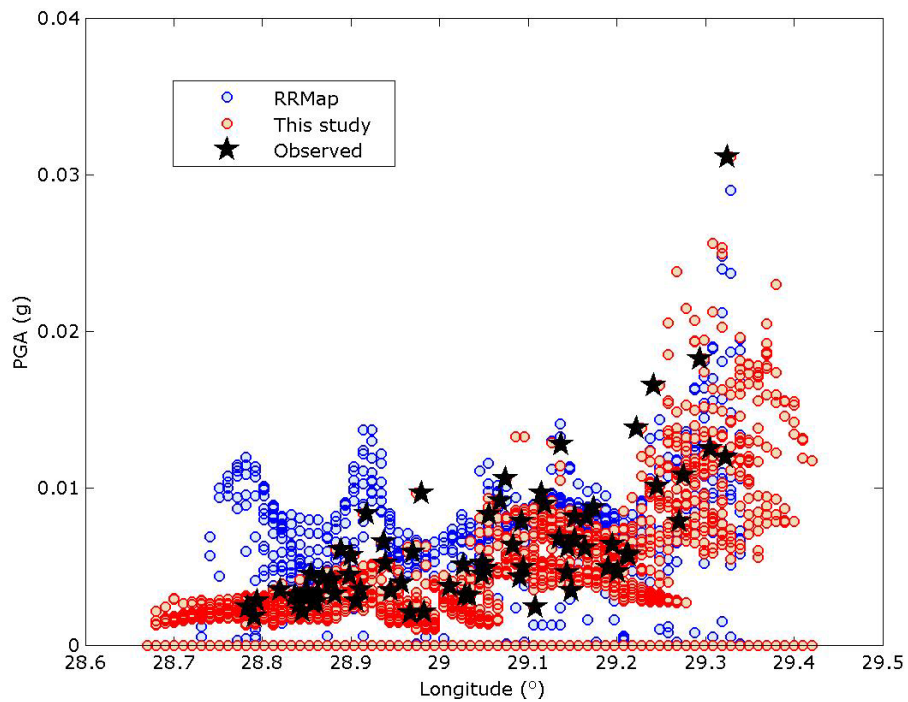


Figure 3.27. Comparison of PGA of the observed data (black stars) with PGA obtained by this study (pink circles) and PGA obtained by RRMap software (blue circles) at each phantom station using the data triggered during the May 16, 2004 earthquake

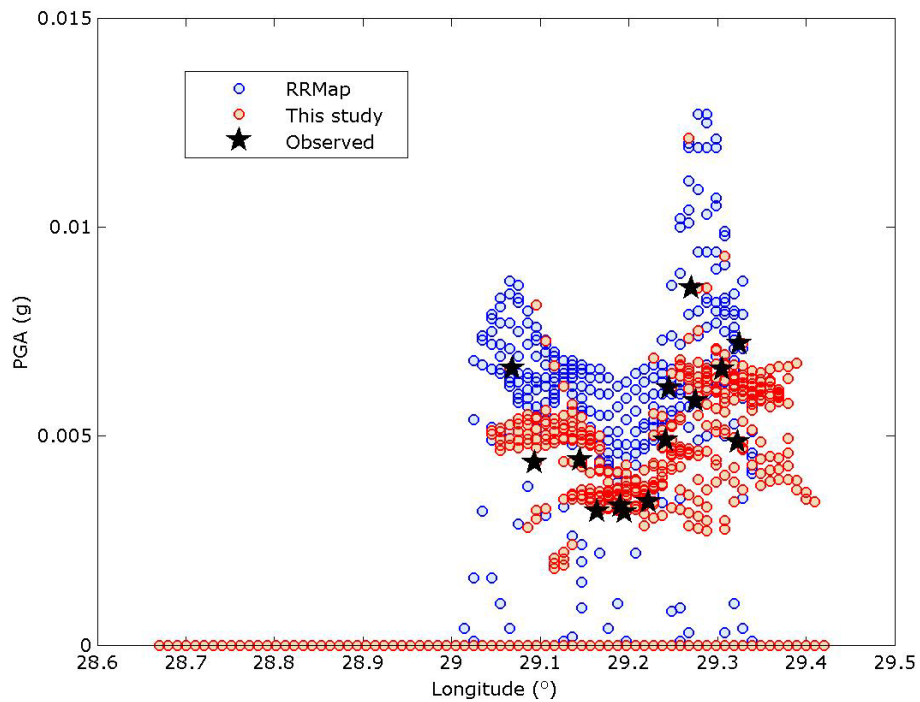


Figure 3.28. Comparison of PGA of the observed data (black stars) with PGA obtained by this study (pink circles) and PGA obtained by RRMap software (blue circles) at each phantom station using the data triggered during the June 24, 2004 earthquake

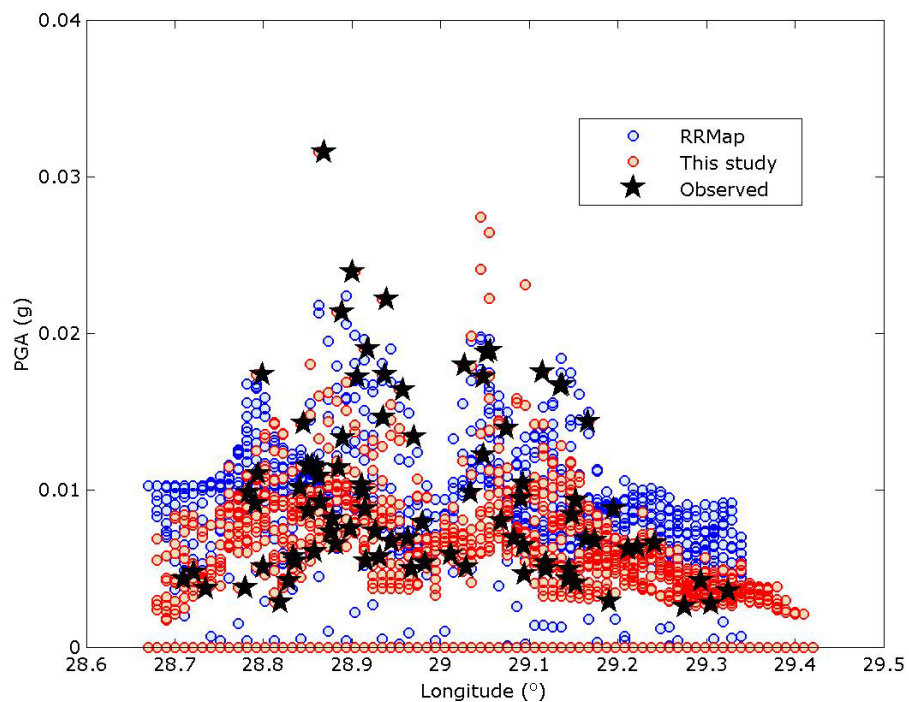


Figure 3.29. Comparison of PGA of the observed data (black stars) with PGA obtained by this study (pink circles) and PGA obtained by RRMap software (blue circles) at each phantom station using the data triggered during the September 29, 2004 earthquake

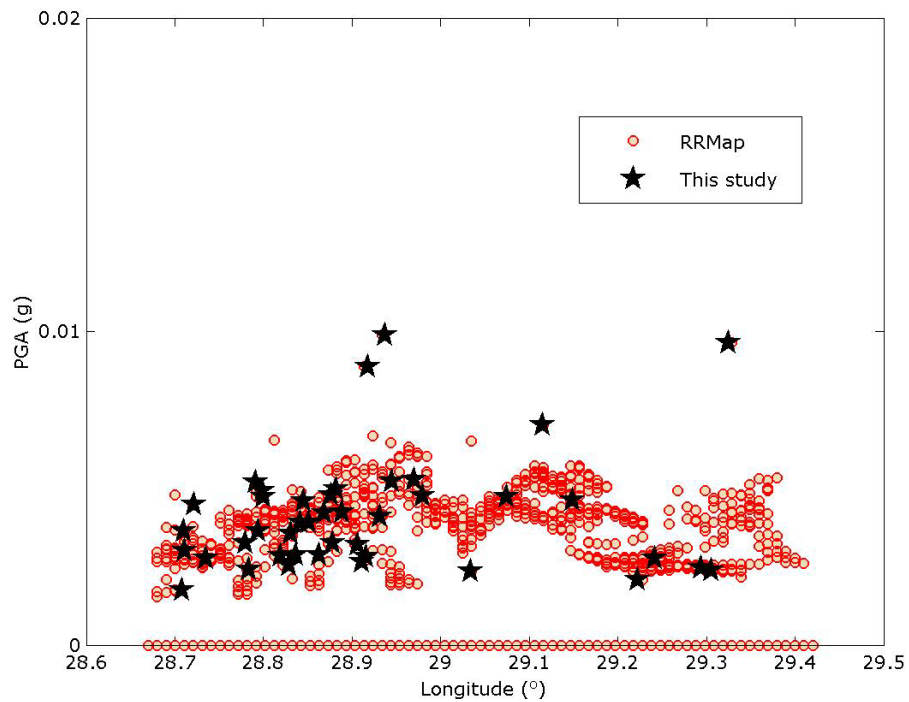


Figure 3.30. Comparison of PGA of the observed data (black stars) with PGA obtained by this study (pink circles) at each phantom station using the data triggered during the October 20, 2006 earthquake

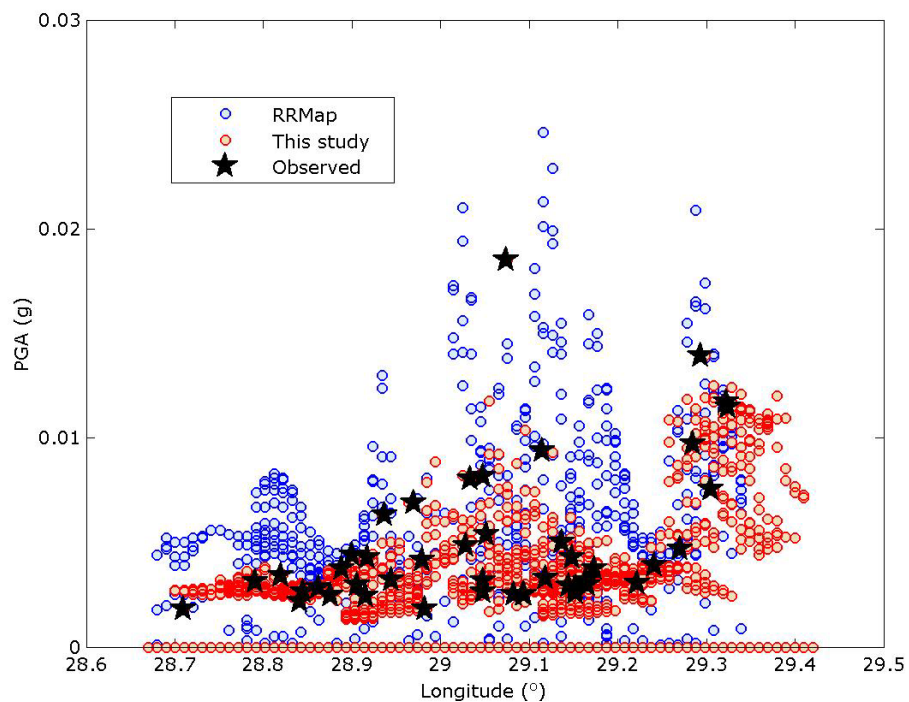


Figure 3.31. Comparison of PGA of the observed data (black stars) with PGA obtained by this study (pink circles) and PGA obtained by RRMap software (blue circles) at each phantom station using the data triggered during the October 24, 2006 earthquake

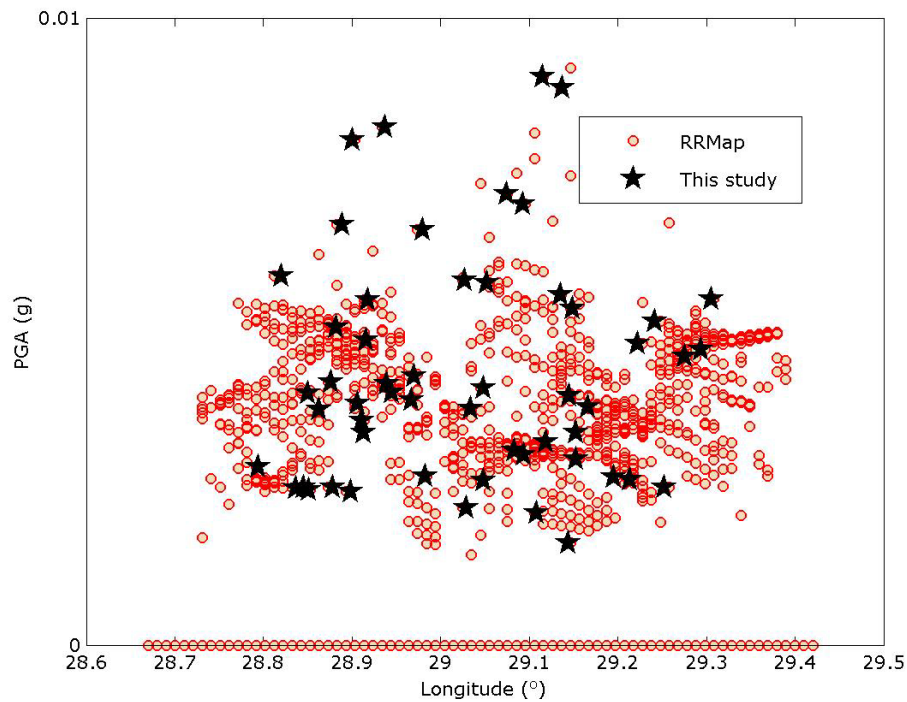


Figure 3.32. Comparison of PGA of the observed data (black stars) with PGA obtained by this study (pink circles) at each phantom station using the data triggered during the March 12, 2008 earthquake

Hereafter, PGA computed by modified kriging method, by RRMap, and by Akkar and Bommer (2007) attenuation relationship at phantom stations are compared. Region based comparisons are shown in Figure 3.33 to Figure 3.39 for seven earthquakes.

The results from this study and from RRMap are in good agreement with each other for the September 19, 2003 earthquake in Figure 3.33. The results from the attenuation relationship are extremely high, because of the limitation of the equations, as discussed before. PGA computed by the proposed method decreases at the European region for the May 16, 2004 earthquake in Figure 3.34.

Consequently, the proposed method is compatible with RRMap using spline interpolation method, especially for the higher values of PGA.

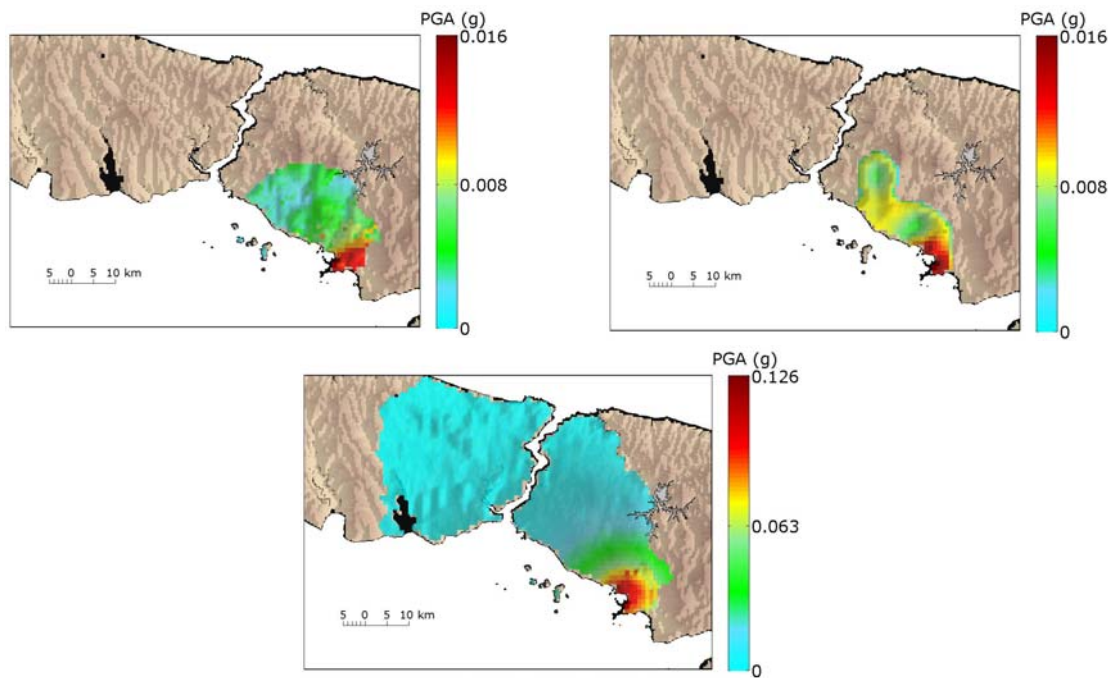


Figure 3.33. Distribution of PGA obtained by this study (left), by RRMap software (right), and by Akkar and Bommer (2007) attenuation relationship (center) at each phantom station using the data triggered during the September 19, 2003 earthquake

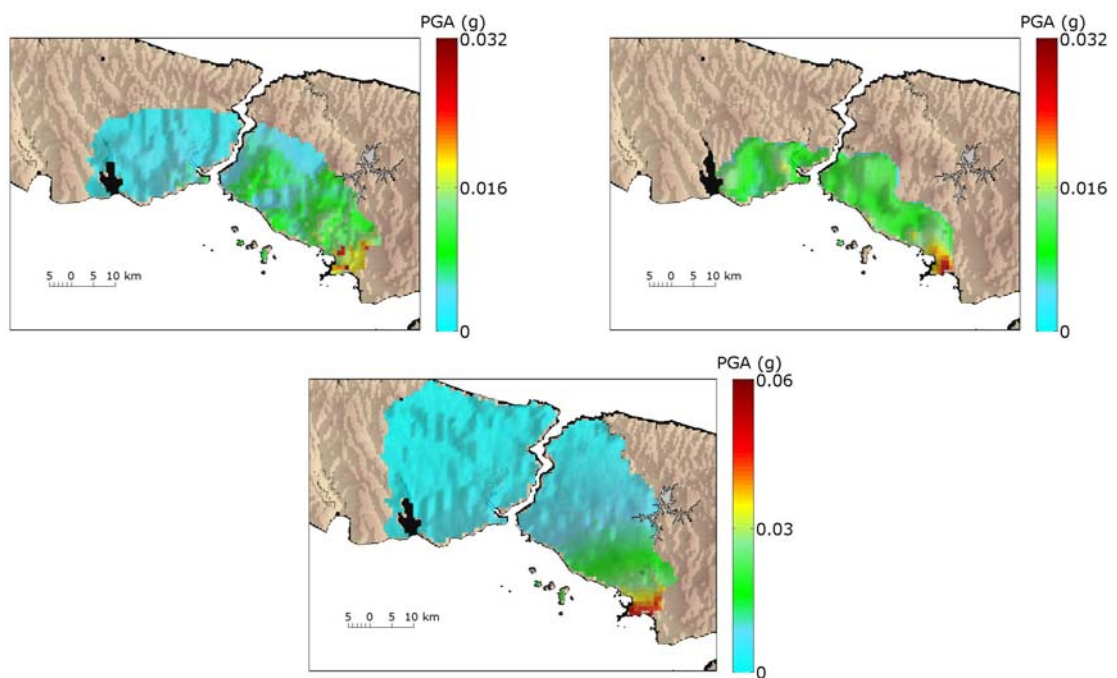


Figure 3.34. Distribution of PGA obtained by this study (left), by RRMap software (right), and by Akkar and Bommer (2007) attenuation relationship (center) at each phantom station using the data triggered during the May 16, 2004 earthquake

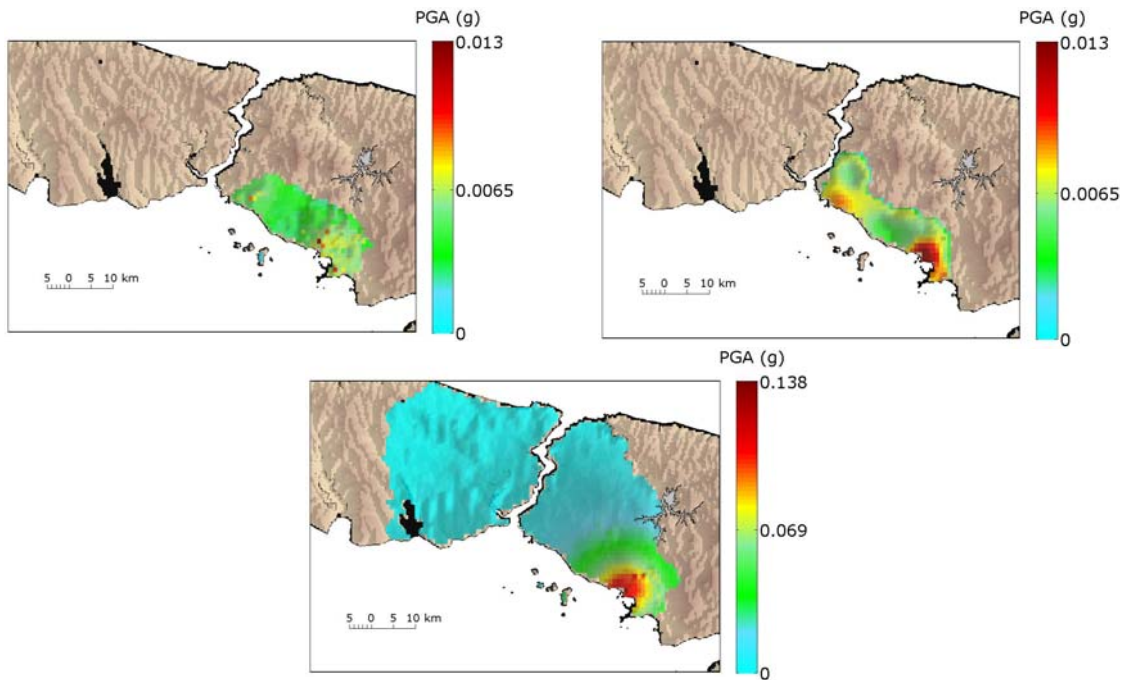


Figure 3.35. Distribution of PGA obtained by this study (left), by RRMap software (right), and by Akkar and Bommer (2007) attenuation relationship (center) at each phantom station using the data triggered during the June 24, 2004 earthquake

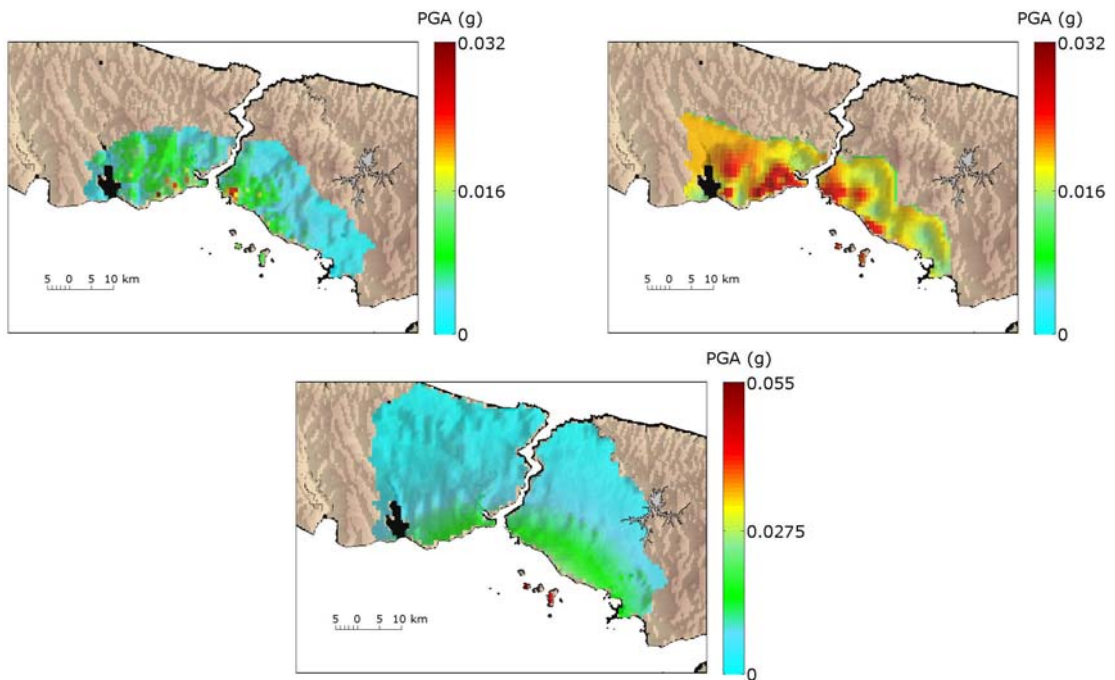


Figure 3.36. Distribution of PGA obtained by this study (left), by RRMap software (right), and by Akkar and Bommer (2007) attenuation relationship (center) at each phantom station using the data triggered during the September 29, 2004 earthquake

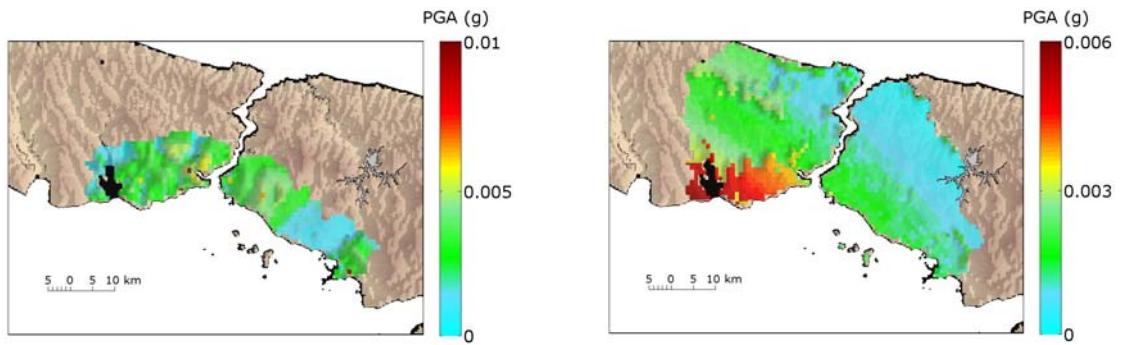


Figure 3.37. Distribution of PGA obtained by this study (left) and by Akkar and Bommer (2007) attenuation relationship (right) at each phantom station using the data triggered during the October 20, 2006 earthquake

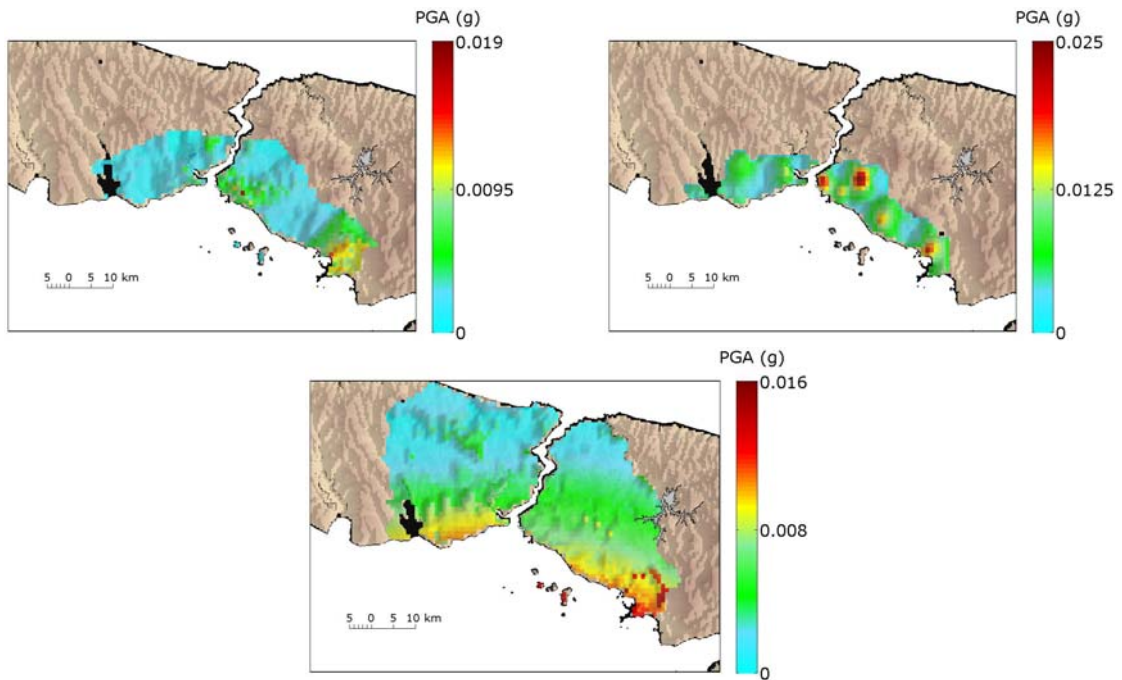


Figure 3.38. Distribution of PGA obtained by this study (left), by RRMap software (right), and by Akkar and Bommer (2007) attenuation relationship (center) at each phantom station using the data triggered during the October 24, 2006 earthquake

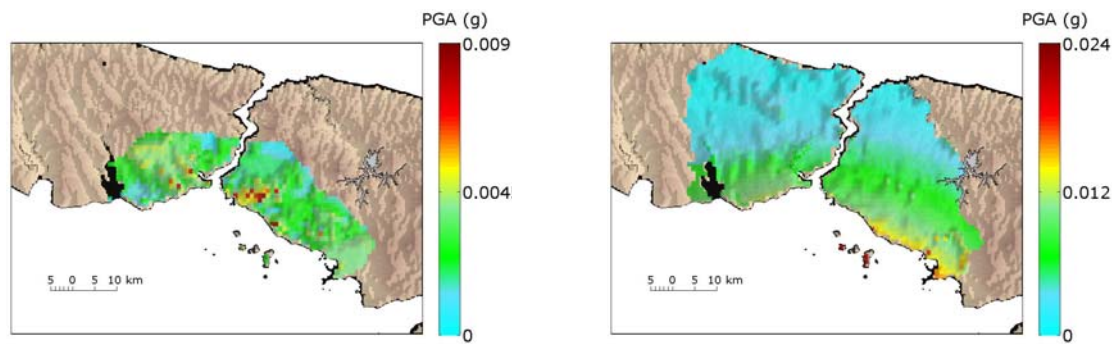


Figure 3.39. Distribution of PGA obtained by this study (left) and by Akkar and Bommer (2007) attenuation relationship (right) at each phantom station using the data triggered during the March 12, 2008 earthquake

3.3. Statistical Spatial Variability of Ground Motion

The spatial variance that remains after estimated effects of site conditions and attenuation have been accounted for constitutes a major ingredient of estimation uncertainty for the ground motion. This uncertainty also needs to be reflected in the code requirements and ShakeMaps. Abrahamson (1988) studied the relationship between the intra-event variation of peak ground acceleration (PGA) and earthquake magnitude. The standard error of PGA based on a log-normal distribution is estimated for each of the 25 events. In Abrahamson (1988), regression of the standard error of the largest horizontal and average horizontal accelerations versus earthquake magnitude showed that the standard errors decrease as magnitude increases. Kawakami and Mogi (2003) analyzed the spatial intra-event variability of PGA's as a function of separation distance. They found that the means and standard deviations of PGA's had an almost linear relationship with the logarithm of the station separation distances ranging from several meters to 100 km. The study of Field *et al.* (1997) addresses the variability of pseudo-velocity response spectra. Evans *et al.* (2003) repeated the analysis by using pseudo-spectral velocity (PSV) response spectra as a function of inter-station distance. They obtained that the sub-kilometer station spacing may be required to map shaking strength substantially more precisely than to the uncertainty of attenuation relations.

Herein, the spatial variation of earthquake strong-ground motion in Istanbul from seven earthquakes recorded by the Istanbul Earthquake Rapid Response and Early

Warning System (IERREWS) is analyzed. The locations of events are shown in Figure 2.3. Their seismological properties are summarized in Table 2.2. The spatial variance of strong-ground motion within Istanbul Earthquake Rapid Response System (IERRS) network is investigated by the analysis of the variation of peak ground accelerations (PGA's) in terms of standard deviation of logarithmic differences of PGA as a function of station-separation distance. For the shorter separation distance, the data recorded by SPITSBERGEN array owned to NORSAR is used. Also, the variation of pseudo spectral velocity (PSV) is also analyzed considering the May 16, 2004 earthquake and September 29, 2004 earthquake.

3.3.1. Methodology

To detect the statistical properties of spatial variability of ground motion recorded by IERREWS, two earthquakes with many recorded data are considered, primarily (Harmandar *et al.*, 2006). As discussed in Chapter 2, the first event (M_L 4.3) took place on 16.05.2004 off the Yalova coast in the Eastern Marmara Sea close to the entrance of the Izmit Bay. The second one (M_L 4.0) occurred on 29.09.2004 to the south of the Prince islands close to Istanbul. Both events can be associated with the North Boundary (or Cinarcik) segment of the North Anatolian Fault in the Marmara Sea. In the first event 73 stations and during the second one 86 stations of the 100-station IERRS were triggered. The locations of events are shown in Figure 2.3. Their seismological properties are summarized in Table 2.2.

The spatial variance of strong-ground motion within IERREWS network is investigated by the analysis of the variation of PGA and pseudo spectral velocities (PSV) as a function of station-separation distance. The spatial variability of PGA is studied by the PGA ratio of two stations as a function of separation distance over a frequency range. The analysis is repeated using ratios of PSV's of station-pairs calculated as the average of PSV's for five per cent critical damping between periods 0.3 and 0.9 s. All possible pair ratios of the values were made as a function of the distance between the paired stations. In both cases, the data are corrected for distance and local site effects. Also, PGA and PSV values were corrected for geometric spreading effect.

The spatial variation of distance and site corrected PGA and PSV values were investigated using the ratios of these values between two stations as a function of mean of distance separation. The ratio represents a spatial difference between two PHA's and PSV's, and is obtained by dividing the smaller value by the larger value (Kawakami and Mogi (2003)). The ratios for both PGA and PSV were calculated for all possible station pairs for each event. In this study, only the stations with inter-station distance from 0 to 5 km were used. The stations were grouped using intervals of 0.2 km. 21 and 22 groups were formed for the May 16, 2004 and September 29, 2004, respectively. The number of stations that fall into each distance interval bin is shown in Figure 3.40 for the May 16, 2004 and September 29, 2004.

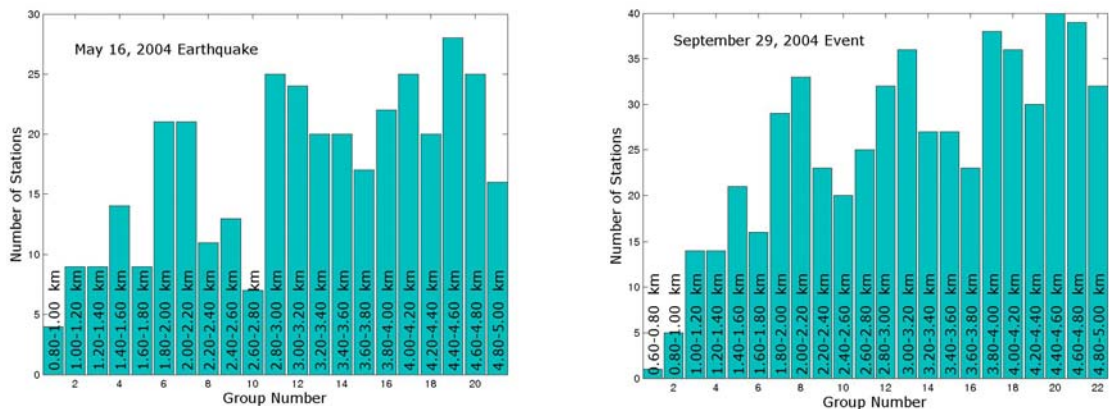


Figure 3.40. Number of stations per group for the May 16, 2004 earthquake and the September 29, 2004 earthquake

As the final step in the estimation of the spatial variation of PGA and PSV values, the logarithm of PGA and PSV ratios were binned for all pairs of stations. The logarithmic standard deviations of PSV against the station separation distances are plotted in Figure 3.41.

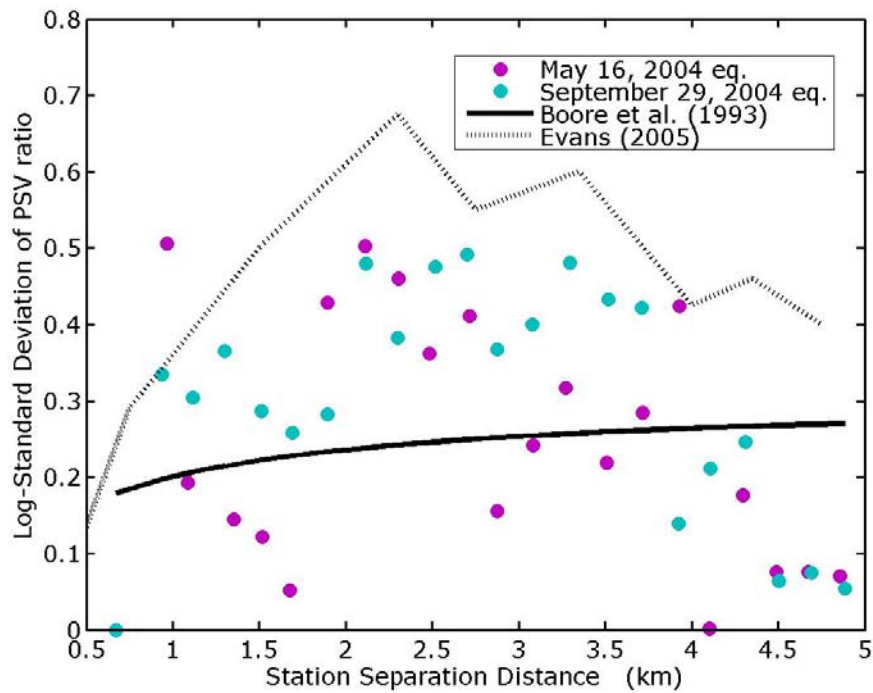


Figure 3.41. Logarithmic standard deviations of PSV ratios as a function of station separation

The logarithmic standard deviations of PGA and PSV ratios vary between 0.0 and 0.5. The station separation distance is in a range of 0.5 to 5 km. For the comparison, Boore *et al.* (1993) for PSV, Evans (2005) for both PGA and PSV are used.

3.3.2. Spatial Variability of Peak Ground Acceleration

The purpose of this study is to examine the spatial variability of PGA's as a function of separation distance. To do this, the PGA ratios are defined as spatial intraevent variations of PGA's and examine their statistical characteristics.

Logarithmic standard deviations of PGA ratios are computed for seven earthquakes from IERREWS described in Chapter 2. In addition to, PGA ratios are derived from data recorded by SPITBERGEN (SPITS) array for the small separation distances. The station separation distances range from 0.2 km to 1 km in SPITS. The mean values are computed to make accurate groups. The mean value of PGA ratios μ_R can be obtained by

$$\mu_R = \exp\left(\frac{\sigma_{P'}^2}{2}\right) \left\{ 1 - \frac{2}{\sqrt{\pi}} \int_0^{\frac{\sigma_{P'}}{\sqrt{2}}} \exp(-t^2) dt \right\} \quad (3.12)$$

where $\sigma_{P'}$ is standard deviation. Thus, the dispersion of PGA's can be represented either by mean value or by standard deviation. The statistical analyses (mean values) were calculated for each station separation group.

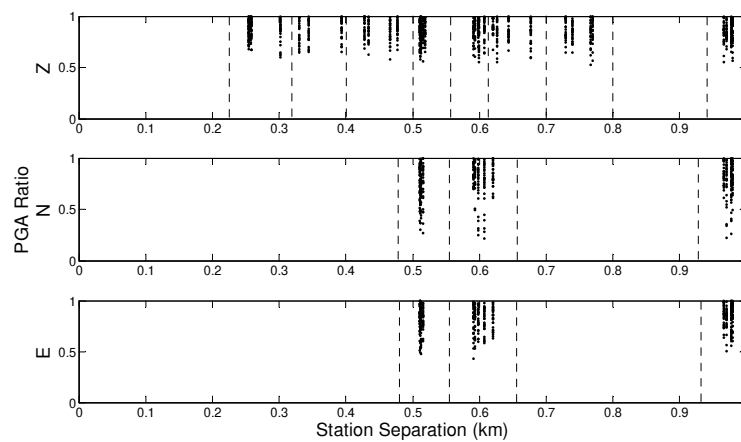


Figure 3.42. PGA ratios of earthquakes recorded by SPITZBERGEN array

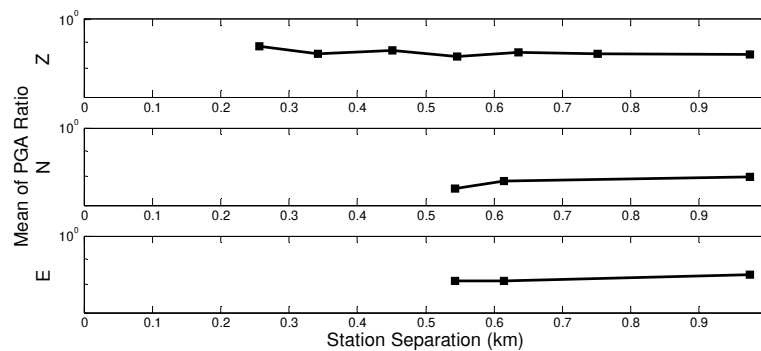


Figure 3.43. Mean values of the PGA ratios of earthquakes recorded by SPITZBERGEN array

Scattered plots for one case (whole data) are shown in Figure 3.42. Taking into account this distribution, the station pairs were divided into groups, demonstrated in the figure with lines. No local site effect correction was done. The mean values of PGA ratios

based on data from SPITS array are plotted in Figure 3.43 for two horizontal and vertical components.

As a result, both ratios from IERREWS and SPITS array are plotted in Figure 3.44. Boore (1997) equation does not match with PGA ratios. The coefficients of Boore (1997) equation are regressed to obtain the relation compatible with IERRS and SPI data.

$$y = 0.155 \left(1 - e^{-\sqrt{4.506 d}} \right) \quad (3.13)$$

where d is the separation distance between the stations.

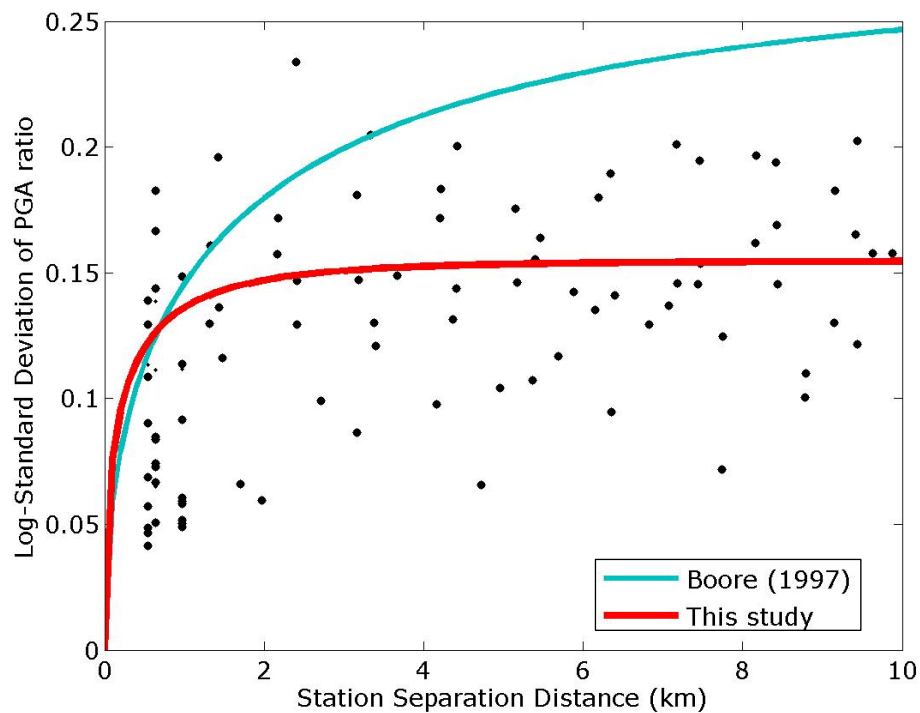


Figure 3.44. Logarithmic standard deviations of PGA ratios as a function of station separation

3.4. Conclusions

The purpose of this study is to examine the spatial variability of PGA's and PSV's in Istanbul as a function of separation distance. The spatial variation was computed by the ratios. The ratio represents a spatial intraevent difference between peak ground

parameters, PGA and PGV. These ratios were obtained by dividing the smaller value by the larger value for all possible station pairs for each earthquake.

It is seen that PGA's increase gradually with the separation distance. The PSV values increase rapidly to the amplitude corresponding to the distance of 3 km. After that distance, a decrease occurs in the values of PSV. Consequently, despite the magnitude range of the studies of Boore *et al.* (1993) and Evans (2005) is different from our magnitude range for PSV values, the results obtained by data from IERREWS and SPITS array match with the studies of Boore *et al.* (1993) and Evans (2005). This comparison may indicate that there is no a significant dependence on earthquake magnitude (Abrahamson *et al.*, 1992) for PSV ratios. However, logarithmic standard deviations of PGA ratios are not compatible with Boore (1997). Because of that reason, the coefficients of Boore (1997) equation for the estimation of the spatial variability in terms of logarithmic standard deviation of PGA differences recalculated for data recorded by IERREWS. The gap for the short station separation distance of IERREWS is filled by SPITS array.

In conclusion, the spatial variability in ground motion reduces to zero as the distance between the stations decreases to zero. On the other hand, for a great enough separation distance (not shown here) the spatial correlation of the ground motion reduces to zero. The two end-member cases suggest the following equation (Boore, 1997) for the variance of peak ground motion as a function of separation distance:

$$\sigma_{\Delta \log Y}^2 = \sigma_{\text{indobs}}^2 \left(1 + \frac{1}{N} \right) F(\Delta)^2 \quad (3.14)$$

where $\sigma_{\Delta \log Y}$ is the standard deviation of differences in the logarithm of the peak motion Y; σ_{indobs} is the standard deviation of an individual observation about a regression; N is the number of recordings; $F(\Delta)$ is a function that accounts for the spatial correlation of the motion, computed by Equation (3.13); and Δ is the average separation distance between the stations.

4. ASSESSMENT OF EARTHQUAKE INDUCED GROUND STRAINS IN THE DÜZCE EARTHQUAKE

4.1. Introduction

The ground strains caused by the seismic waves can have a significant effect on earthquake triggering, ground failure, and damage to man-made structures. The transient deformation of the ground surface during an earthquake is closely related to the spatial variability of the seismic motion (Zerva, 2009). Herein, ground strains in Düzce Earthquake are analyzed.

In the absence of earthquake induced permanent displacements and deformations, the seismic response of buried structures, and water pipelines, depends mainly on the amplitude of transient strains induced in the ground (Scandella *et al.*, 2007). Wave propagation phenomenon is studied nowadays using several techniques, such as finite element method, finite difference method, boundary element method, and spectral element method. Three-dimensional wave propagation has been of interest, after the computational power is increased by parallel computers. Three-dimensional wave propagation problems are typically defined by three major elements: the source, the propagation path and the structure itself. The accurate modeling of each of such elements is a hard task: The source may not be well defined, such as in the earthquake case, or it may involve a very large frequency spectrum, such as for traffic-induced vibrations; the propagation path, in terms of spatial variability of dynamic soil properties, is seldom well constrained by suitable geophysical/geotechnical prospecting; finally, the dynamic behavior of the structure and the supporting soil may be strongly affected by nonlinear effects, the influence of which can be assessed reliably only in few cases (Stupazzi *et al.*, 2006). Considering these parameters to obtain accurate results for the solution of the wave propagation problem causes extreme difficulties from the computational point of view. To reduce the computational effort required by such a large scale numerical problem, a powerful substructuring method, termed Domain Reduction Method (DRM), was generated by Bielak *et al.* (2003). This method has been applied to the case of Düzce, using data from the November 12, 1999 Düzce earthquake. Düzce earthquake with a magnitude of hit

Turkey on November 12, 1999. The damage to the buildings was similar to that sustained during the Kocaeli 1999 earthquake. Two viaducts and one tunnel under construction exhibited extensive damage.

4.2. Domain Reduction Method

The Domain Reduction Method (DRM) is a modular two-step, finite element methodology for modeling earthquake ground motion in highly heterogeneous localized regions with large contrasts in wavelengths (Bielak *et al.*, 2003). The problem of multiple physical scales is overcome by subdividing the original problem (Figure 4.1-a) into two simpler ones. The first (Figure 4.1-b) is an auxiliary problem that simulates the earthquake source and propagation path effects with a model that encompasses the source and a background structure from which the localized feature has been removed. The second problem (Figure 4.1-c) models local site effects. Its input is a set of equivalent localized forces derived from the first step. These forces act only within a single layer of elements adjacent to the interface between the exterior region and the geological feature of interest. This enables to reduce the domain size in the second step.

The Domain Reduction Method is equipped with the spectral element approach developed by Faccioli (1997). This spectral element approach is implemented in the computational code GeoELSE (GeoELasticity by Spectral Elements), for 2D/3D wave propagation analyses (Maggio, 2001, Stupazzini, 2004).

The spectral element method is usually regarded as a generalization of the finite element method based on the use of high order piecewise polynomial functions. The crucial aspect of the method is the capability of providing an arbitrary increase in accuracy simply enhancing the algebraic degree of these functions (the spectral degree SD). On practical ground, this operation is completely transparent for the users, who limit themselves to choose the spectral degree at runtime, leaving to the computational code the task of building up suitable quadrature points and new degrees of freedom. Obviously, the increasing spectral degree implies the raise the computational effort of the problem (Stupazzi *et al.*, 2006).

The computational code GeoELSE is used to study the seismic response of the Düzce basin during the November 12 earthquake. The original problem is subdivided into two simpler ones solved in two steps. First is an auxiliary problem as mentioned before, (Step I) from which the Düzce basin has been removed and replaced by the same material as the surrounding domain. The second problem is a reduced model (Step II) which contains the Düzce basin, the geological feature of interest, but not the causative fault. The excitation applied to the reduced model is a set of equivalent localized forces derived from the first step. These forces are equivalent to and replace the original seismic forces applied in the first step to reproduce the seismic source (Scandella *et al.*, 2007). In the analysis, the free field displacements are evaluated at the effective boundary (Figure 4.1-b) from the first step, and are used as input for the second step. In the first step, 3D analysis has been carried out using the semi-analytical method of Hisada and Bielak (2003); in the second step, 2D numerical analysis has been computed by means of the Spectral Element Method.

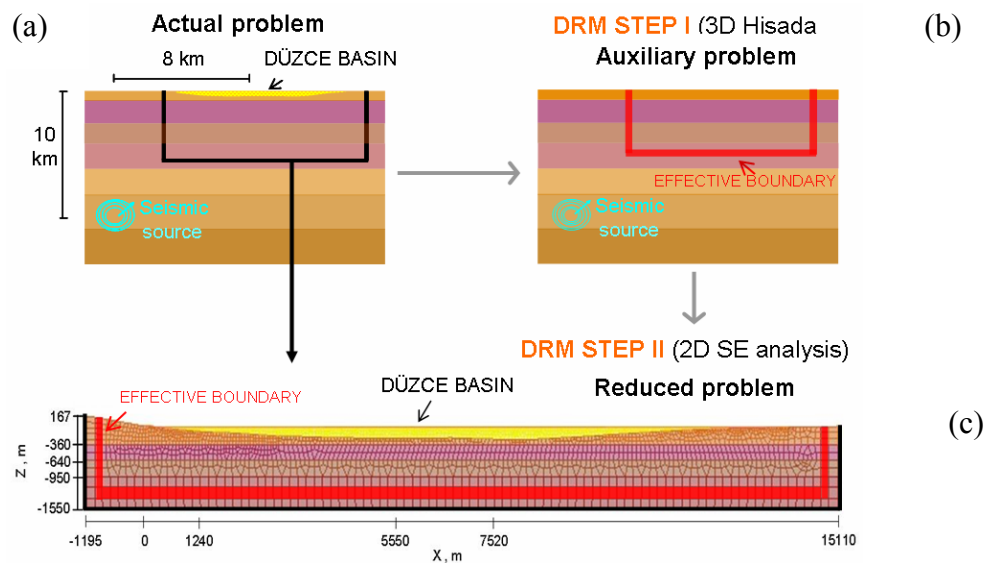


Figure 4.1. The scheme of the DRM procedure applied to the Düzce urban area (Scandella *et al.*, 2007)

The methodology for the analysis of the seismic response of Düzce basin is summarized as follows:

1. The reduced model (Step II) is subdivided into several meshes using spectral elements to obtain the locations of the nodes at the effective boundary.

2. The semi-analytical method of Hisada and Bielak (2003) is used to derive the velocity time histories at these nodes. For this semi-analytical method, source parameters and velocity profile should be presented. Several studies have been performed to reproduce the rupture process of the November, 1999 Düzce earthquake (*i.e.* Yagi and Kikuchi, 2000, Birgören *et al.*, 2004). The source parameters, inferred from Yagi and Kikuchi (1999), are listed in Table 4.1.
3. The velocity time histories are integrated to obtain displacement time histories to pass the second step.
4. These displacement time histories at the effective boundaries are used as input parameters in GeoELSE to obtain seismic response of the basin.

Table 4.1. Source parameters of the rupture model for the November 12, 1999 earthquake

Lat. Long.	Depth <i>km</i>	M_0 <i>Nm</i>	M_W	Δu_m <i>m</i>	W_f <i>km</i>	L_f <i>km</i>	v_R <i>km/s</i>	Rise time <i>s</i>	Strike	Dip	Rake
40.77°N 31.20°E	10.00	4.9×10^{19}	7.1	5.6	16.5	16.5	2.80	2.80	265°	65°	168°

The geological maps and borehole data provided by KOERI, together with several soil profiles from deep borings provided by AUTH. The NS cross-section has been obtained from these data as shown in Figure 4.2. A standard rock model proposed by Boore and Joyner (1997) successfully used by Faccioli *et al.* (2002) to reproduce the seismic response recorded at Düzce and neighboring cities during the November 1999 earthquake. Herein, this velocity profile used in Step I is shown in Figure 4.3. The site properties are listed in Table 4.2.

Table 4.2. Site properties of the auxiliary problem

Layer No	ρ (t/m^3)	v_p (m/s)	v_s (m/s)	Q_p	Q_s	Depth (m)
1	2.20	2312.5	1352.5	200	100	<i>from 0 to 490</i>
2	2.25	3750.0	2185.0	250	150	<i>from 490 to 770</i>
3	2.30	4000.0	2350.0	350	200	<i>from 770 to 1080</i>
4	2.30	4600.0	2700.0	350	200	<i>from 1080 to 1680</i>
5	2.40	5050.0	3000.0	350	200	<i>from 1680 to 2500</i>
6	2.50	5500.0	3300.0	500	300	<i>from 2500 to 4500</i>
7	2.70	6300.0	3700.0	800	500	<i>from 4500 to ∞</i>

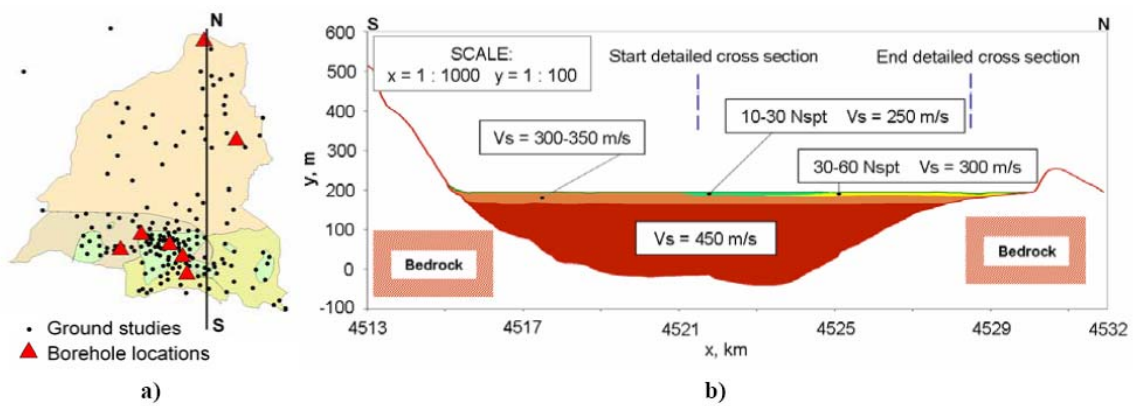


Figure 4.2. Location of available Borehole and shallow ground studies and soil profile of the NS cross-section of Düzce

The results of the analysis using the standard rock model proposed by Boore and Joyner (1997) are used in comparison of observed velocity and displacement time histories, and Fourier amplitude spectrum of Bolu and Karadere stations with the simulated ones at the same stations. The location of these sites is reported by Faccioli *et al.* (2002).

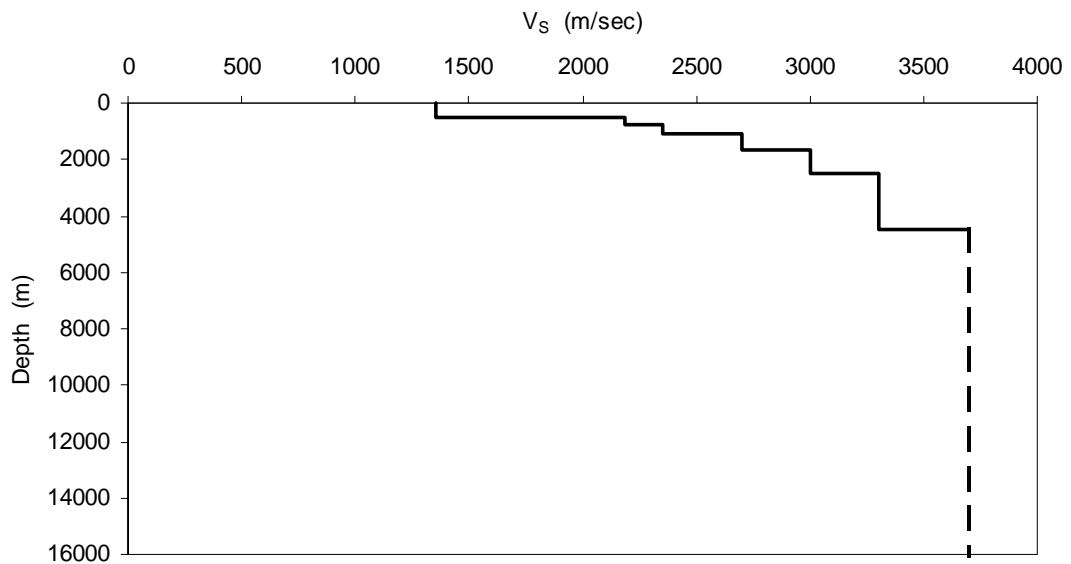


Figure 4.3. V_s profile used in Step I

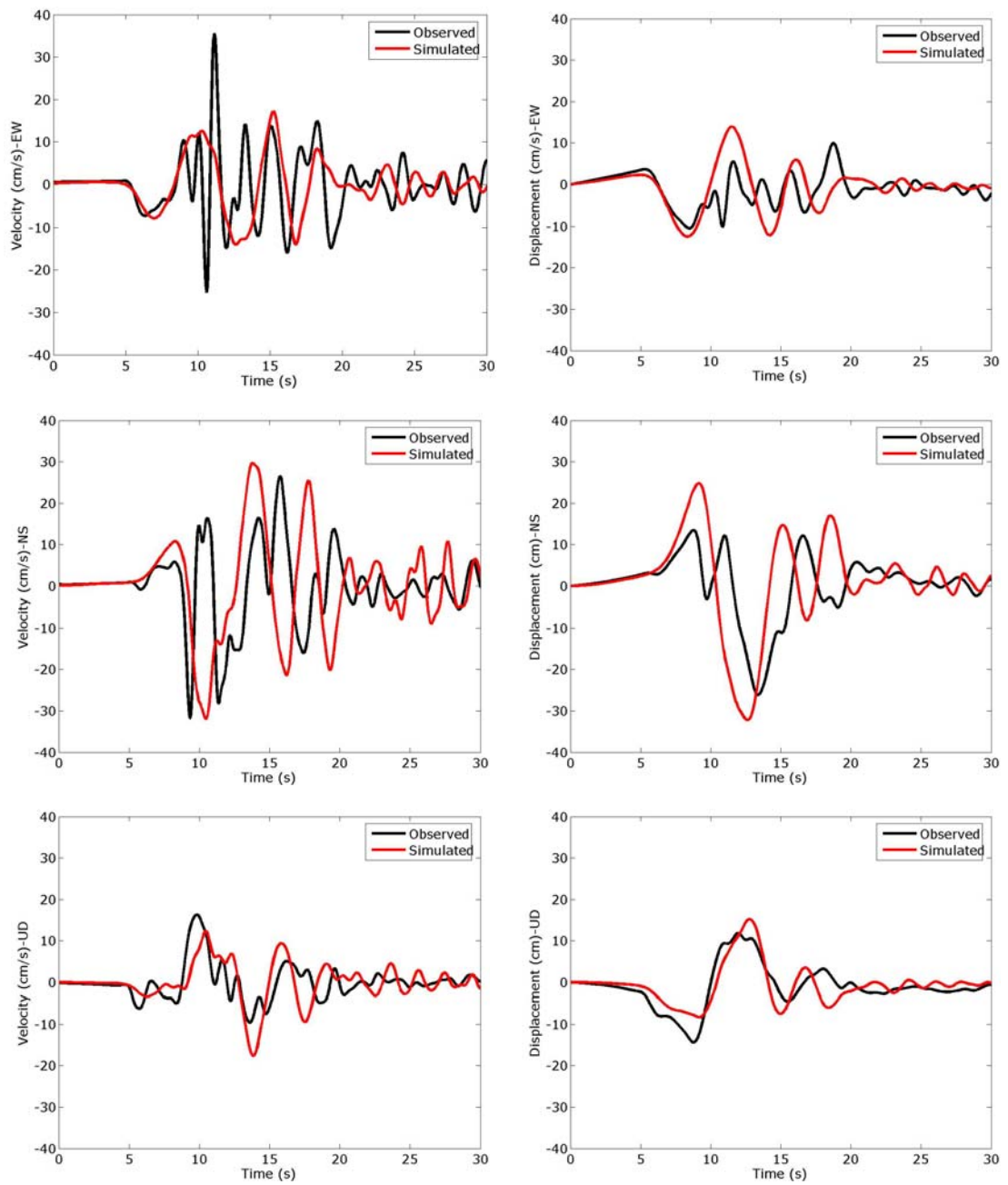


Figure 4.4. Observed and simulated velocity and displacement time histories of EW, NS, and UD components at Bolu station

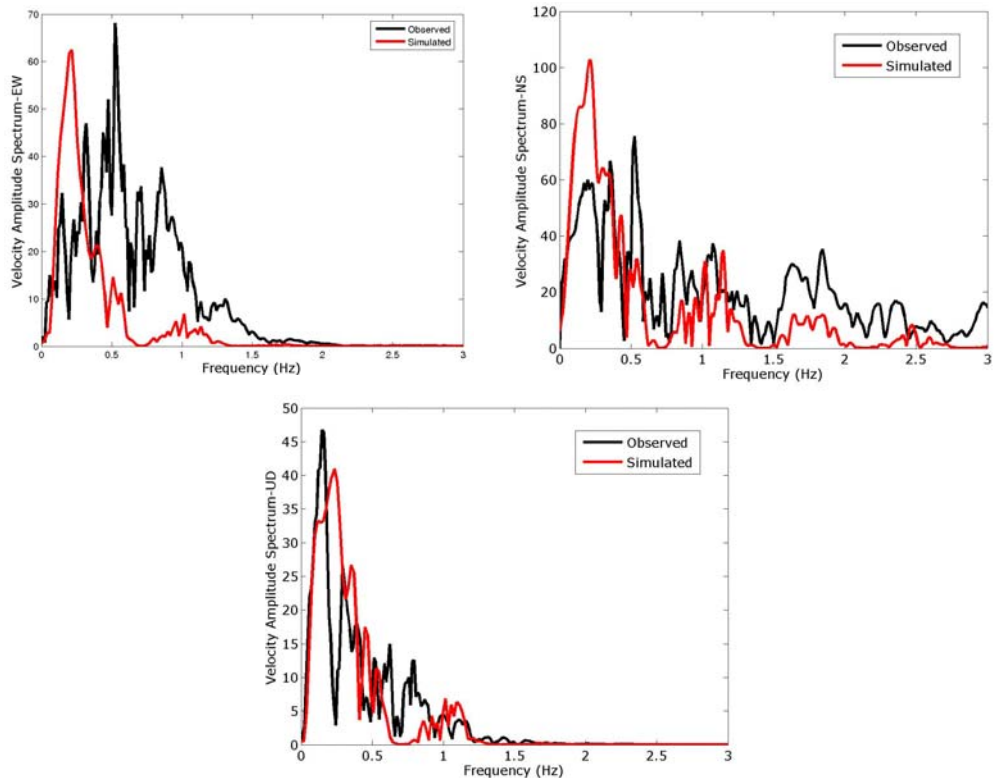


Figure 4.5. Fourier Amplitude Spectra of EW, NS, and UD components at Bolu station

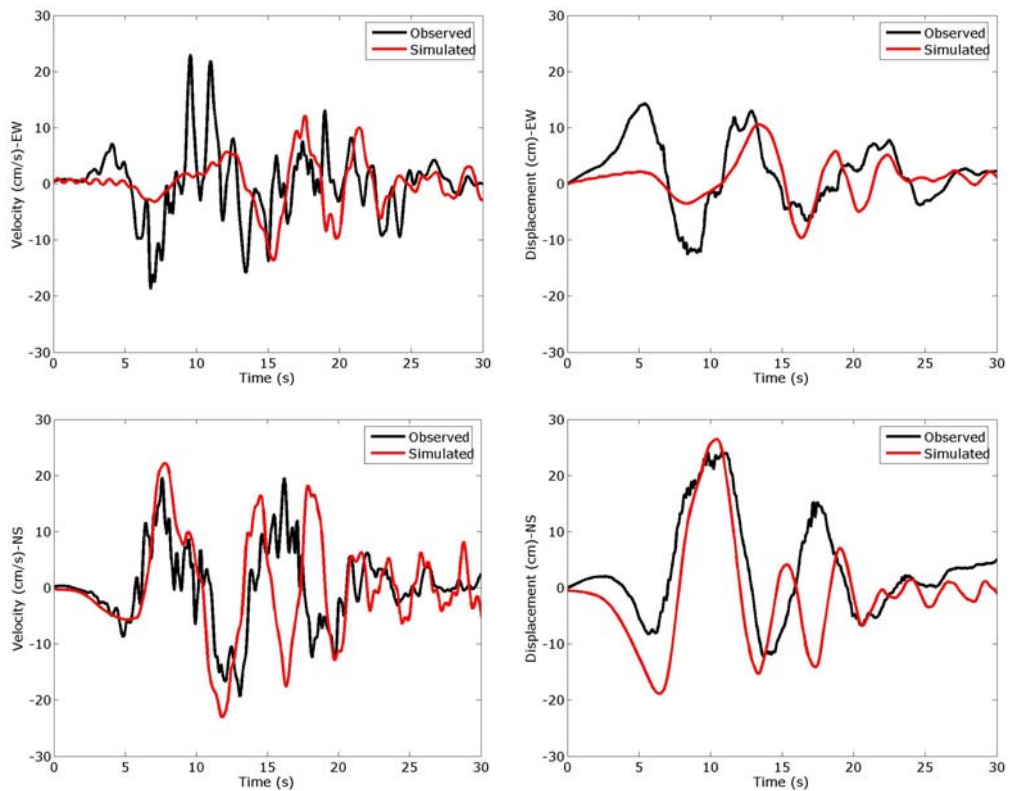


Figure 4.6. Observed and simulated velocity and displacement time histories of EW and NS components at Karadere station

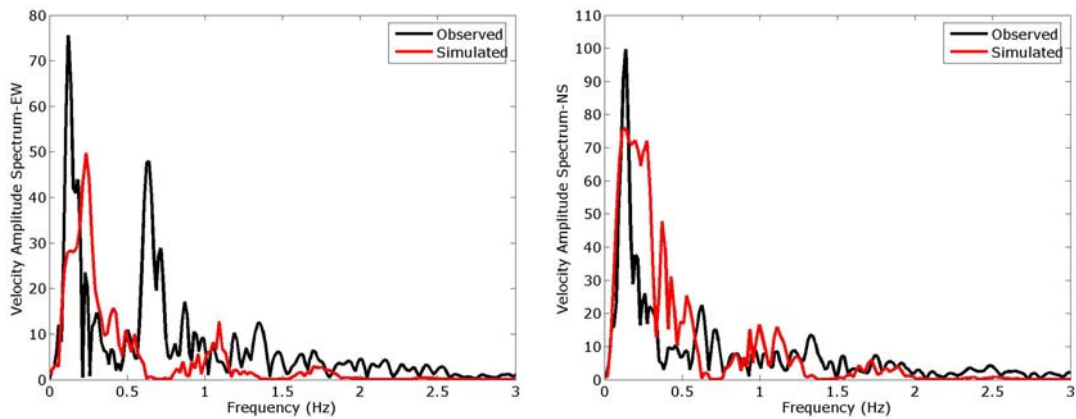


Figure 4.7. Fourier Amplitude Spectra of EW and NS components at Karadere station

The comparisons, shown in Figure 4.4 to Figure 4.7, represent the correlation of the simulated time histories with the observed time histories. Velocity time histories are evaluated at the boundary nodes using the standard rock model proposed by Boore and Joyner (1997) for the second step. In the second step, the GeoELSE numerical code is used to obtain the seismic response in Düzce basin.

The S-wave profile used in the second step for the reduced model is shown in Figure 4.8. The site properties of the reduced model are listed in Table 4.3. The vertical and horizontal displacements are used as the effective forces that represent the wave propagation from the seismic source at the boundary of the reduced model.

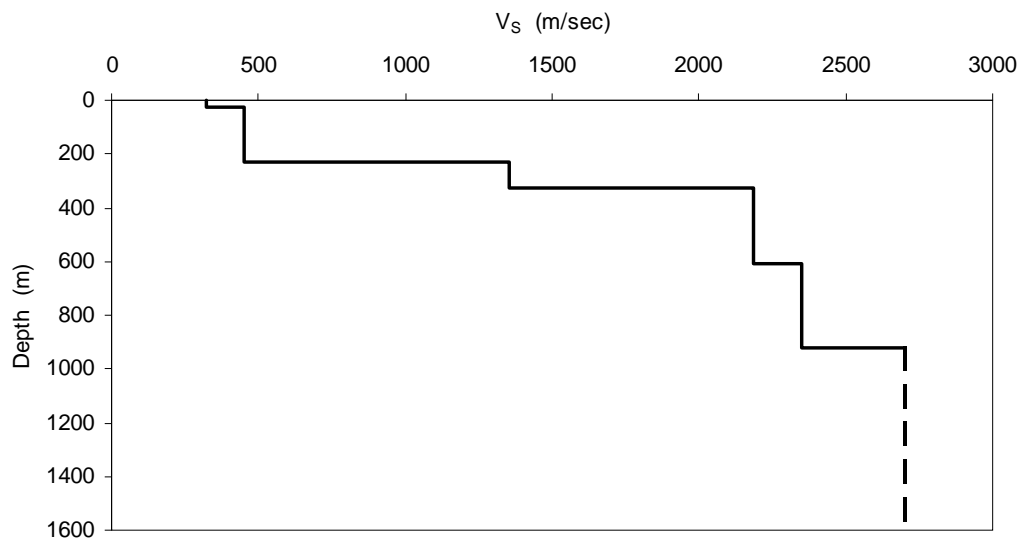


Figure 4.8. V_s profile used in Step II

Table 4.3. Dynamic soil properties for the reduced model

Layer No	ρ (t/m ³)	v_p (m/s)	v_s (m/s)	Q_s
1	1.80	796.0	325.0	20
2	2.00	937.0	450.0 <td 30	
3	2.20	2312.5	1352.5	100
4	2.25	3750.0	2185.0	150
5	2.30	4000.0	2350.0	200
6	2.30	4600.0	2700.0	200

The spectral element scheme of Düzce basin is shown in Figure 4.9. The cross sections are selected as the critical regions for the basin, and the ground motions is generated at these significant points along the basin.

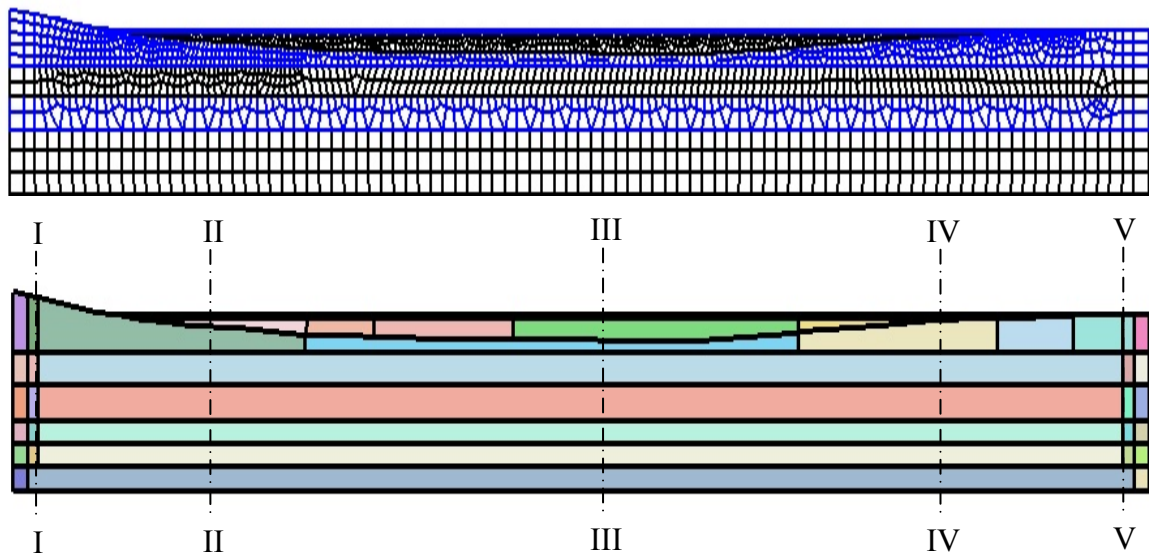


Figure 4.9. Mesh model of Düzce basin

4.3. Results and Conclusions

The results after the second step are compared for the station that recorded data during the earthquake is Düzce station at the basin surface. Figure 4.10 and Figure 4.11 represent the comparison of the observed and simulated displacement time histories (left), and Fourier amplitude spectra (right) at Düzce station. Despite the difficulty and

complexity of analysis of Düzce basin, the simulated waveforms of displacement time histories for EW and UD components are good in agreement with the observed waveforms.

Actually, higher sharp peaks are observed for both time histories and Fourier amplitude spectra at Düzce station. The reason is the irregular increase of V_S with depth, *i.e.* soft basin effect.

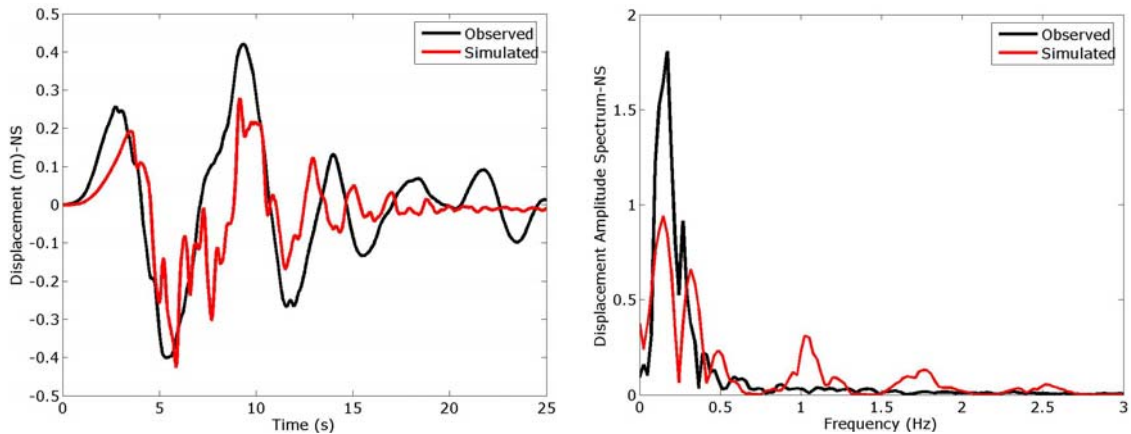


Figure 4.10. Observed and simulated displacement time histories (left) and Fourier amplitude spectra of NS component at Düzce station

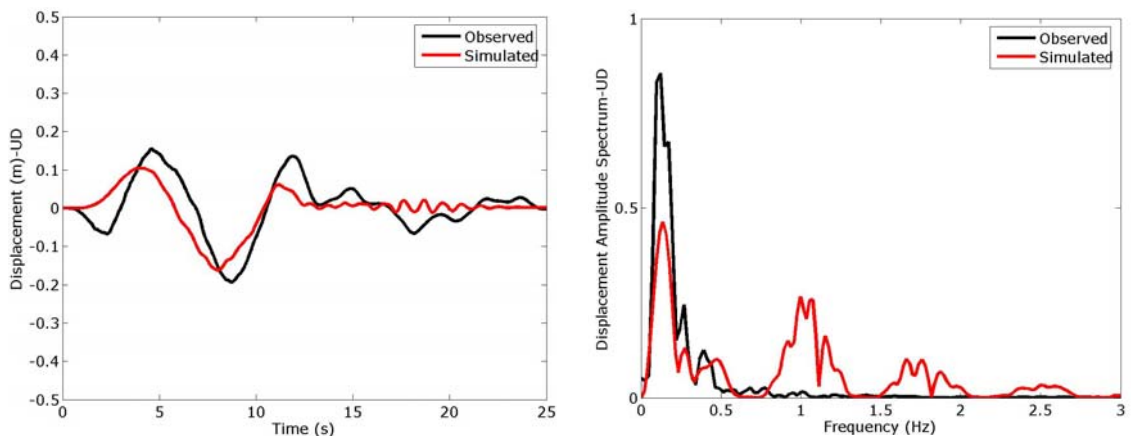


Figure 4.11. Observed and simulated displacement time histories (left) and Fourier amplitude spectra of UD component at Düzce station

The seismic response of Düzce basin is determined in terms of time histories at several surface receivers. The spatial variation of displacement time histories and displacement Fourier spectra are shown in Figure 4.12 to Figure 4.16 for the locations (Figure 4.9) along the eight receivers at the vertical direction.

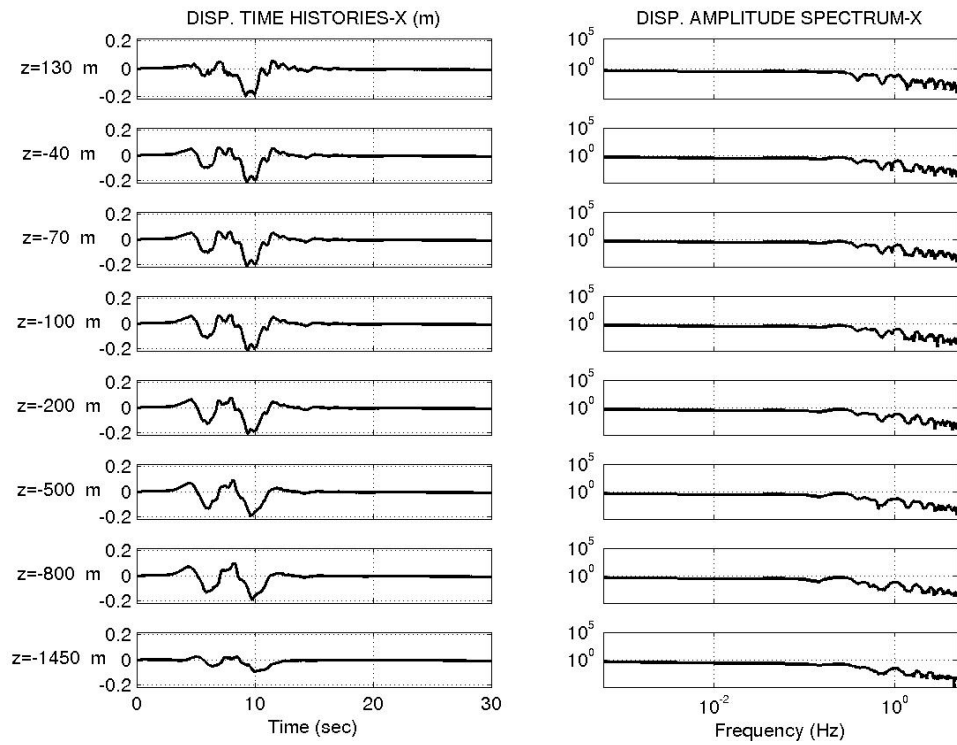


Figure 4.12. Variation of displacement time histories and displacement amplitude spectra w.r.t. depth at cross section I along the NS cross-section

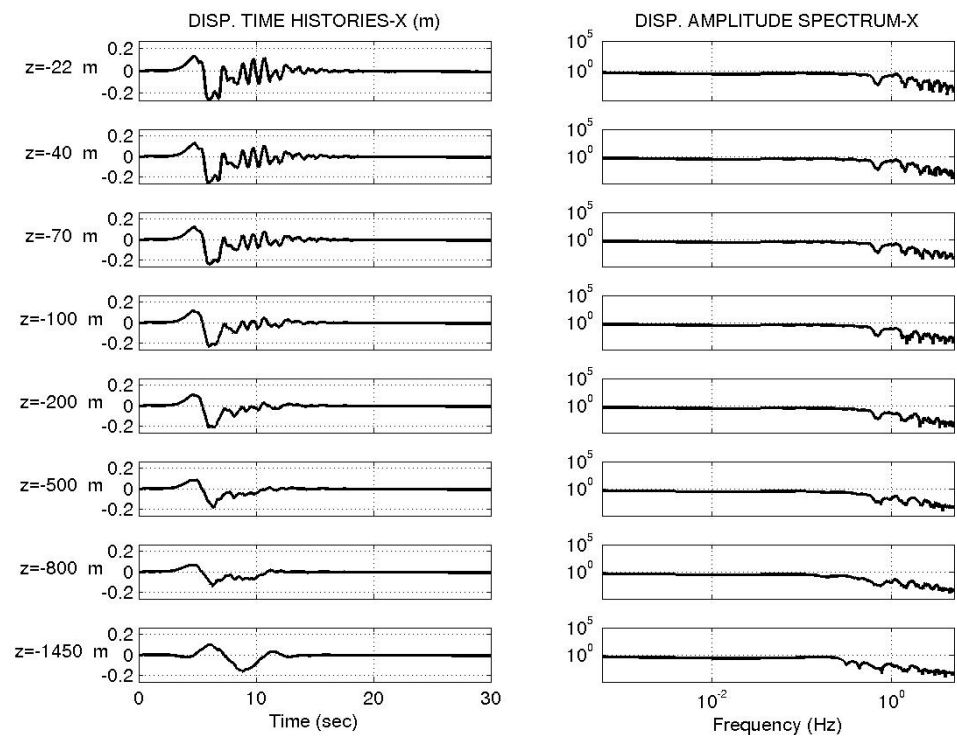


Figure 4.13. Variation of displacement time histories and displacement amplitude spectra w.r.t. depth at cross section II along the NS cross-section

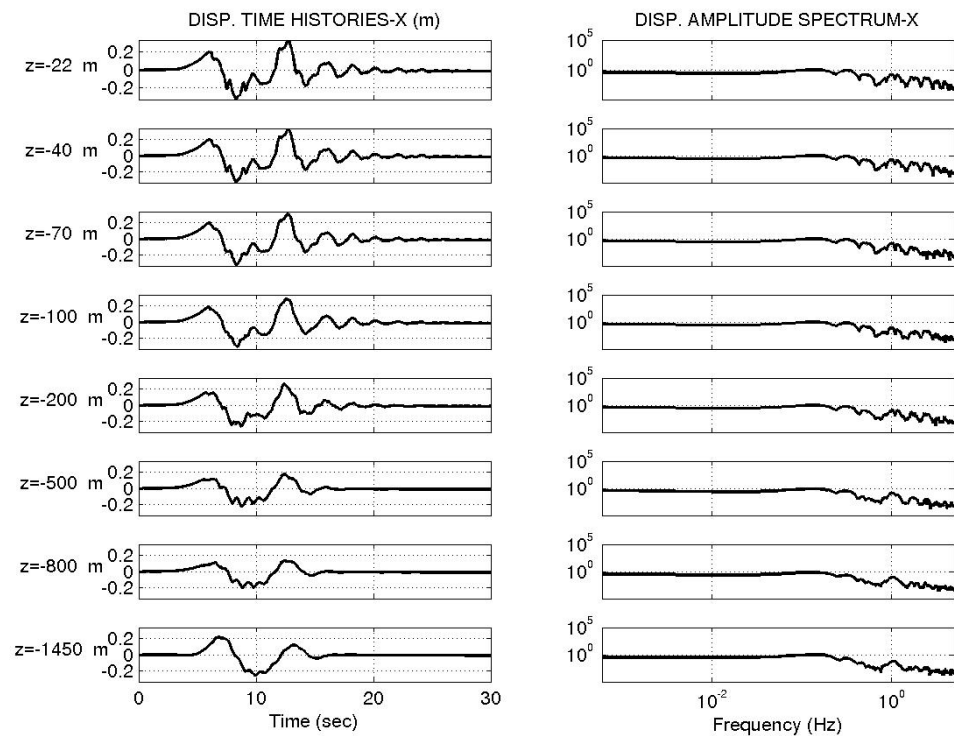


Figure 4.14. Variation of displacement time histories and displacement amplitude spectra w.r.t. depth at cross section III along the NS cross-section

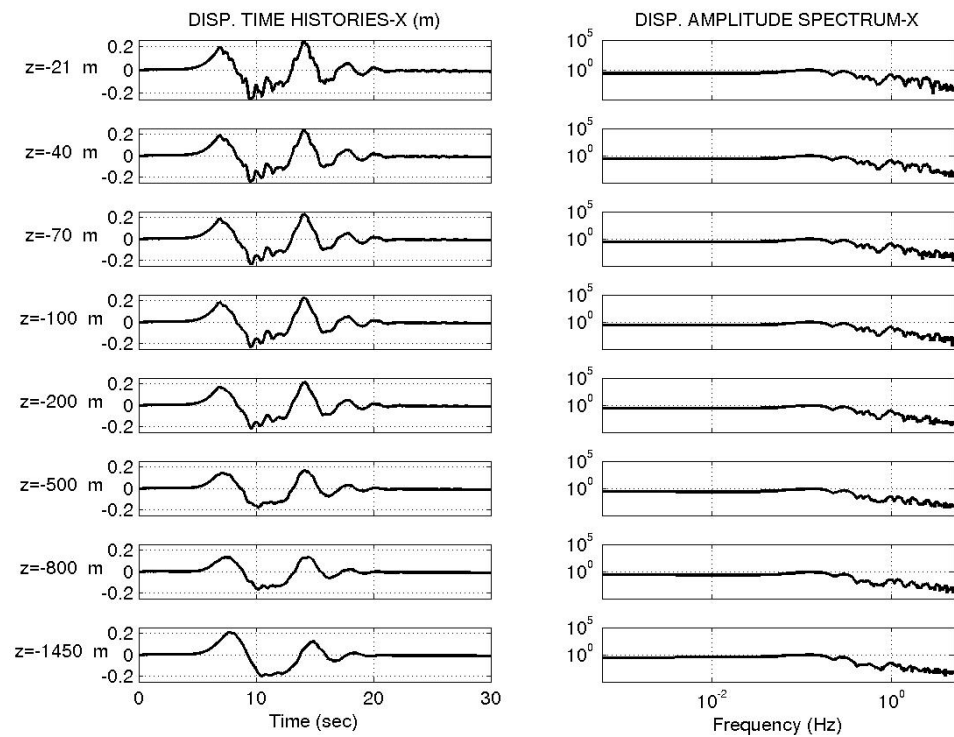


Figure 4.15. Variation of displacement time histories and displacement amplitude spectra w.r.t. depth at cross section IV along the NS cross-section

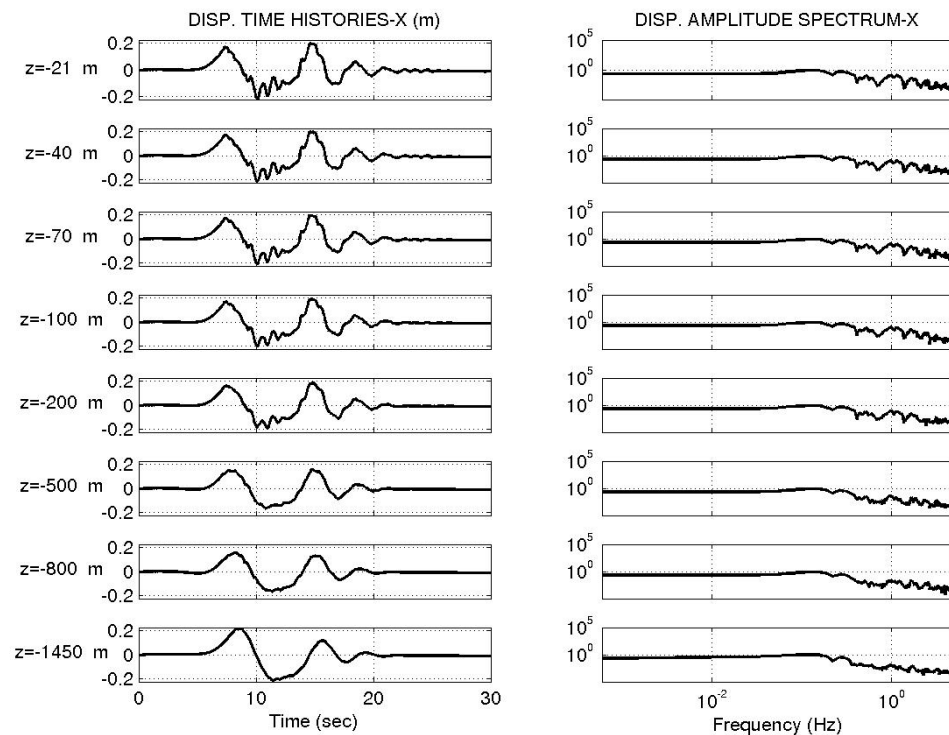


Figure 4.16. Variation of displacement time histories and displacement amplitude spectra w.r.t. depth at cross section V along the NS cross-section

The ground motion parameters; peak ground acceleration (PGA), peak ground velocity (PGV) and peak ground displacement (PGD) are calculated along NS cross section of Düzce basin (Figure 4.17). It is observed that the selected ground motions parameters have highest values at the southern part of the basin. The reason is that the basin represents irregular increase in shear wave velocity values.

The peak ground strains are obtained along NS cross section of the basin. The spatial variation of peak ground strains of the horizontal and vertical directions is shown in Figure 4.18. Also, peak ground strains increase at the southern boundary of Düzce basin. Consequently, as it is mentioned before, the ground strains caused by the seismic waves can have a significant effect on earthquake triggering, ground failure, and damage to man-made structures. So, this topic has been examined in detail nowadays.

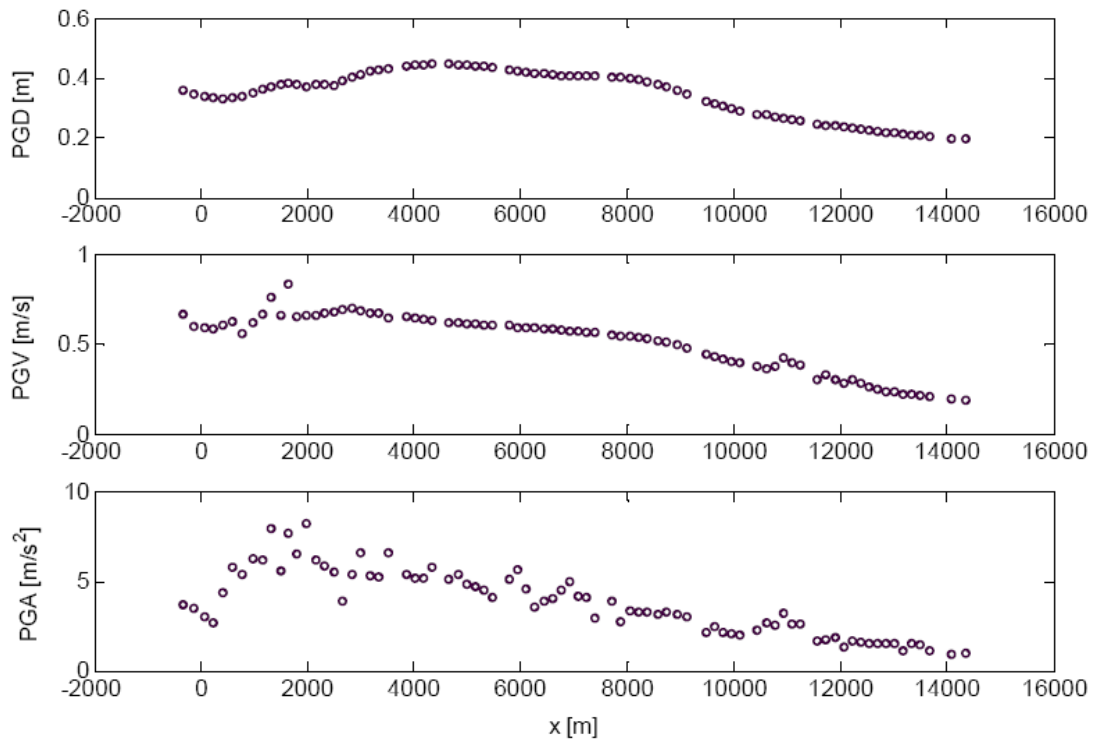


Figure 4.17. Variation of peak ground displacement, velocity and acceleration along the NS cross-section at the basin surface

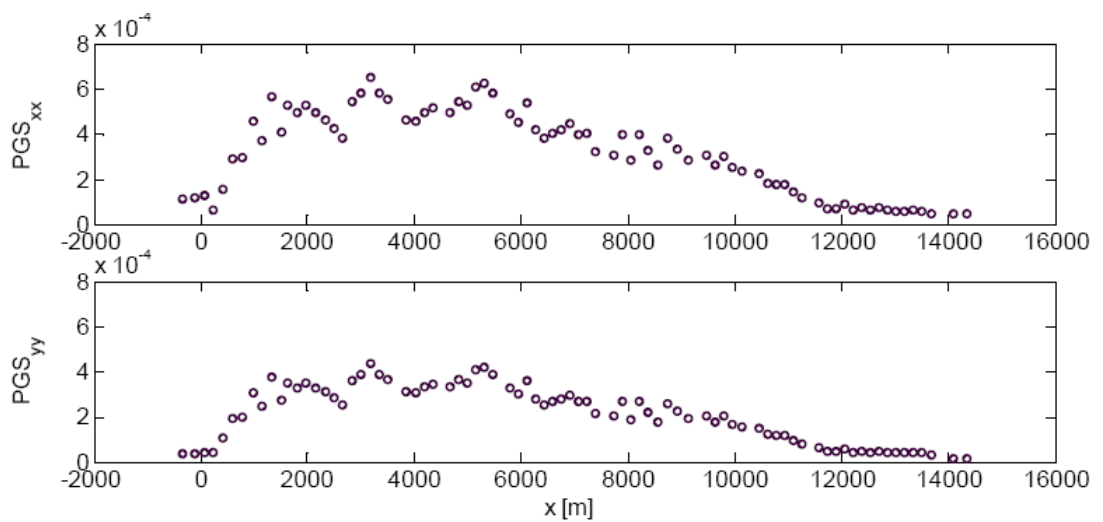


Figure 4.18. Variation of peak ground strains in the horizontal and vertical directions along the NS cross-section at the basin surface

5. STOCHASTIC DESCRIPTION OF THE SPATIAL VARIATION OF SEISMIC GROUND MOTION

As indicated in Chapter 1, the spatial variation of seismic ground motion can significantly affect the seismic responses of extended structures, and the characterization of the spatial variation is important for the accurate seismic analysis of pipelines, tunnels, dams, suspensions, bridges, nuclear power plants, as well as on conventional building structures. Considering that a lot of extended structures, *e.g.* bridges, are situated in sedimentary basins, a large number of researchers have indicated that the analysis of the variability between the ground motion of the adjacent and/or relatively far supports are essential.

The spatial variation of strong ground motion has two parts: variation in waveform (phase) and variation in amplitude. The coherency explains the variation in waveform. This means that the coherency describes the similarity between ground motions at different locations in frequency domain. So that, the degree of correlation between the amplitudes and phase angles of two time histories is interpreted in the frequency domain.

In this chapter, the seismic ground motion spatial variation in İstanbul is analyzed. First the concept of coherency function and its conventional estimation procedure are introduced, and then a parametric model is developed. The lagged coherency is estimated by applying a conventional coherency estimation scheme to seven seismic events recorded at Istanbul Earthquake Rapid Response System (IERRS). The general properties of the IERRS and the recorded data of the seven events are explained in Chapter 2.

5.1. Definition of Coherency

As a first step, the covariance function is used for the derivation of the coherency. For engineering applications, generally the covariance function, intended as second-order statistics, between the accelerograms recorded at different stations are used to characterize ground motion spatial variation. The frequency domain description of the second-order statistics is used because of its mathematical convenience in random vibration analysis.

Matsushima (1977); Abrahamson (1990); Harichandran (1991); Zerva and Zervas (2002) are some of the authors studied on the variation in frequency domain. Specifically, the normalized cross-power spectrum, namely coherency function $\gamma_{xy}(\omega)$, between two accelerograms recorded at two stations x and y given as follows:

$$\gamma_{xy}(\omega) = \frac{S_{xy}(\omega)}{\sqrt{S_{xx}(\omega)S_{yy}(\omega)}} \quad (5.1)$$

in which $S_{xx}(\omega)$ is the power spectral density at station x , $S_{xy}(\omega)$ is the cross-power spectral density between stations x and y . Therefore, the coherency is generally a complex function and can be written as:

$$\gamma_{xy}(\omega) = |\gamma_{xy}(\omega)| \exp[i \theta_{xy}(\omega)] \quad (5.2)$$

in which i denotes the complex number $\sqrt{-1}$, and the phase spectrum is

$$\theta_{xy}(\omega) = \tan^{-1} \left(\frac{\text{Im}[S_{xy}(\omega)]}{\text{Re}[S_{xy}(\omega)]} \right) \quad (5.3)$$

The lagged coherency $|\gamma_{xy}(\omega)|$ indicates the degree of linear correlation between the random processes recorded at two stations. From the definition, it is obvious that $0 \leq |\gamma_{xy}(\omega)| \leq 1$. The real part of the coherency function $\text{Re}[\gamma_{xy}(\omega)]$ is commonly referred as unlagged coherency; and the square of the lagged coherency $|\gamma_{xy}(\omega)|^2$ is referred as coherence function. However, lagged coherency is the most commonly recommended format to characterize the spatial variation of ground motion.

To evaluate coherency functions, the three items on the right side of Equation (5.1) need to be identified by applying spectral estimation techniques to recorded accelerograms. The main techniques to estimate the spectra of time series are: Conventional Spectral Analysis, Maximum Likelihood Method and Maximum Entropy Method (Marple, 1987). Both Maximum Likelihood Method and Maximum Entropy Method can yield higher

resolution than the Conventional Spectral Analysis method. For the broadband seismic ground motion, however, the resolution of spectral estimate the Conventional Spectral Analysis method is sufficient and appropriate for practical engineering application (Harichandran and Vanmarcke, 1986; Harichandran, 1991). Consequently, the current coherency estimation studies are mainly based on the Conventional Spectral Analysis (Zerva, 2009).

As noted above, the coherency is a complex number. The real part of coherency describes the similarity of the two ground motion without any adjustment for wave propagation and therefore includes the effect of the deviation from vertical plane wave propagation. It is more common to use the absolute value of coherency which removes the effects of simple plane wave propagation. It measures the similarity between the ground motion at two stations for a given frequency band. Physically, it is the ratio of the power of the ground motion at the given frequency band that can be modeled by a plane-wave to the total power of the ground motion at that frequency band.

The complex coherency has an amplitude and a phase for each frequency band. The amplitude is the aforementioned as lagged coherency. The phase is the phase difference between the recordings from stations separated by distance. The phase difference accounts for the different arrival times at the two stations. For a given station pair, the apparent velocity of the “best fit” plane-wave for a given frequency band can be computed from phase.

For the generation of the coherency values, selection of the specific time windows is necessary to handling the assumption of homogeneity, stationarity and ergodicity. The shear wave part of the accelerograms is generally appropriate for this purpose, because in most cases the shear wave contains the strongest energy in earthquake recordings and, generally, is the most damaging component from the engineering point of view. The selected time window is seen as a segment of a stationary process with limited duration. Different time window lengths can be used depending on specific earthquake events and the recorded time histories (for example: 5, 9, 10, 21 seconds (Hao *et al.*, 1989); 2 seconds (Schneider *et al.*, 1990); 10 seconds (Harichandran, 1991; Boissieres and Vanmarcke, 1995)).

5.2. Data Processing

Before applying the spectral estimation schemes to the selected time window, the entire time history should be preprocessed for baseline adjustment and instrumentation correction. To better characterize the homogeneity of ground motion random fields, the selected time windows can be aligned with respect to a reference station to remove the apparent wave propagation effect across the array. The time lags in the alignment can be determined by estimating the correlation between stations and evaluating the positive maximum correlation coefficients (Boissieres and Vanmarcke, 1995). After the preprocessing and alignment operations, the coherency function can be obtained by estimating the power spectral densities and cross-spectral density, as indicated in Equation (5.1)

The application of smoothing windows is indispensable in the coherency spectrum estimation procedure, otherwise the sample coherency spectrum is identically equal to unity irrespective of what properties the random processes possess (Jenkins and Watts, 1968). In addition, the smoothing window controls the statistics (variance and bias) of coherency estimates as well as its resolution. Common smoothing windows in conventional spectrum estimation, *e.g.* Bartlett, Hamming and Hanning windows can be used (Stoica and Moses, 1997). These smoothing windows yield similar results as long as the equivalent bandwidths of the spectral windows are the same (Harichandran, 1991). Therefore, the selection of an appropriate equivalent bandwidth of spectral windows is more important than choosing smoothing spectral window types. As such, the lengths of smoothing windows are selected by considering the tradeoff between the bias and variance of the estimators. Abrahamson *et al.* (1991) indicated that the selection of the smoothing window should be based on not only the statistical properties of coherency estimates, but also on the purpose of the application. They suggested an 11-point Hamming window when the time window length is less than 2000 steps and the coherency estimates are to be used in structural analysis. In this study, eight cases using hamming window is studied. The coherency is calculated for 11-point hamming window for east-west and north-south directions; and for radial and transversal directions. Also, the procedure is done for 15-point Hamming window for east-west and north-south directions; and for radial and transversal directions. Figure 5.1 shows the variation of the coherency values of R31-R44

pair with respect to the window length. Similar relation between the coherency values and the window length for each pair is observed. The more the window length, the less the resolution is occurred. On the contrary, decrease in window length causes more details in coherency values. As a result, for the estimation of the coherency values, the window length is selected as 11 point based on Abrahamson *et al.* (1991) suggestions and based on the observations that one of it shown in Figure 5.1.

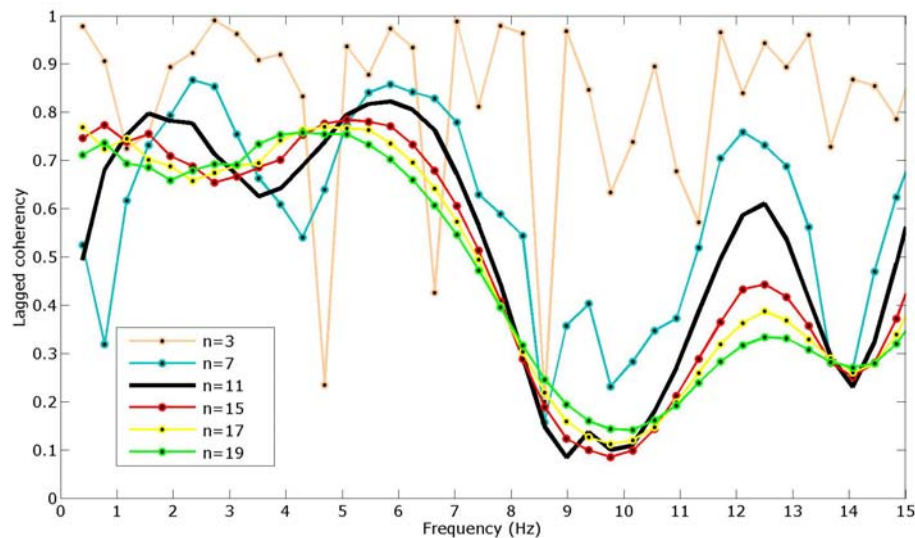


Figure 5.1. Comparison of the number of data points for Hamming window for the pair R31-R44 (September 19, 2003 earthquake)

The filter range is calculated using the Fourier Amplitude Spectrum and signal to noise ratio. This band-pass filter interval is separately detected for each data. Figure 5.2 is shown as an example of data recorded at the September 19, 2003 earthquake from the station R51. Then, S-wave window lengths are identified. After the selection of S-wave window, the data is tapered with 5 per cent cosine taper. The acceleration ground motion for ten records from only one earthquake are shown as an instance in Figure 5.3. Totally, 332 recorded data triggered by Istanbul Earthquake Rapid Response System (IERRS) is used. The coherency values are calculated for 9837 pairs.

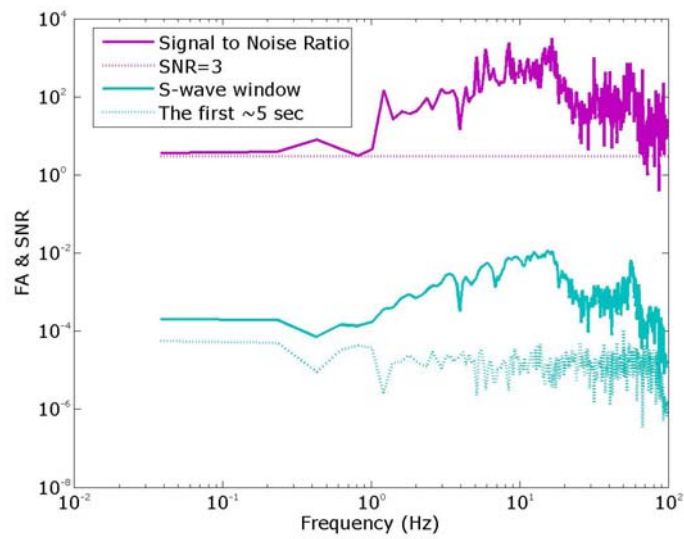


Figure 5.2. Fourier Amplitude Spectrum of the noise and signal part of the station R51 for the September 19, 2003 earthquake; and the signal to noise ratio

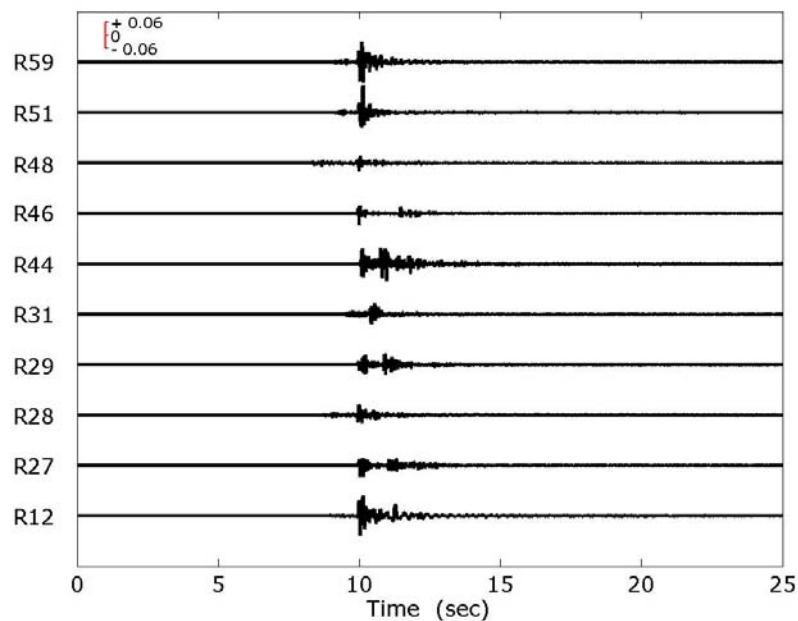


Figure 5.3. Acceleration time history (m/s^2) for ten records taken from the September, 19 2003 earthquake

5.3. Evaluation of Coherency

Let $a(\vec{r}_x, t)$ and $a(\vec{r}_y, t)$ be the selected acceleration time windows at two stations whose locations are denoted as \vec{r}_x and \vec{r}_y . Assume the duration of the time windows is

$T = N \cdot \Delta t$, which is the product of the number of data samples N and the time step Δt . The discrete form of the Fourier transform of a time window at the n^{th} frequency step ($\omega_n = n \cdot \Delta \omega$) can be first obtained as (Zerva and Zervas, 2002):

$$A_x(\omega_n) = \sqrt{\frac{\Delta t}{2\pi N}} \sum_{s=0}^{N-1} a_x(s \cdot \Delta t) \exp(-i\omega_n s \Delta t) \quad (5.4)$$

The procedure for the evaluation of the stochastic spatial variation of seismic motion from recorded data considers that the motions are realizations of space-time random fields. In order to extract valuable information from the available limited amount of data, such as the recorded time histories at the array stations during an earthquake, certain assumptions need to be made (Zerva and Zervas, 2002):

- It is assumed that the random field is homogeneous in space, *i.e.*, all stochastic descriptors of the motion (joint probability distribution functions) are functions of the separation distance between stations, but independent of absolute location. This assumption implies that the frequency content (amplitude) of the seismic motion at different recording stations does not vary significantly. Since the majority of dense instrument arrays are located on fairly uniform soil conditions, the assumption of homogeneity is valid. Significant variation in the frequency content of the motion can be expected if the stations are located at different local soil conditions (*e.g.*, one on rock and the other on alluvium).
- It is further assumed that the time histories recorded at the array stations are stationary random processes. Stationarity implies that the probability functions do not depend on the absolute time, but are functions of time differences (or time lag); in this sense, the time histories have neither beginning nor end. Although this assumption appears to be unrealistic, this is not the case: Most characteristics of seismic ground motion for engineering applications are evaluated from the strong motion shear (S) wave window, *i.e.*, a segment of the actual seismic time history. This strong motion segment from the actual time history can be viewed as a segment of an infinite time history with uniform characteristics through time, *i.e.*, a stationary process. For a stationary process, the amplitude and phase of the motion are not

functions of time. It is also assumed that the stationary time histories at the recording stations are ergodic. A stationary process is ergodic, if averages taken along any realization of the process are identical to the ensemble averages, *i.e.*, the information contained in each realization is sufficient for the full description of the process.

5.3.1. Cross Spectral Density

The means of the cross spectral density of the data recorded at two stations (locations) on the ground surface is described by the random field of seismic ground motion (accelerations).

The discrete-form smoothed cross spectrum is:

$$S_{xy}(\omega_n) = \sum_{m=-M}^M W(m \cdot \Delta\omega) (A_x(\omega_n + m \cdot \Delta\omega)) (A_y^*(\omega_n + m \cdot \Delta\omega)) \quad (5.5)$$

in which * indicates complex conjugate, the frequency step $\Delta\omega$ is equal to $2\pi/T$, and $W(\omega)$ denotes spectral smoothing windows.

5.3.2. Power Spectral Density

The power spectral densities of the motion (ie, $x=y$) are estimated from the analysis of the data recorded at each station and are commonly referred to as point estimates of the motion:

$$S_{xx}(\omega_n) = \sum_{m=-M}^M W(m \cdot \Delta\omega) |A_x(\omega_n + m \cdot \Delta\omega)|^2 \quad (5.6)$$

Based on the smoothed power spectra and cross-spectrum, the corresponding coherency function can then be calculated with Equation (5.1). With the coherency spectrum estimates, the corresponding coherency model parameters can be further determined via least-squares fitting schemes (Harichandran and Vanmarcke, 1986; Hao *et*

al., 1989; Abrahamson *et al.*, 1991). In addition to acceleration time histories, the velocity and displacement time histories can also be used for coherency estimation in accordance with the availability of the data. Theoretically, the coherency functions obtained from acceleration, velocity and displacement time histories are the same; nevertheless, there are minor differences between the estimated coherency functions due to the different dominant frequency ranges and the smoothing operations, but the general trend is similar in all cases (Zerva and Zervas, 2002).

5.3.3. Coherency

For the calculation of the coherency values, a code is written in MATLAB software. Firstly, data taken from Event 5 triggered by SMART-1 array are used for the verification of the code. The calculated coherencies based on the SMART-1 data are compared with the results from the reference (Zerva and Zervas, 2002) that used the same data for the calculation of coherency. As illustrated in Figure 5.4 and Figure 5.5, results are almost identical.

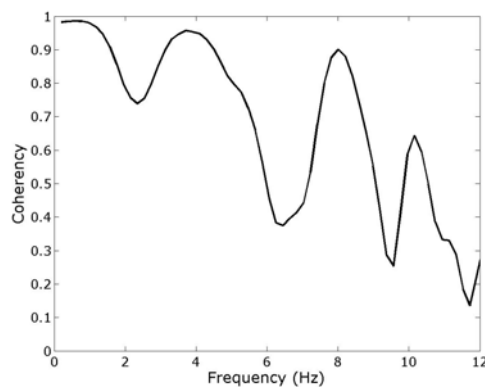


Figure 5.4. The lagged coherency between stations I06 and I12 recorded by SMART-1 (this study)

After the substantiation of the code, the coherency values for the seven events were calculated for the different distance bins using Equation (5.1). But the June, 24 2004 earthquake is eliminated because of the irregular shape of coherency values.

The coherency values are calculated using the data from east-west; north-south; radial; and transversal directions considering both 11- and 15- point hamming windows.

Seven distance bins are used. The bins are: Less than 2.0 km; between 2.0 and 2.5 km; between 2.5 and 3.0 km; between 3.0 and 3.5 km; between 3.5 and 4.0 km; between 4.0 and 4.5 km; and between 4.5 and 5.0 km. The coherencies are averaged in each distance bins. In Figure 5.6; (a), (b), (c), (d), (e), (f), and (g) demonstrate the coherency values for these distance bins for the September, 29 2004 earthquake. The demonstrated values are calculated for the east-west component using 11-point hamming window. The average values for all bins are shown in Figure 5.6 (h). In Figure 5.7, the computed average coherency values are illustrated for different directions and smoothing window lengths. The coherencies of east-west component of the data using 11-point hamming window show more appropriate distribution with distance and frequency than the others. Hereafter, these values are used.

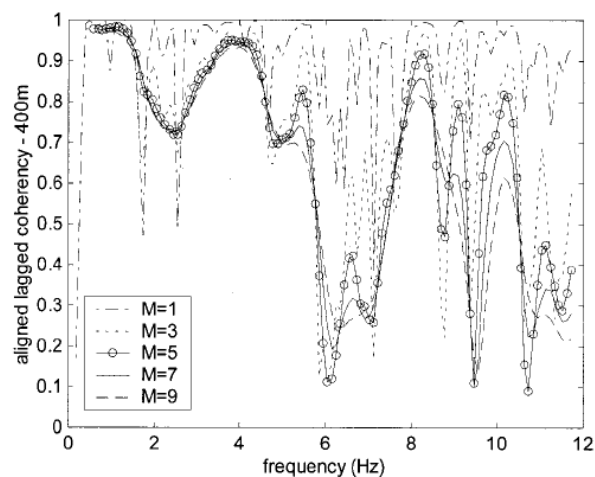


Figure 5.5. The lagged coherency between stations I06 and I12 recorded by SMART-1 (Zerva and Zervas, 2002)

The coherency values computed using data from the September 19, 2003 earthquake; the May 16, 2004; the October 20, 2006 earthquake; the October 24, 2006; and the March 12, 2008 earthquake are shown in Figure 5.8 to Figure 5.17.

The coherencies changing with both distance and frequency in 3-D are represented in Figure 5.18. The coherency values for all data generally increase for the lowest separation distance and frequency, as expected. Only the data from the September 19, 2003 earthquake show more or less a mixed distribution due to the lack of recorded data at the moment.

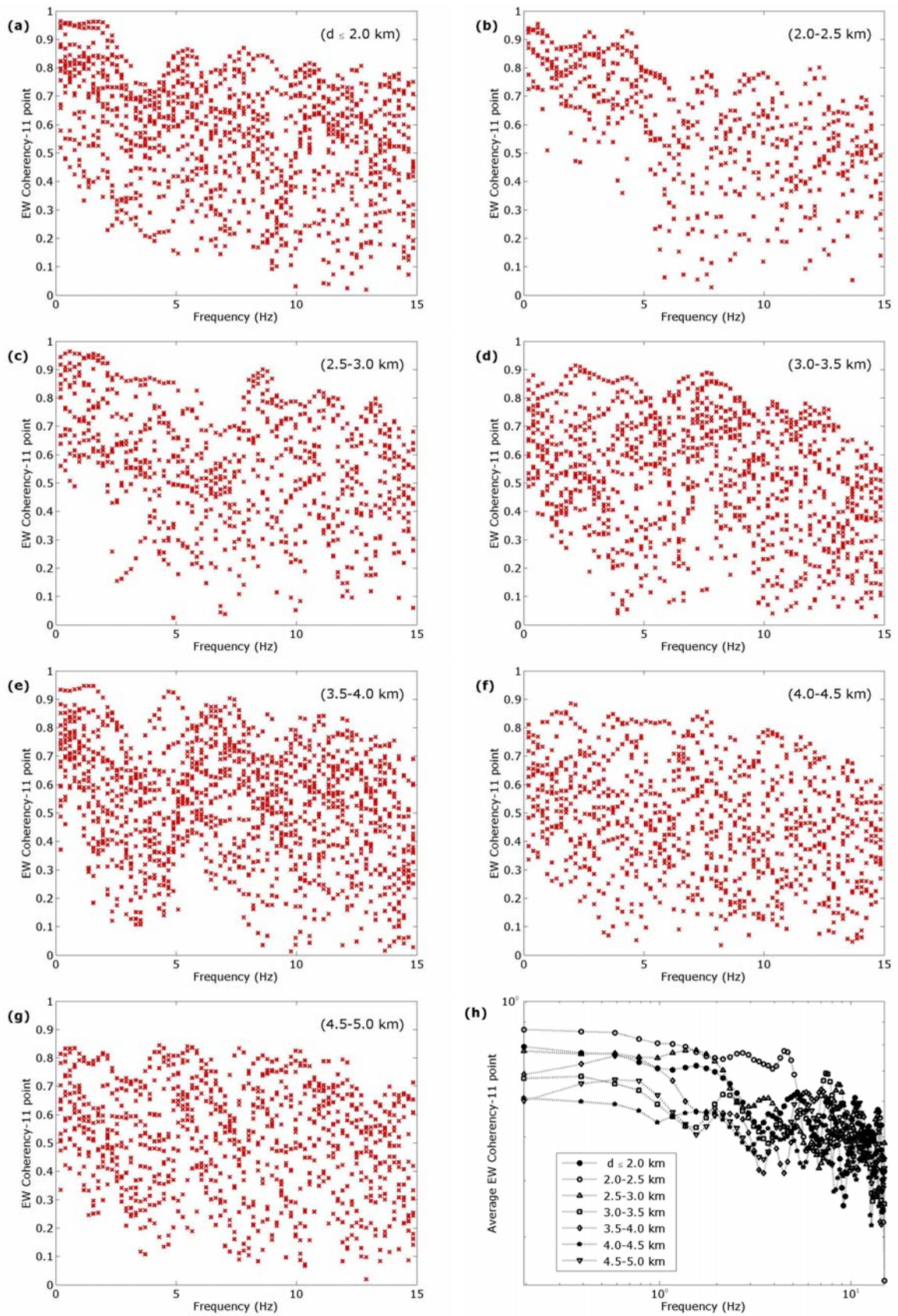


Figure 5.6. Coherency values for each distance bins and average coherency values for EW direction (11-point) –September 29, 2004 earthquake

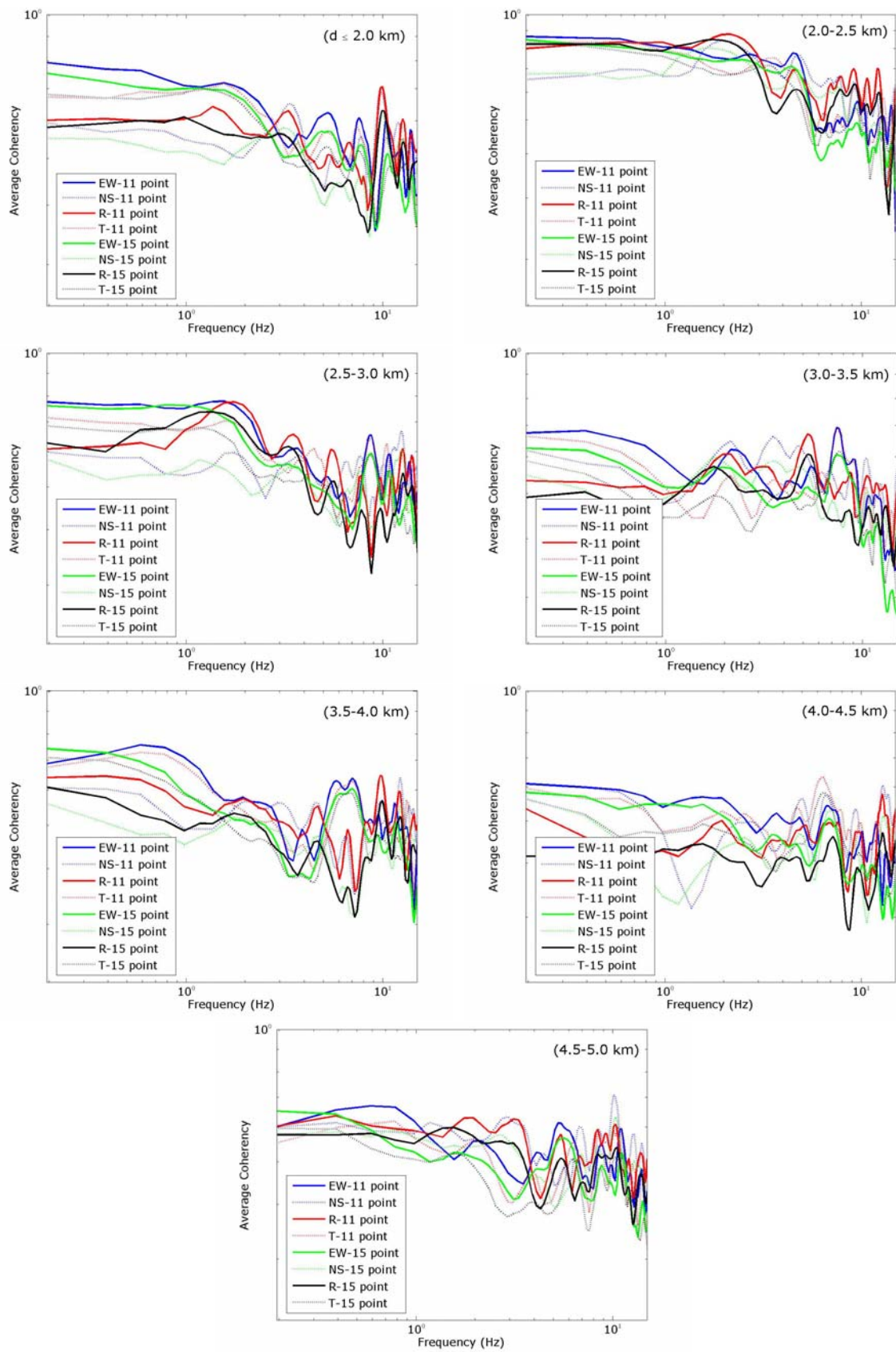


Figure 5.7. Average coherency values of each distance bins with respect to direction and smoothing window length –September 29, 2004 earthquake

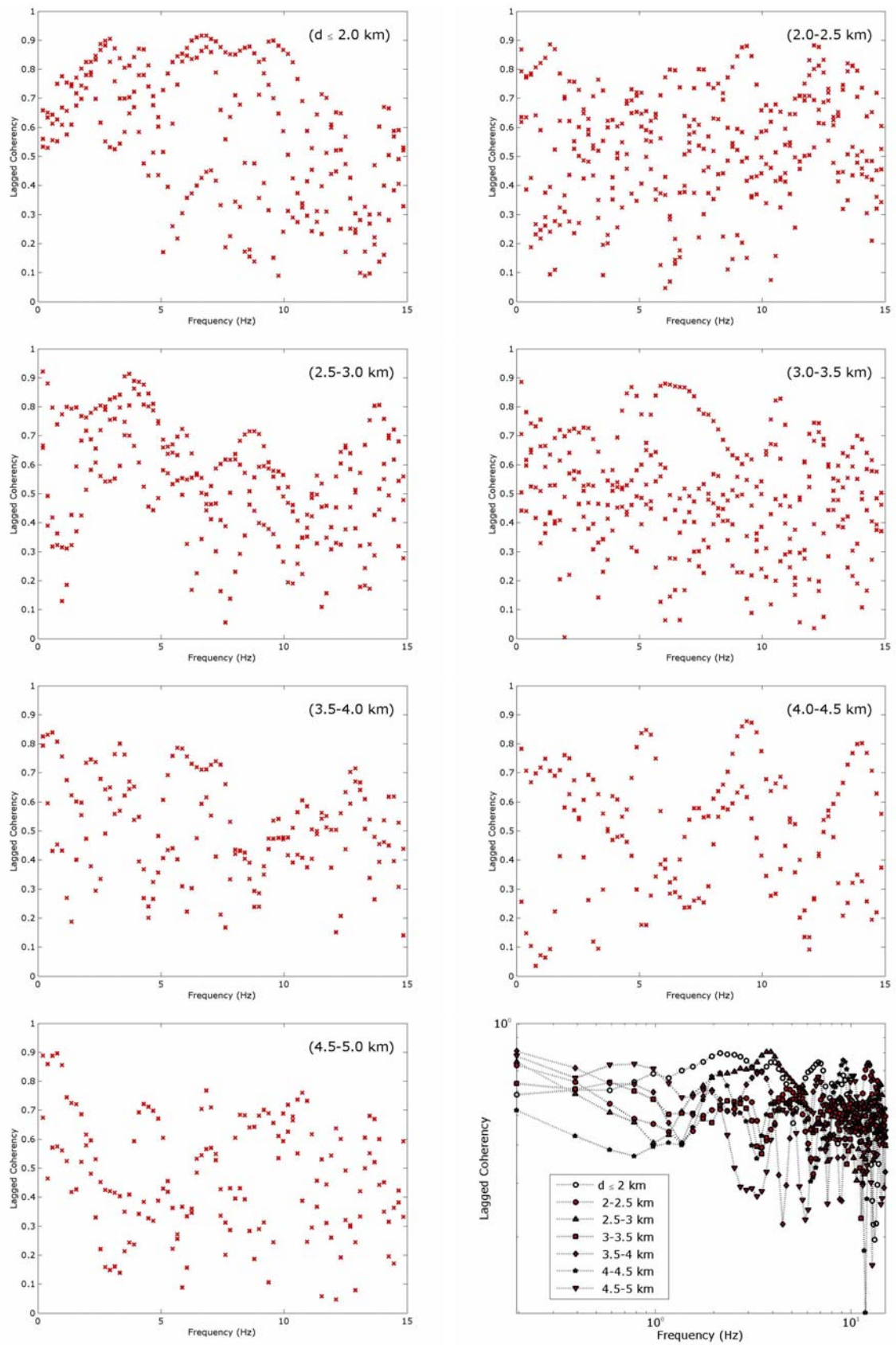


Figure 5.8. Coherency values for each distance bins and average coherency values for EW direction (11-point) – September 19, 2003 earthquake

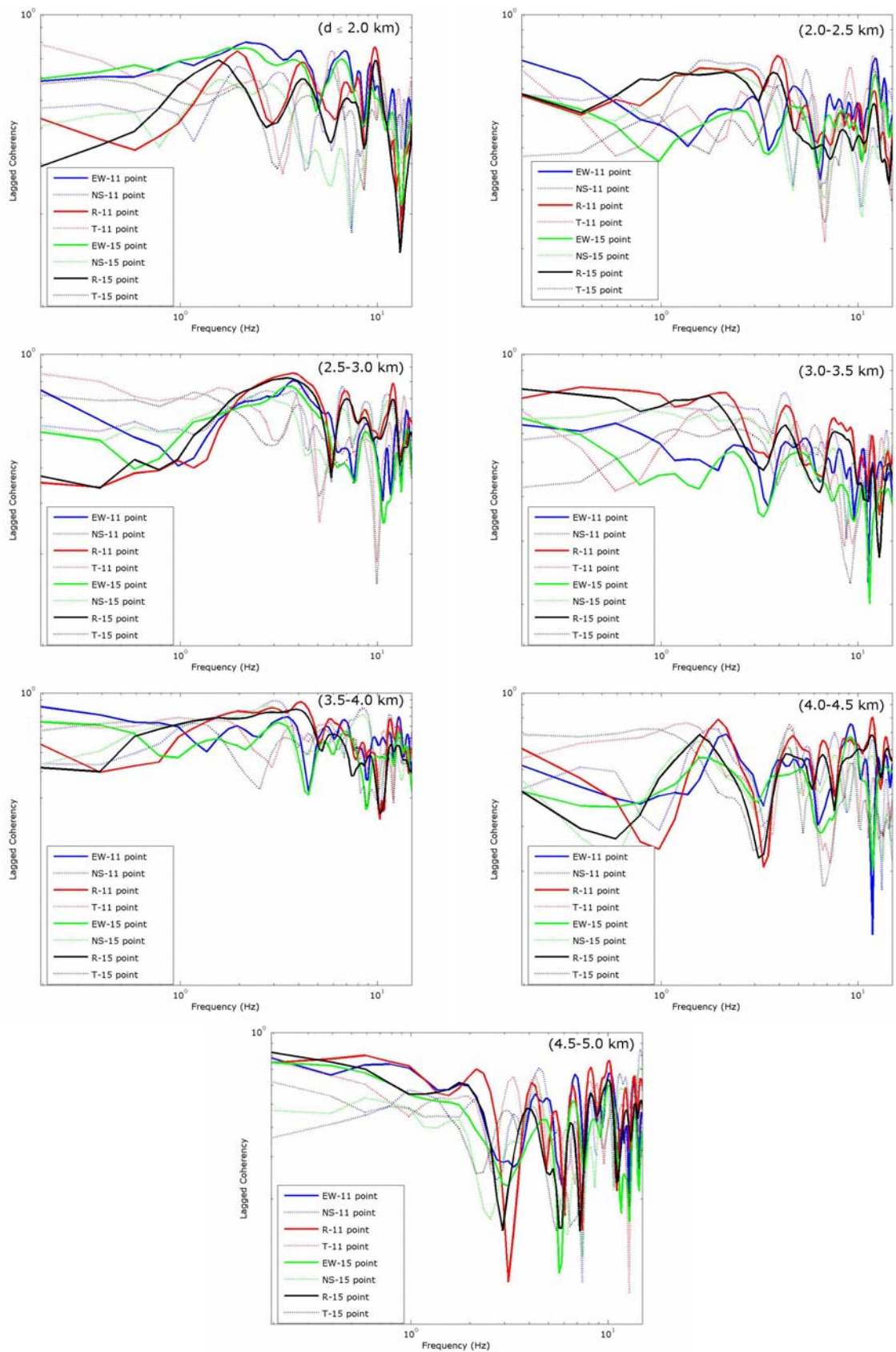


Figure 5.9. Average coherency values of each distance bins with respect to direction and smoothing window length – September 19, 2003 earthquake

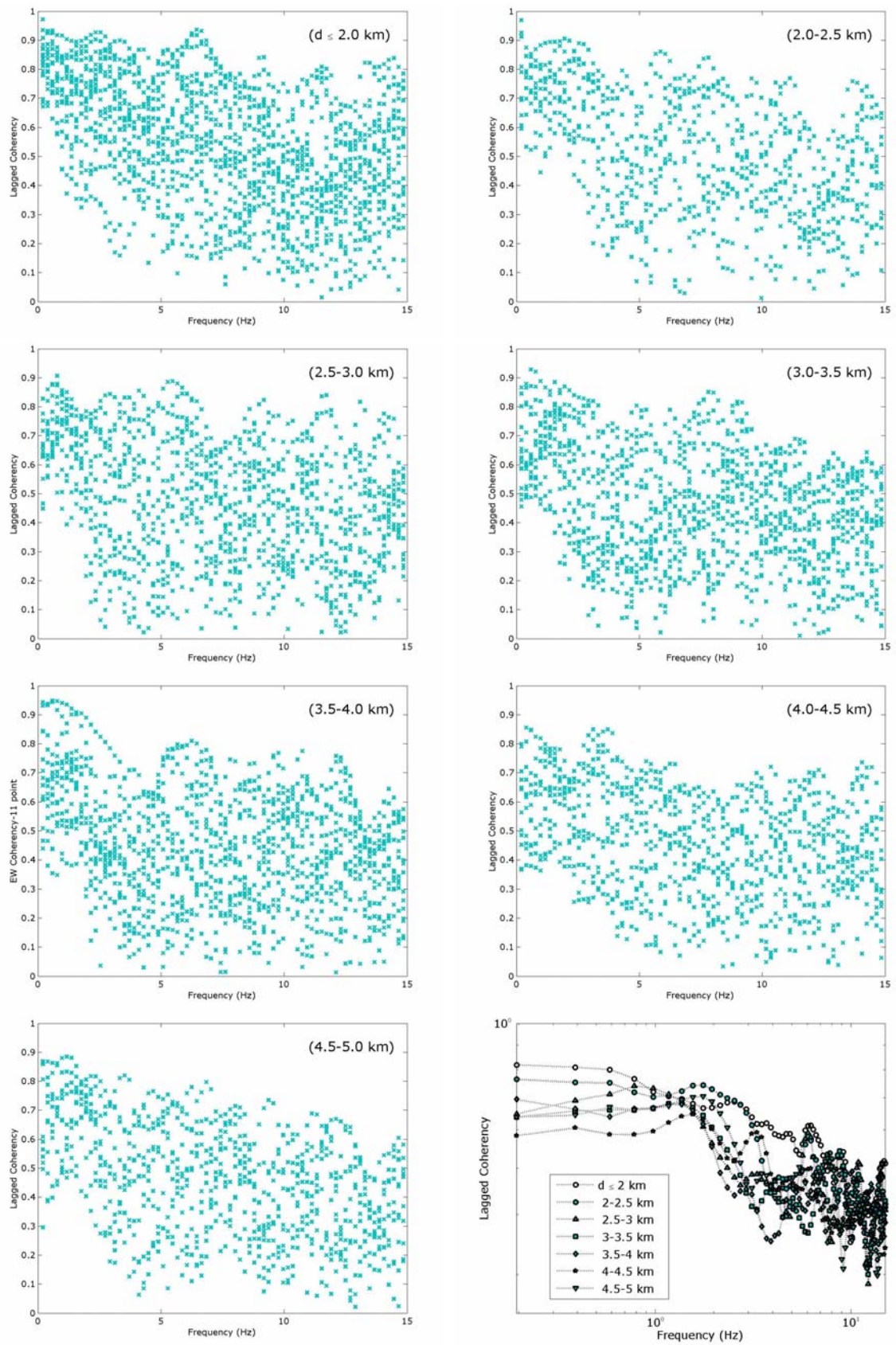


Figure 5.10. Coherency values for each distance bins and average coherency values for EW direction (11-point) – May 16, 2004 earthquake

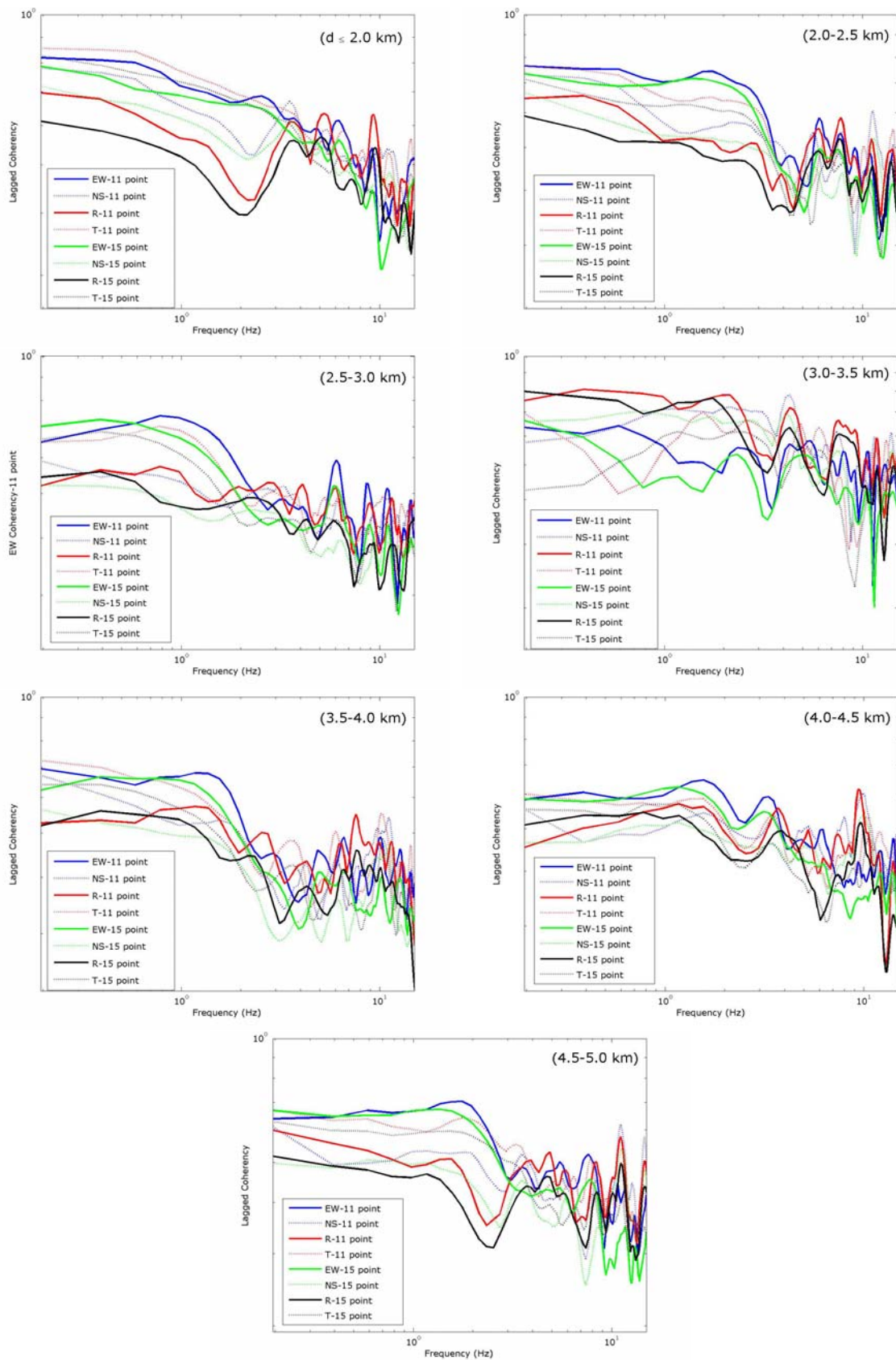


Figure 5.11. Average coherency values of each distance bins with respect to direction and smoothing window length – May 16, 2004 earthquake

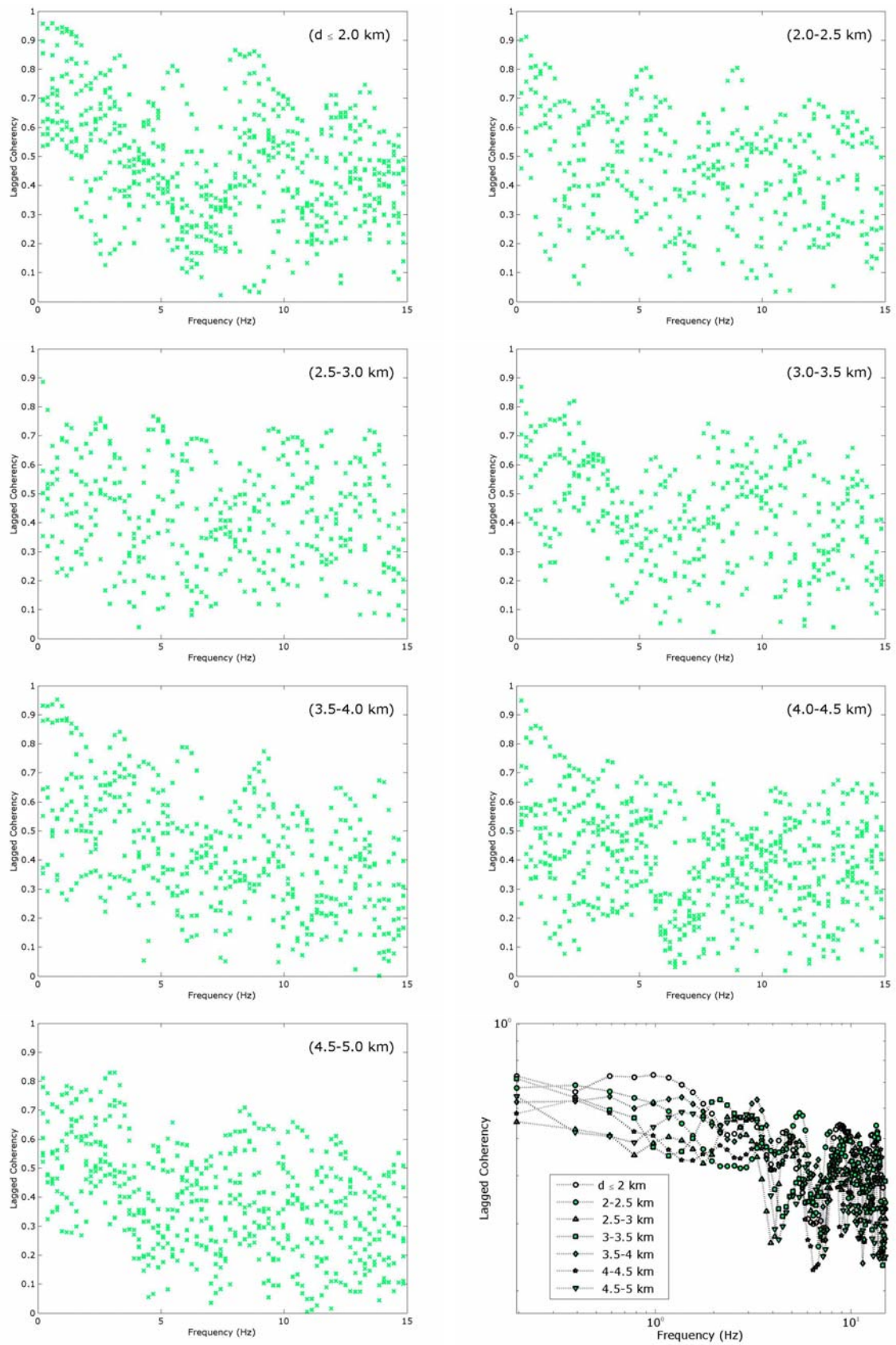


Figure 5.12. Coherency values for each distance bins and average coherency values for EW direction (11-point) – October 20, 2006 earthquake

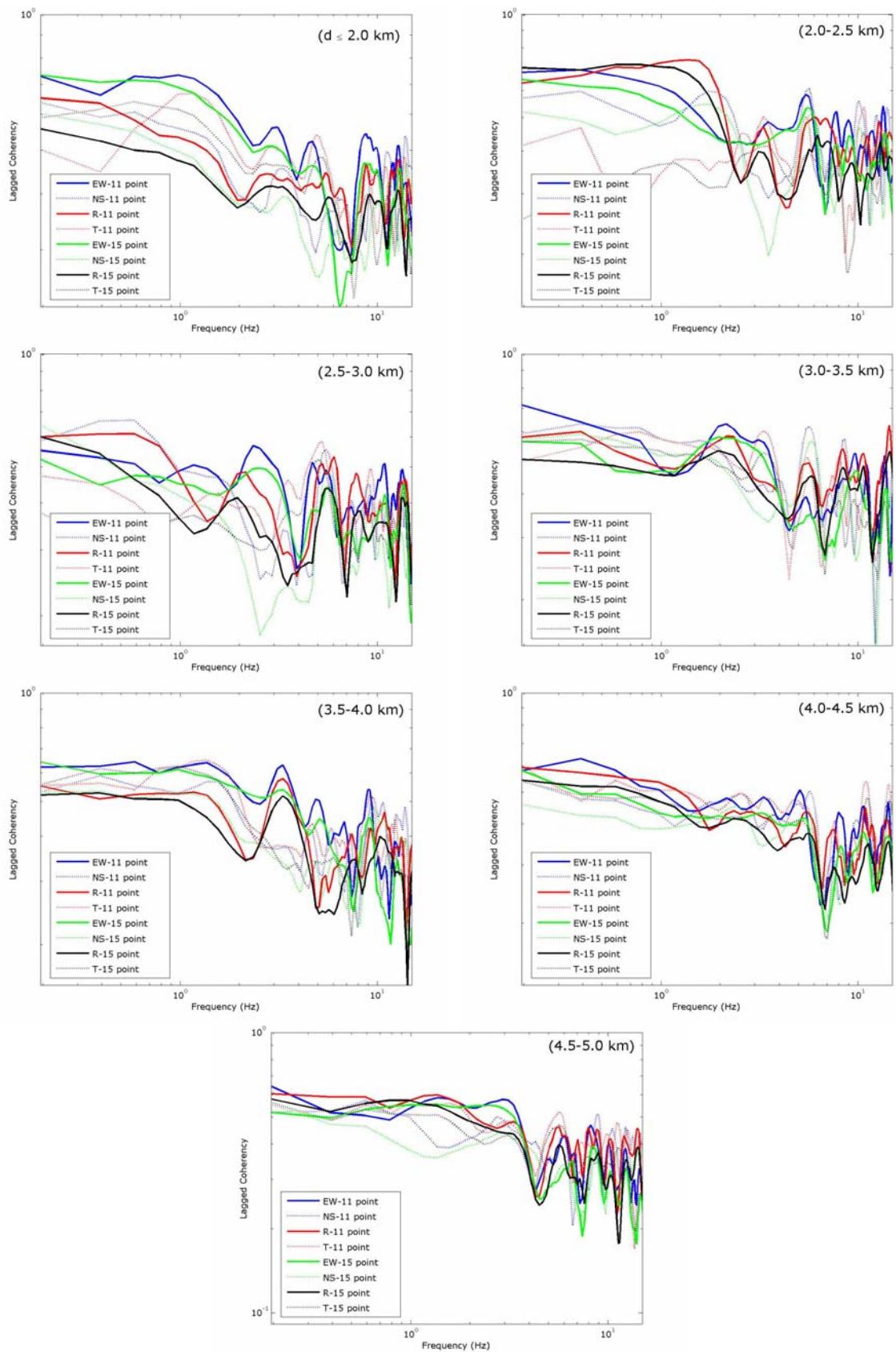


Figure 5.13. Average coherency values of each distance bins with respect to direction and smoothing window length – October 20, 2006 earthquake

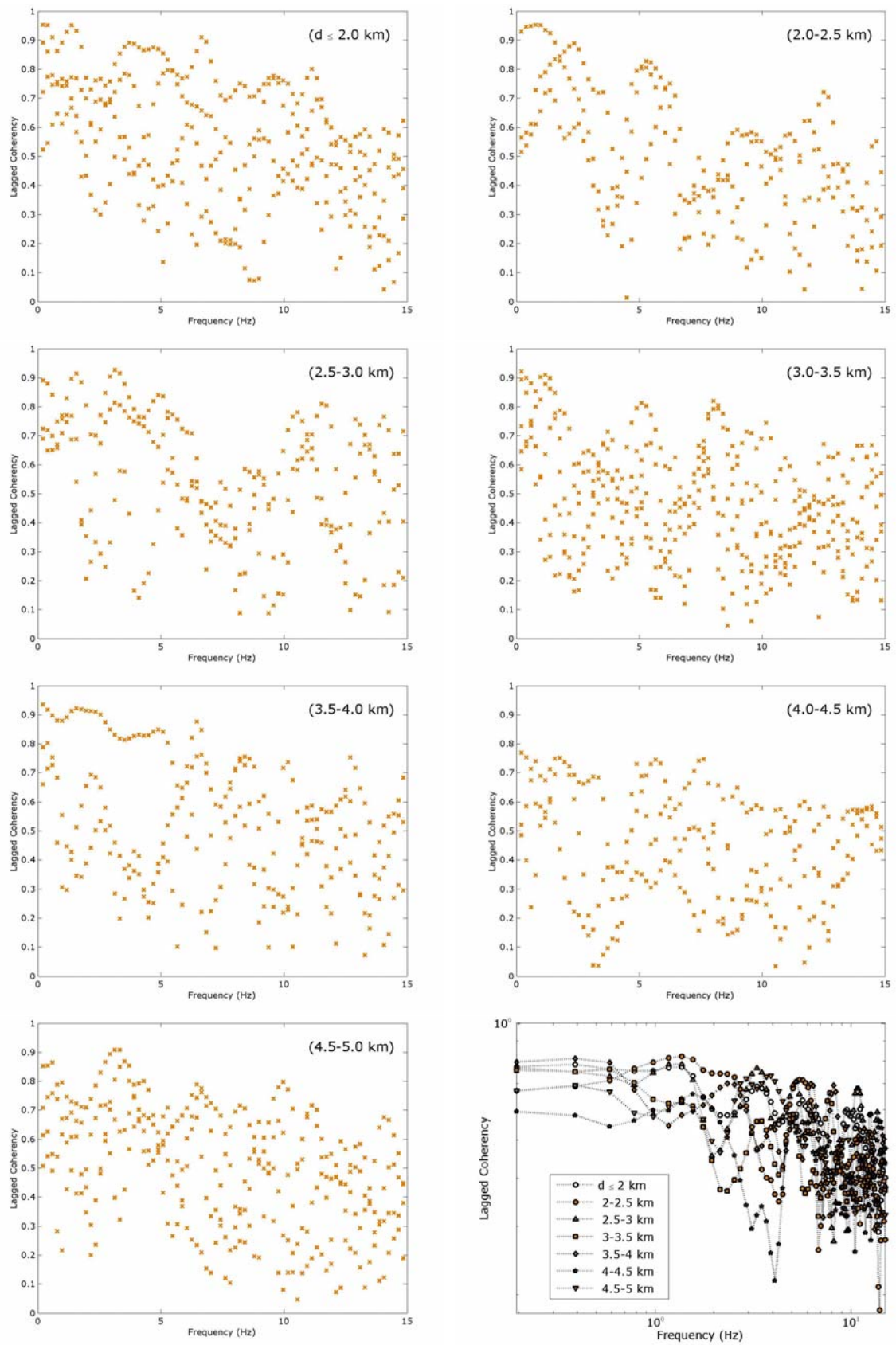


Figure 5.14. Coherency values for each distance bins and average coherency values for EW direction (11-point) – October 24, 2006 earthquake

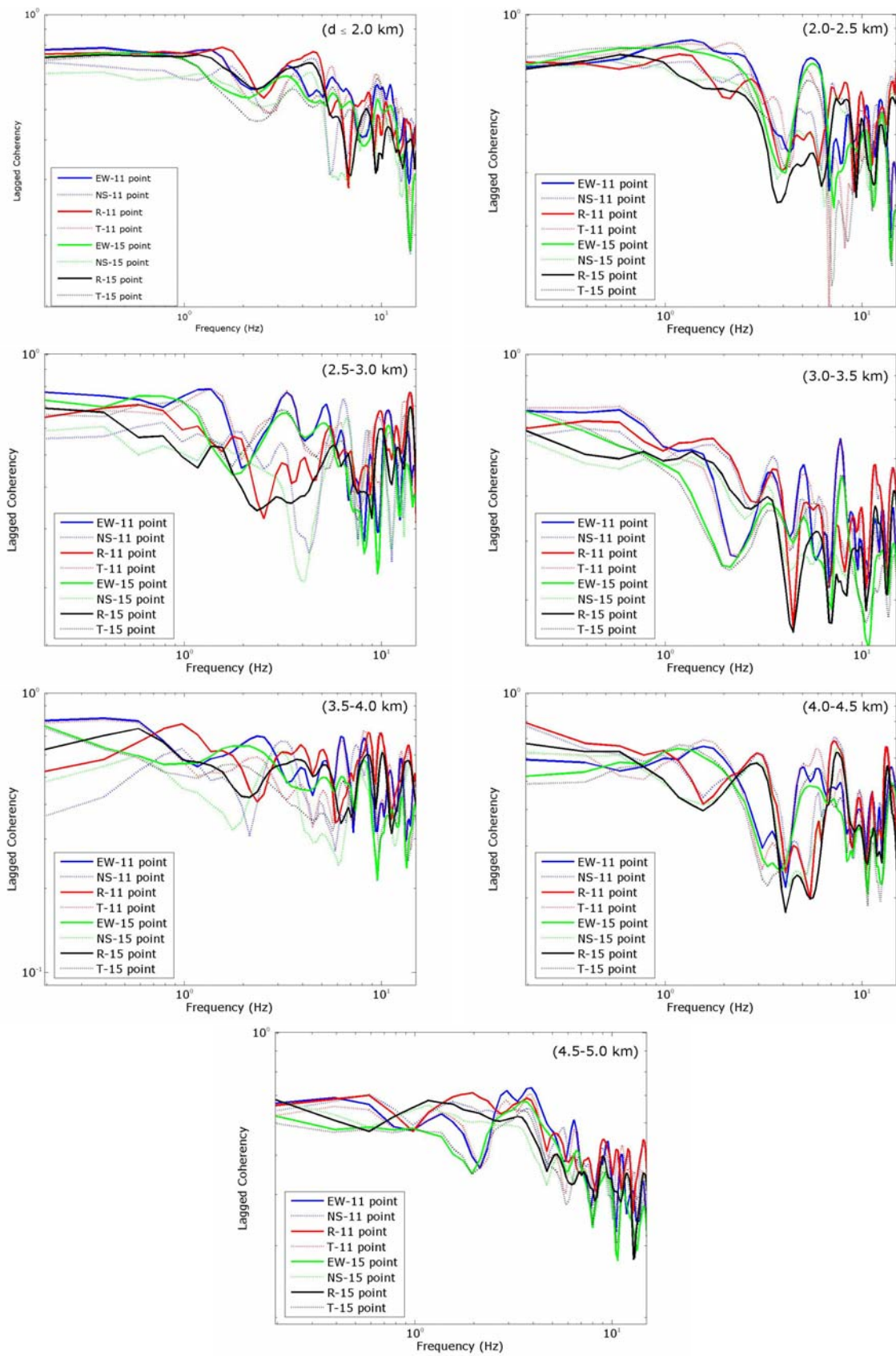


Figure 5.15. Average coherency values of each distance bins with respect to direction and smoothing window length – October 24, 2006 earthquake

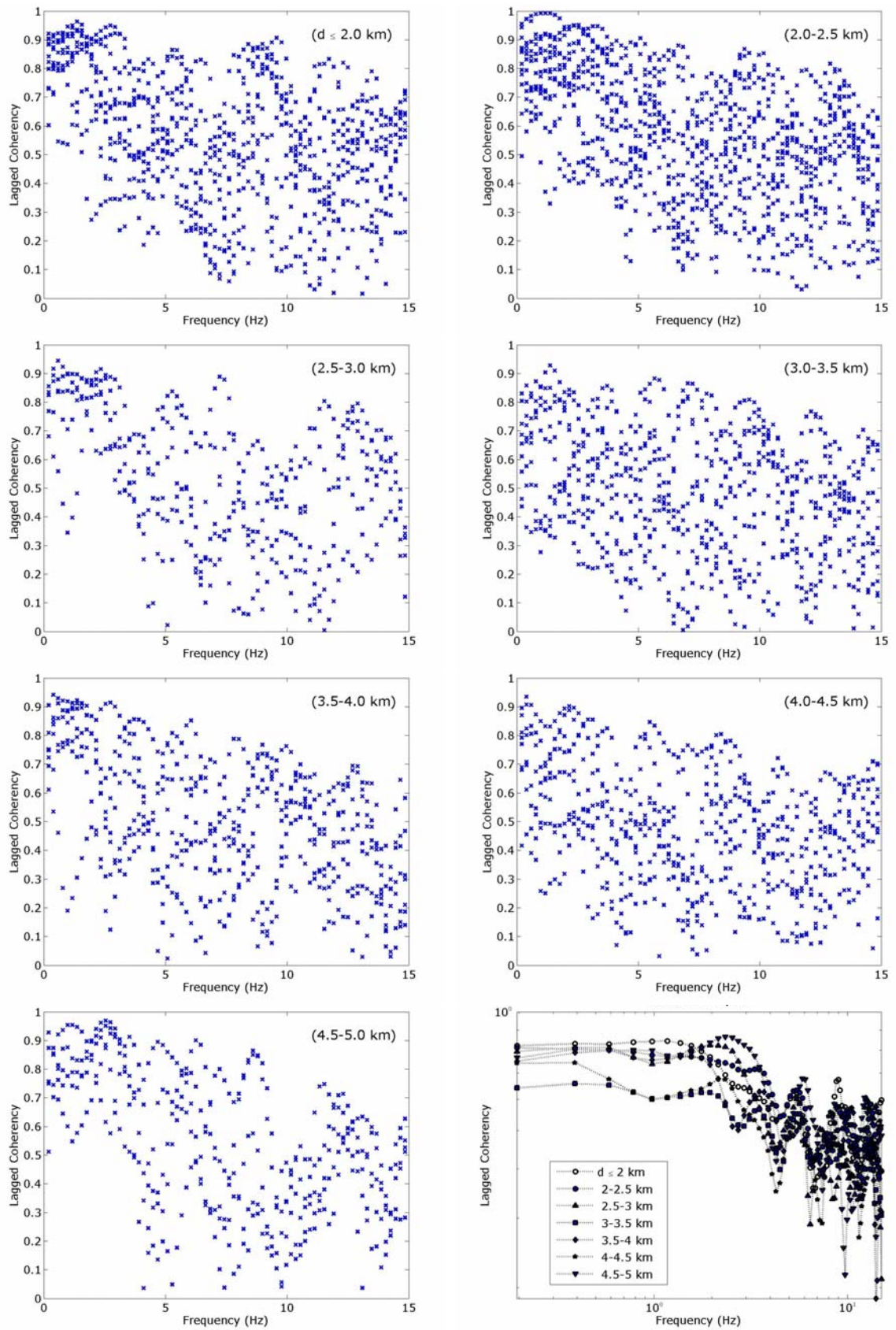


Figure 5.16. Coherency values for each distance bins and average coherency values for EW direction (11-point) – March 12, 2008 earthquake

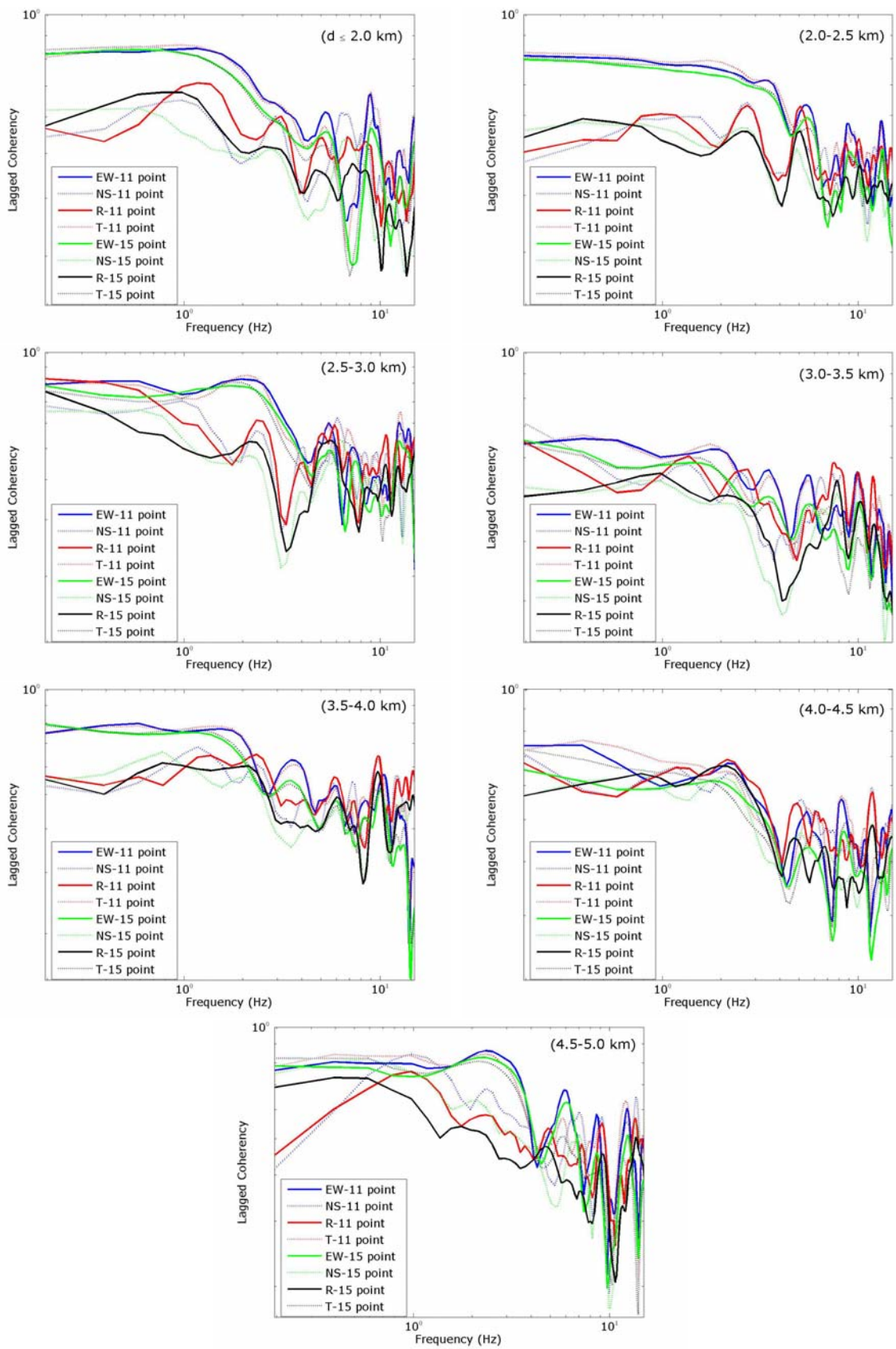


Figure 5.17. Average coherency values of each distance bins with respect to direction and smoothing window length – March 12, 2008 earthquake

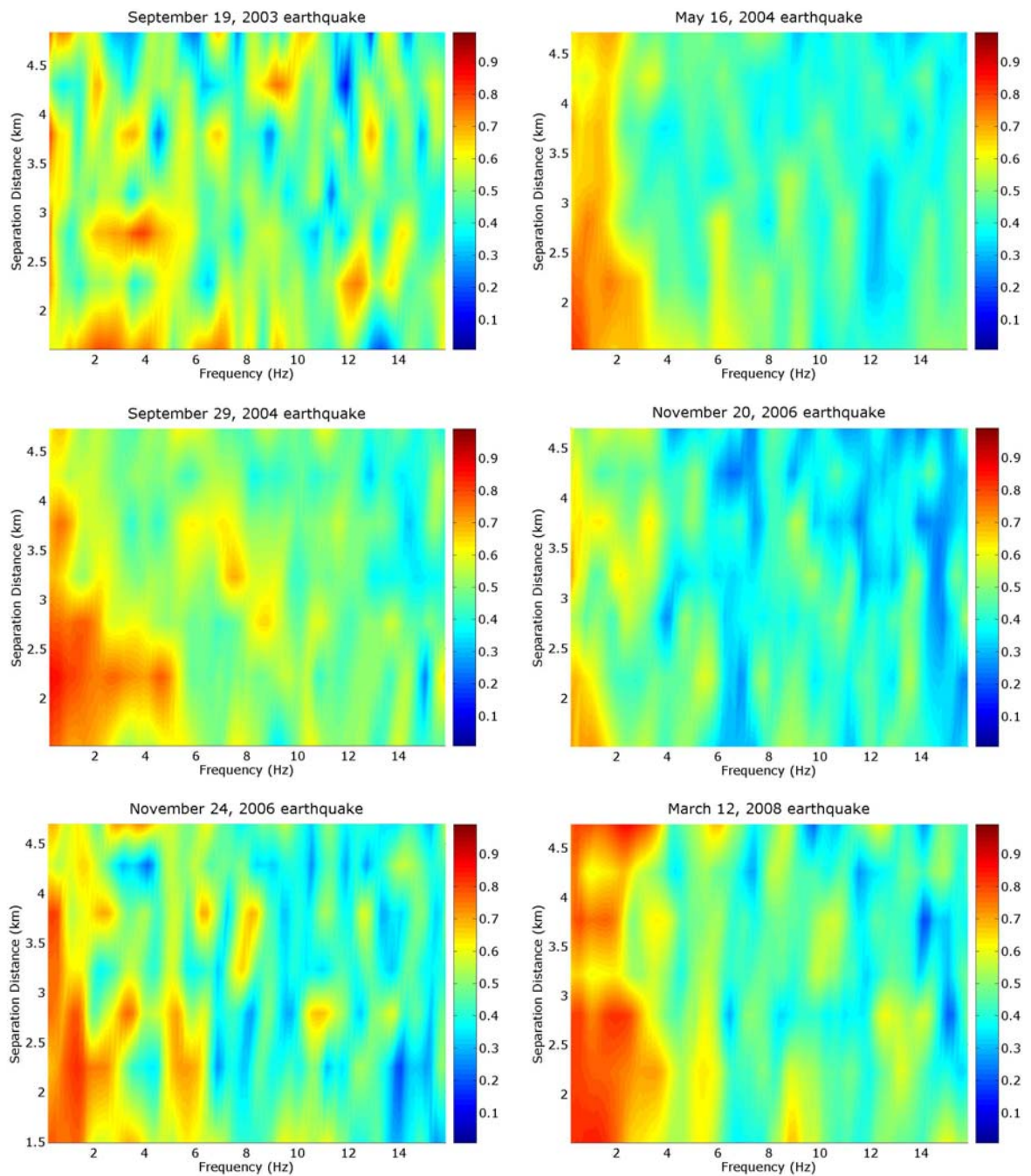


Figure 5.18. Average coherency values of six earthquakes recorded by IERRS with respect to separation distance and frequency

From another perspective, the coherencies are arranged with respect to the earthquake source, in other words, direction of the wave propagation to search a relation between the coherencies and orientation. Eventually, there was no relation between wave propagation and the coherency for data taken from aforementioned seven earthquakes.

5.4. Spatial Variability Models

5.4.1. Introduction

A mathematical description for the coherency was first introduced in earthquake engineering by Novak and Hindy in 1979. The expression, originally based on wind engineering, was:

$$|\gamma(\xi, \omega)| = \exp\left[-\kappa\left(\frac{\omega\xi}{V_s}\right)\right] \quad (5.7)$$

where, κ and ν are constants and V_s is an appropriate shear wave velocity. It should also be noted that Novak and Hindy presented the first stochastic analysis of a lifeline system (buried pipeline) subjected to seismic motion experiencing loss of coherence. Prior to this time only the propagation property of the motion was considered in deterministic analysis of lifelines, with the exemption of the work of Bogdanoff *et al.* (1961) who considered random earthquake type excitations and Sandi, 1970, who presented a stochastic analysis of lifeline response to non-synchronous seismic motion. After the installation of strong motion arrays, in particular, the SMART-1 array, the stochastic description of the seismic motion and the stochastic response analysis of lifelines have been extensively investigated by researchers.

5.4.2. Empirical Coherency Models

Because of 1) the variability in seismic data recorded at different sites and during different events; 2) the differences in the numerical processing of the data used by various investigators; and 3) the different functional forms used in the regression fitting of a function through data with large scatter, there is a multitude of spatial variability expressions in the literature. The procedures for the removal of the wave passage effects in lagged coherency estimates also vary: some procedures evaluate coherency directly from the data, some remove the apparent propagation effects first and then evaluate the coherency, while others align the data before the coherency is estimated. Some of the

expressions developed for the description of the coherency of the seismic ground motion at the SMART-1 array are presented in the following:

Loh (1985):

$$|\gamma(\xi, \omega)| = \exp(-a(\omega)|\xi|) \quad (5.8)$$

Loh and Yeh (1988):

$$|\gamma(\xi, \omega)| = \exp\left(-a \frac{\omega |\xi|}{2\pi c}\right) \quad (5.9)$$

Loh and Lin (1990):

$$|\gamma(\xi, \omega)| = \exp\left((-a_1 - b_1\omega^2)|\xi \cos\theta|\right) \exp\left((-a_2 - b_2\omega^2)|\xi \sin\theta|\right) \quad (5.10)$$

Hao *et al.* (1989), and Oliveira *et al.* (1991):

$$|\gamma(\xi_1, \xi_t, \omega)| = \exp(-\beta_1|\xi_1| - \beta_2|\xi_t|) \times \exp\left[-\left(\alpha_1(\omega)\sqrt{|\xi_1|} + \alpha_2(\omega)\sqrt{|\xi_t|}\right) \times \left(\frac{\omega}{2\pi}\right)^2\right] \quad (5.11)$$

Abrahamson *et al.* (1990):

$$\tanh^{-1}[\gamma(\xi, \omega)] = (2.54 - 0.012\xi) \times \left\{ \exp[(-0.115 - 0.00084\xi)\omega] + \frac{\omega^{-0.878}}{3} \right\} + 0.35 \quad (5.12)$$

5.4.3. Semi-empirical Models

Semi-empirical models for the spatial variation of the seismic ground motion, *i.e.*, models for which their functional form, are based on analytical considerations but their parameter evaluation requires recorded data.

Somerville *et al.* (1988) proposed a model that attributes the spatial variation of the motion to the wave propagation effect, the finite source effect, the effect of scattering of the seismic waves as they propagate from the source to the site, and the local site effects. It has been shown, however, from data analyses and seismological observations, that earthquake magnitude may not particularly influence coherency estimates.

Spudich (1994) gives a possible explanation for the reason why the source finiteness may not significantly affect coherency estimates: For large earthquakes of unilateral rupture propagation, the waves radiating from the source originate from a spatially compact region that travels with the rupture front, and, thus, at any time instant, a relatively small fraction of the total rupture area radiates. Unilateral rupture at the source constitutes the majority of earthquakes

Der Kiureghian (1996) developed a stochastic model in which the total spatial variation of the seismic motion is composed of terms corresponding to wave passage effects, bedrock motion coherence effects, and site response contribution; in the model evaluation,

Zerva and Harada (1997) introduced a semi-empirical model for the coherency that approximates the site topography by a horizontally extended layer with random characteristics overlaying a half-space (bedrock).

Perhaps the most quoted coherency model was introduced by Luco and Wong (1986), and is based on the analysis of shear waves propagating a distance R through a random medium:

$$\left| \gamma(\xi, \omega) = \exp \left[- \left(\frac{R}{r_0} \right) \left(\frac{\mu \omega \xi}{v_{rm}} \right)^2 \right] \right| \quad (5.13)$$

where **Error! Bookmark not defined.** v_{rm} is an estimate for the elastic shear wave velocity in the random medium, r_0 the scale length of random inhomogeneities along the path, and μ^2 a measure of the relative variation of the elastic

properties in the medium. Luco and Wong's model also considers that the exponential decay with separation distance and frequency is the same.

5.4.4. Development of the Coherency Model for Istanbul

The decay of the coherency calculated from the data recorded by IERRS suggests that the frequency decay is approximately exponential. Therefore, the following initial coherency model is selected:

$$|\gamma(d, f)| = a_1 + e^{-(a_2 \cdot d)^2} + e^{-(a_3 \cdot f)^2} \quad (5.14)$$

where a_1 , a_2 , and a_3 are constants; d is the station separation distance; f is the frequency content. The least-squares regression of the coherency on frequency by distance bin yields parameters a_1 , a_2 , and a_3 . The analysis has done for eight cases: East west directions of coherency values using 11- and 15- point hamming; Radial and transversal directions of coherency values using 11- and 15- point hamming. Equation (5.14) does not match for all data and the each earthquake, especially considering the distance variable.

As an alternative to Equation (5.14), a new model is improved:

$$|\gamma(d, f)| = a_1 + \left(\frac{a_2}{d} \right) \left(e^{-(a_3 \cdot d)^2} + e^{-(a_4 \cdot f)^2} \right) \quad (5.15)$$

In this formula, due to the irregularities of coherency values with respect to distance, the parameter a_3 which related to distance, does not converge, listed in Table 5.1.

Table 5.1. Regression coefficients based on Equation (5.15) for East-West direction of the earthquakes data recorded by IERRS (11-point)

	2003.09.19 earthquake	2004.05.16 earthquake	2004.09.29 earthquake	2006.10.20 earthquake	2006.10.24 earthquake	2008.03.12 earthquake	All data
a₁	0.4369	0.4238	0.4762	0.3846	0.4298	0.4551	0.440
a₂	0.3951	0.6719	0.5082	0.5497	0.5888	0.062	0.564
a₃	508.6517	17.4640	-43.7637	-1.2550	2177.3574	108.9232	35.239
a₄	0.0999	0.2577	0.1899	0.2887	0.1845	0.2569	0.214

By the elimination of the uncorrelated parameter a_3 , the coherency formula becomes:

$$|\gamma(d, f)| = a_1 + \left(\frac{a_2}{d}\right) \left(e^{-(d)^2} + e^{-(a_3 \cdot f)^2} \right) \quad (5.16)$$

The coefficients for East-West directions are listed in Table 5.2. The coefficients for eight cases (*i.e.* East west directions of coherency values using 11- and 15- point hamming; Radial and transversal directions of coherency values using 11- and 15- point hamming) are correlates well with each other. Therefore, the coefficients calculated from the coherency values of East-West directions using 11-point hamming window, will be considered as a result.

Table 5.2. Regression coefficients based on Equation (5.16) for East-West directions of the earthquakes data recorded by IERRS (11-point)

	2003.09.19	2004.05.16	2004.09.29	2006.10.20	2006.10.24	2008.03.12	All
	earthquake	earthquake	earthquake	earthquake	earthquake	earthquake	data
a₁	0.4451	0.4224	0.4788	0.3829	0.4320	0.4528	0.4398
a₂	0.3681	0.6623	0.4765	0.5273	0.5428	0.7463	0.5373
a₃	0.1099	0.2809	0.2070	0.2931	0.1963	0.2624	0.2272

When the separation distance is taken as zero or almost zero, the coherency values should be one or close to one. Equation (5.15) and Equation (5.16) have an inverse separation distance parameter that causes not to provide aforementioned rule when the separation distance considered as zero. That's why, a new equation related to Equation (5.16) needs to be developed. The frequency and distance variables are considered for both exponential terms in the formula. The equation is expressed as

$$|\gamma(d, f)| = a_1 e^{(a_2 - a_3 \sqrt{f})d} + (1 - a_1) e^{(-a_4 - a_5 f^2)d^2} \quad (5.17)$$

Again, regression analyses are done for six earthquakes, separately. The results are listed in Table 5.3. The last column of Table 5.3 represents the results of the regression analysis done for whole data containing all coherency values taken from six earthquakes.

It is seen that these five parameters, a_1 , a_2 , a_3 , a_4 , and a_5 , are close to each other for every event and whole data.

Table 5.3. Regression coefficients based on Equation (5.17) for East-West directions of the earthquakes data recorded by IERRS (11-point)

	2003.09.19	2004.05.16	2004.09.29	2006.10.20	2006.10.24	2008.03.12	All
	earthquake	earthquake	earthquake	earthquake	earthquake	earthquake	data
a_1	0.5298	0.4813	0.5620	0.4708	0.4702	0.5023	0.5130
a_2	0.0253	0.0867	0.4155	0.0777	0.1071	0.1320	0.0781
a_3	0.0170	0.0399	0.0263	0.0446	0.0398	0.0517	0.0380
a_4	0.3795	0.1925	0.1444	0.3081	0.2137	0.1926	0.2643
a_5	0.0067	0.0233	0.0409	0.1000	0.0248	0.0302	0.0301

5.4.5. Regression Results

For each earthquake, the coherency values are grouped into seven separation distance ranges as discussed previous section. The mean of the coherency are computed for each earthquake at frequencies up to 100 Hz. The mean coherencies are shown in Figure 5.19. The derived coherency functions (Equation (5.17)) as a function of frequency are plotted in the same figure for each separation distance groups.

For each earthquake, the residuals of Equation (5.17) are computed. The mean residuals of these earthquakes are plotted in Figure 5.20 for seven separation distance bins. The mean residual are reasonable for the derived coherency function but any systematic trends do not appear in the residuals.

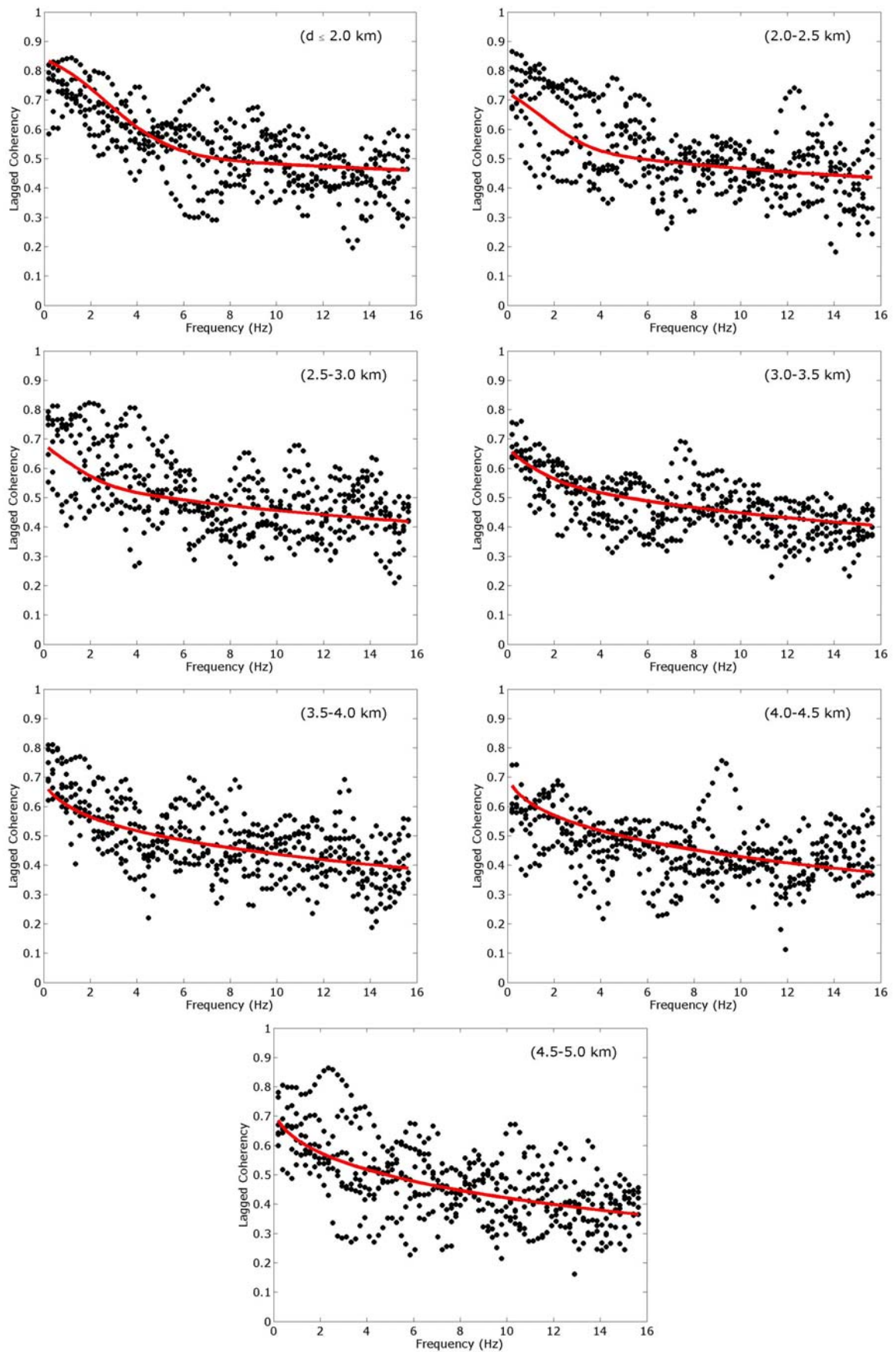


Figure 5.19. The derived coherency model for each distance bins using all earthquake data

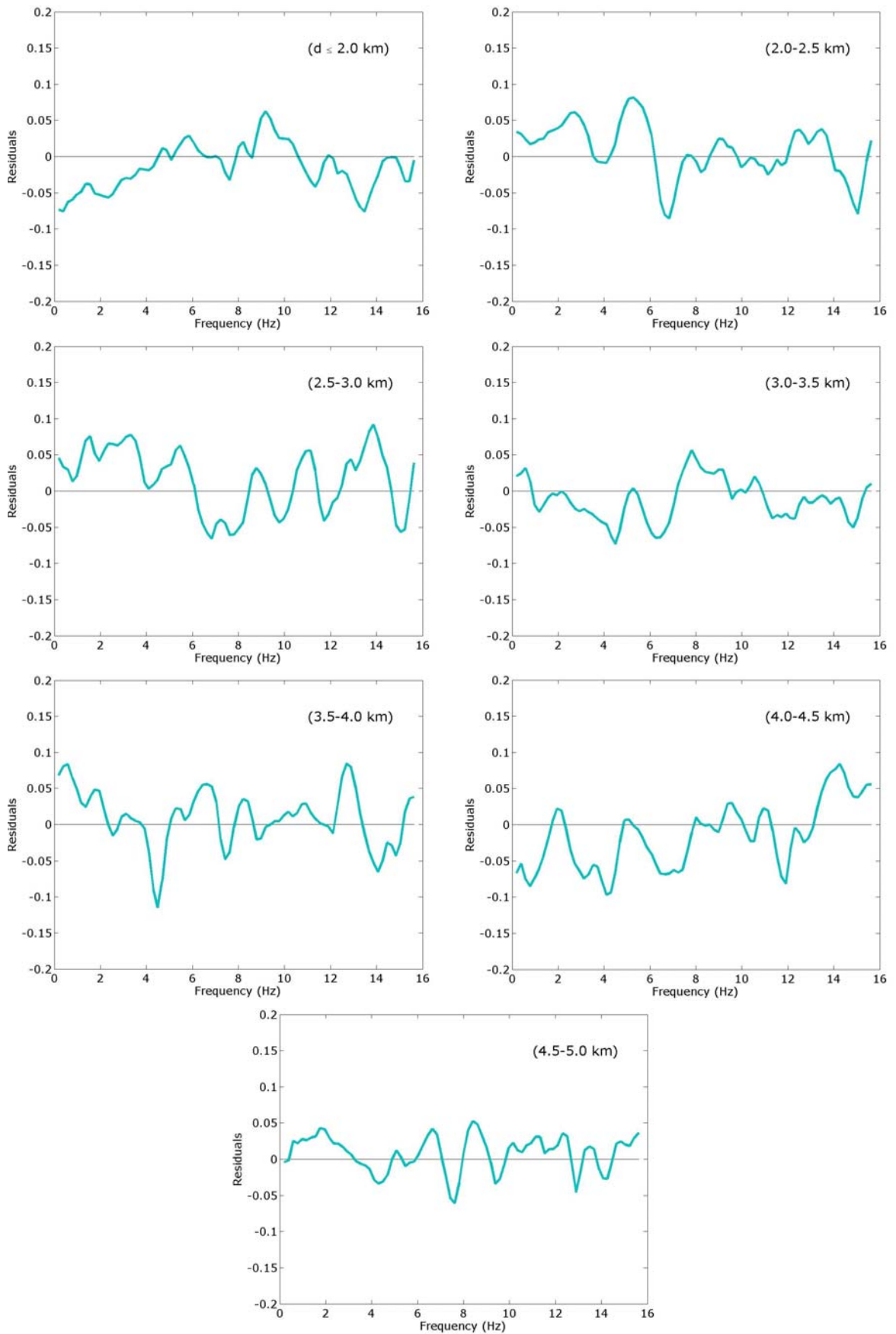


Figure 5.20. Residuals of the coherency model (Eq. (5.17)) for each distance bins

6. SIMULATION OF SPATIALLY VARIABLE GROUND MOTION

6.1. Introduction

In addition to the realistic characterization of spatial variation, simulation of spatially variable time histories is an indispensable part of the study of the effects of seismic spatial variation on structural response, especially for future performance-based design of extended lifeline structures (Porter, 2003). Actually it is recognized that high-quality ground motion characterization is vital to the success of performance-based design, and ground motion evaluation procedures for single point structures has been proposed within the performance-based design framework (Stewart *et al.*, 2001). However, the generation of spatially variable ground motion for the performance-based design of lifeline structures, such as bridges, dams, pipelines, power transmission systems, etc., has not yet received the attention it deserves (Songtao, 2006).

Currently, a large number of approaches are available to simulate the seismic random fields. Some unconditional simulation schemes are: spectral representation method (Shinozuka and Deodatis, 1991), covariance matrix decomposition method (Hao *et al.*, 1989, Zerva and Katafygiotis, 2000), auto-regressive-moving-average approximation method (Spanos and Zeldin, 1996), hybrid discrete Fourier Transform and digital filtering approach (Li and Kareem, 1997), etc. Besides, several conditional simulation schemes, which can inherit the physical characteristics of recorded time histories, have been proposed as well, such as conditional probability density function method (Kameda and Morikawa, 1992; 1994), Kriging method and multivariate linear prediction method (Vanmarcke *et al.*, 1993) etc. The conditional simulation is a natural way to generate spatially variable ground motion for performance-based design of extended structures.

In general, the generated time histories from the simulated techniques are examined through their compliance with the properties of the target random field, *i.e.* the prescribed power spectral density and coherency models. However, based on the studies of Zerva and Zhang (1997), the simulated time histories should comply with the observations of actual time histories. This compliance is especially important for the observation that amplitude

variability and phase variability increase with frequency in a correlated pattern and reach constant values at higher frequencies when the coherency values between stations tend to zero. Katafygiotis *et al.* (1999a, 1999b) examined several unconditional simulation schemes. Their studies indicate that some techniques conform to the observations, while others do not. Therefore, caution should be used when using the simulation techniques.

Lilhanand and Tseng (1988) and Tseng *et al.* (1993) proposed a method for generation of realistic synthetic earthquake time histories compatible with multiple-damping design spectra.

Das and Gupta (2008) described a wavelet-based procedure to simulate ensembles of accelerograms by replicating temporal variations in the frequency content of a parent recorded accelograms. The procedure is based on an extension of the stochastic decomposition technique to wavelet domain while using the analytic form of the modified Littlewood-Paley (L-P) basis function.

Bi and Hao (2003) presents a method to generate spatial ground motion time histories to be compatible with different power spectral density functions and a coherency loss function. The method is applied to generate spatial ground motion on surface of a canyon site with multiple soil layers.

Abrahamson (1992) and Abrahamson (1993) proposed a method for generating spatially incoherent ground motion given a target spectrum, coherency function and an initial time history. The method is based on the relation between the absolute value of coherency and statistical properties of the Fourier phase angles. The algorithm using an iterative procedure to estimate the suite of incoherent ground motion is presented.

Hancock *et al.* (2006) presented an improved method for the wavelet adjustment of recorded ground motion to achieve a match between the target design spectrum and the response spectra of the accelerograms. New wavelets have been developed that have zero final velocity and displacement, ensuring that records do not require a baseline correction after wavelet adjustment. The procedure is applied using pseudo-spectral acceleration so that spectral displacements can be matched. This method enables records to be adjusted so

that they match the target response spectrum at more damping levels than previously possible, although the goodness-of-fit to the target spectrum reduces as the number of target damping levels increases.

Shama (2007) developed an approach for the simulation of spatially correlated ground motion statistically analogous with a reference record. This procedure makes use of a discrete representation of the ground motion as a random process in terms of its frequency components and subdivides the known record into a sequence of time windows to account for its temporal variation. Ground motion, consistent with both the target autospectrum of the known record and a frequency-dependent coherency function, were simulated at different stations. As a result, model diagnostic checking showed that this simplified procedure is accurate and applicable for discretely supported systems such as suspension and cable-stayed bridges, particularly when used in conjunction with seismological models to generate strong motion spatially correlated accelerograms.

Artificial records constitute a convenient tool but their shortcomings, arising from their dissimilarity with real earthquake ground motion in terms of number of cycles, phase content and duration, are widely recognized, and their use in nonlinear analyses is not recommended. These problems are avoided by using real strong-motion accelerograms, appropriately scaled to the target spectrum (at least in the vicinity of the structure's natural period of vibration), but the inherent variability of real earthquake motion means that it will often be necessary to run large numbers of dynamic analyses in order to obtain stable estimates of the inelastic response of the structure. The required number of inelastic dynamic analyses can be significantly reduced if the real records are first matched to the target response spectrum, by eliminating the largest differences between the target spectrum and the spectral ordinates of individual accelerograms. This is clearly a compromise and in some sense the records become 'artificial' as a result, although the records can retain most (if not, in fact, all) of the characteristics of real earthquake records. The choice is essentially one of compromise between engineering pragmatism and seismological rigour, reducing the number of time-consuming structural analyses whilst avoiding the use of completely artificial accelerograms generated from modified white noise.

The objective herein is to generate earthquake ground motion for a finite array of ground surface stations, including the reference station; such that they are design-response-spectrum compatible with given a prescribed design response spectrum at a reference station and their coherencies are consistent with the target coherency function with a prescribed spatial coherency function. First, target response spectrum compatible earthquake ground motions are simulated. Then, these simulated ground motion are used to generate the ground motion that produce coherencies in unison with the target coherency function.

6.2. Methodology to Simulate Target Spectrum Compatible Ground Motion

A methodology is developed by Abrahamson (1993) and improved by Hancock *et al.* (2006). A time domain modification of an acceleration time history to make it compatible with a user specified target spectrum is preformed by Lilhanand and Tseng (1988) and the computer code (RspMatch) was written by Abrahamson (1993). The modification of the time history can be performed with a variety of different modification models. In doing so, the long period non-stationary phasing of the original time history is preserved. The program RspMatch performs spectral matching using wavelets. Whereupon, Hancock *et al.* (2006) improved the new version of the program, RspMatch2005, enables the accelerograms to be matched to the pseudo-acceleration or displacement spectral ordinates as well as the spectrum of absolute acceleration, and additionally allows the matching to be performed simultaneously to a given spectrum at several damping ratios.

A commonly used method to reduce the spectral mismatch of the individual ground motion is to apply spectral matching in the frequency domain by adjusting the Fourier amplitude spectra (*e.g.* Rizzo *et al.*, 1975; Silva and Lee, 1987). This is useful in that it generates accelerograms that are based on real ground motion and also have a close match to the target spectrum. However, adjusting the Fourier spectrum corrupts the velocity and displacement time-series and can result in motion with unrealistically high energy content (Naeim and Lew, 1995).

An alternative approach for spectral matching adjusts the time history in the time domain by adding wavelets to the acceleration time-series. Wavelet adjustment of recorded

accelerograms has the same advantages as the Fourier adjustment methods but leads to a more focused correction in the time domain thus introducing less energy into the ground motion and also preserves the non-stationary characteristics of the original ground motion.

The method proposed by Lilhanand and Tseng (1988) employs wavelets but uses the response of elastic SDOF systems rather than the Continuous Wavelet Transform (CWT). This enables accelerograms to be made spectrum compatible with smaller adjustments than the wavelet adjustment methodologies which use the CWT.

A flowchart showing the procedure as employed in RspMatch2005 is given in Figure 6.1. The essence of the methodology is as follows:

- Calculate the response of an elastic SDOF system under the action of the acceleration time-series for each period and damping level to be matched.
- Compare the peak of each SDOF response with the target amplitude and determine the mismatch.
- Add wavelets to the acceleration time-series with the appropriate amplitudes and phasing so that the peak of each response matches the target amplitude. One wavelet is used to match one SDOF response.

Each wavelet is applied to the time series so that the time of maximum SDOF response under the action of the wavelet is the same as the time of the peak response to be adjusted from the unadjusted acceleration time-series. New wavelets have been developed that have zero final velocity and displacement, ensuring that records do not require a baseline correction after wavelet adjustment.

Although the algorithm (Figure 6.1) prevents the solution from diverging it does not guarantee that the solution will converge to within the requested tolerance. A balance needs to be maintained between the goodness-of-fit to the response spectra and the degree of adjustment made to the accelerogram.

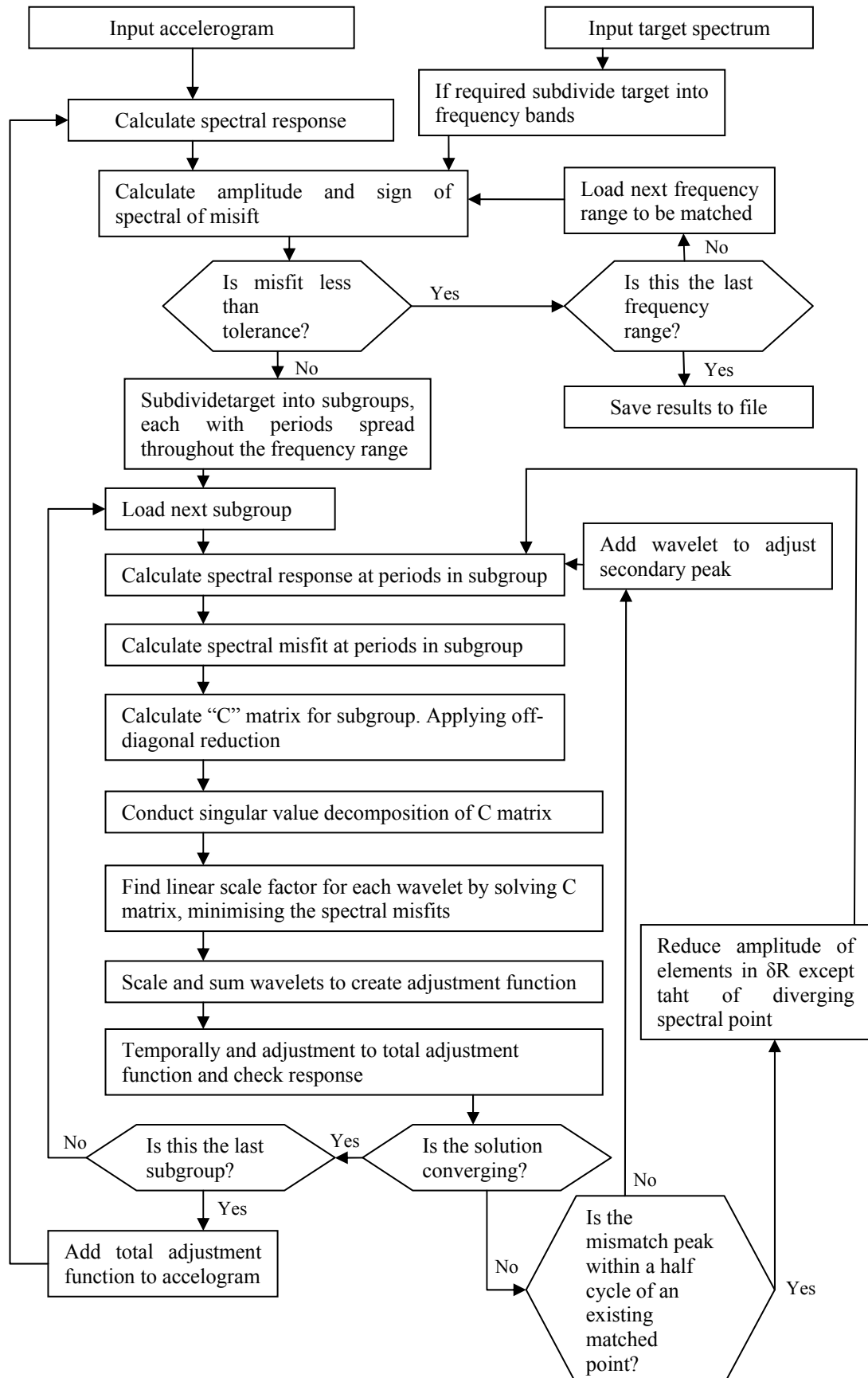


Figure 6.1. Methodology of RspMatch2005 (Hancock *et al.*, 2006)

6.3. Methodology to Simulate Ground Motion Consistent with the Target Coherency Model

Some of the methods (Zerva, 1992; Ramadan and Novak, 1993, 1994; Laouami and Labbe, 2001) that have been developed in the past few years for the simulation of spatially correlated synthetic accelerograms employed theoretical equations for the earthquake's power spectrum, such as the Kanai-Tajimi equation, and theoretical time envelope functions to account for the non-stationarity characteristics (*i.e.*, build-up and decay) of the generated motion. Studies by Ohsaki (1979) showed that introducing time envelope functions might disturb the phase properties of the simulated accelerograms and hence change the correlation characteristics of the developed ground motion. Therefore, this class of method is considered to be inadequate from a practical perspective.

Stochastic procedures which employ either covariance matrix decomposition (Vanmarcke *et al.*, 1993) or spectral factorization (Shrikhande and Gupta, 1996) have been proposed to simulate non-stationary spatially correlated ground motion that are conditioned by recorded earthquakes at near points. Other approaches that analyze the spatial variation of the ground motion using the theory of wave propagation and finite-element techniques have also been developed (Zendagui and Berrah, 2002). These procedures may be computationally demanding, particularly when the number of unknown stations increases.

Shama (2007) is proposed an alternative approach for the simulation of incoherent accelerograms conditioned by a recorded motion at a reference station. To represent the temporal variation of the known accelerogram precisely, this approach subdivides it into a sequence of time windows. The target power spectrum for each time window was established using an autoregressive (AR) model and used in conjunction with a simple approach of the superposition of trigonometric functions. The statistical dependence of the ground motion at a second station was introduced by means of an exponential coherency function.

Herein, the generated target coherency spectrum compatible earthquake ground motion using RspMatch2005 software are simulated with the aforementioned method proposed by Shama (2007).

6.3.1. Estimation of the Power Spectrum

The harmonic process model, as defined by Priestley (1981), is used in the proposed method to idealize the ground motion accelerogram as a stationary random process, which can be expanded approximately into a set of discrete frequency components

$$a(t) = \sum_{i=1}^n A_i \cos(\omega_i t + \phi_i) \quad (6.1)$$

where $a(t)$ is ground acceleration at time t , A_i is the amplitude, and ϕ_i ($i=1, \dots, n$) are independent random phases, each assumed to have a uniform distribution on the interval $(0, 2\pi)$.

In general, there is some relation of proportionality between a measure of the squared amplitude of the stochastic process and the one-sided local power spectrum in the form (Gasparini and Vanmarcke, 1976)

$$\sum \frac{A_i^2}{2} = \sum S_g(\omega_i) \Delta\omega = \int_0^{\alpha} S_g(\omega) d\omega \quad (6.2)$$

where $S_g(\omega_i) \Delta\omega$ is the contribution to the total power of the motion from the sinusoid with frequency ω_i . Hence, by allowing the number of sinusoids in the motion to become very large (*i.e.* the frequency approaches the Nyquist frequency of the process), the discrete power will approach the continuous power spectrum curve.

By substituting Equation (6.2) into Equation (6.1), the ground motion acceleration can be expressed as (Shinozuka, 1971)

$$a(t) = \sqrt{2} \sum_{i=1}^{N_f} \sqrt{S_g(\omega_i) \Delta\omega} \cos(\omega_i t + \phi_i) \quad (6.3)$$

in which N_f is the number of frequency intervals; $\Delta\omega = \frac{\omega_u}{N_f}$, with ω_u as the cut-off frequency (Nyquist frequency); and $\omega_i = k \Delta\omega$. For the application of Equation (6.3) to non-stationary earthquake accelerograms, in which frequencies as well as amplitudes are time dependent, it is essential to analyze separately segments of the record, which are short enough to be stationary but still convenient for containing sufficient data for the determination of the power spectrum. By assuming ergodicity of the ground motion random process, segments of a known accelerogram can be computationally simulated using Equation (6.3).

Since each segment of the accelerogram is assumed as a stationary stochastic process with a zero mean, it can be described by its power spectrum. The significance of the power spectrum arises from the fact that it illustrates how the variance of the stochastic process is distributed with frequency. The power spectrum is determined by assuming a time series model of the data. Time series models include the autoregressive (AR), the moving average (MA), and the autoregressive moving average (ARMA) models. Since estimates of the AR parameters can be obtained as solutions to linear equations, they are more preferable when compared to MA and ARMA models (Marple, 1987). Hence, AR spectral estimates were employed, where the time series of interest (segment of the known accelerogram) is assumed to be a linear random process.

In the AR model, the current value of the process is expressed as a finite linear filter of previous values plus a white noise. The coefficients of the autoregressive model were computed from the auto covariance function using the Levinson–Dubrin recursive method for solving the Yule–Walker equations (Box *et al.*, 1994).

The theoretical continuous power spectrum for the autoregressive process is determined as

$$S_g(\omega) = \frac{\Delta t \sigma^2}{\pi \left| 1 + \sum_{j=1}^N \psi_j e^{-i\omega_j \Delta t} \right|^2} \quad (6.4)$$

where Δt is the sampling interval for the known accelerogram; and i is the complex value of $\sqrt{-1}$.

Phase spectrum for each window was obtained directly from the Fourier transform of the record as

$$\phi_i = \tan^{-1} \left(\frac{\text{Im}(\omega_i)}{\text{Re}(\omega_i)} \right) \quad (6.5)$$

in which ϕ_i is the phase angle of the i^{th} contributing sinusoid with frequency ω_i ; and $\text{Im}(\omega_i)$ and $\text{Re}(\omega_i)$ are the imaginary and real parts of the Fourier amplitude of the ground acceleration at ω_i . By substituting Equation (6.4) and Equation (6.5) into Equation (6.3), a computational simulation for a known accelerogram can be obtained.

6.3.2. Adaptation of Coherency Model

Studies conducted by Harichandran and Vanmarcke (1986) and Harichandran (1991) showed that local variation in the power spectrum of the ground motion could be neglected within areas of uniform soil conditions and geology. In this method proposed by Shama (2007), it is assumed that this condition exists within the dimensions of most engineered structures, and the spatial variation of ground motion was prescribed in terms of wave scattering as well as wave passage effects, which can be incorporated into Equation (6.3) to produce the discrete version of the acceleration process at another successive station j . The inclusion of wave scattering effects on the simulated motion can be achieved by introducing a coherency model in the form of phase difference $\mu_{i,j}$, henceforth called coherency phase, while wave travel effects can be incorporated by introducing a time lag between the two stations as

$$a(t) = \sqrt{2} \sum_{i=1}^{N_f} \sqrt{S_g(\omega_i) \Delta \omega} \cos[\omega_i(t - \tau_j) + \phi_i + \mu_{i,j}] \quad (6.6)$$

in which τ_j is the time lag between the two stations given by $\tau_j = \frac{d_j}{V}$, where d_j is the separation between the two stations projected parallel to the dominant wave propagation direction; V is the apparent seismic wave velocity in the medium; and $\mu_{i,j}$ is the coherency phase for the i^{th} frequency at station j , assumed to be uniformly distributed between 0 and 2π .

6.3.3. Coherency Phase

The coherency phase $\mu_{i,j}$ for the i^{th} frequency is defined as

$$\mu_{i,j} = \cos^{-1} \left[\gamma(d_j, \omega_i) \beta \left(\phi_i, \frac{\omega_i d_j}{V} \right) \right] \quad (6.7)$$

where $\gamma(d_j, \omega_i)$ is the coherency model to represent the spatial variation of the ground motion between any two stations, described in this study as Equation (5.17) derived in Chapter 5.4.4, written again as

$$|\gamma(d, f)| = 0.513 e^{(0.0781 - 0.038\sqrt{f})d} + (1 - 0.513) e^{(-0.2643 - 0.0301 f^2)d^2} \quad (6.8)$$

where d is the separation distance between two stations and f is the frequency.

β is a function used to locate the coherency phase angle in one of the four quadrants of the trigonometric circle, depending on both the phase angle of the original record and the normalized frequency as (Shama, 2007):

$$\beta = \begin{cases} +1 & 0 < \phi \leq 2\pi \\ \end{cases} \quad \text{for } \frac{\omega d}{V} \leq 0.8 \quad (6.9a)$$

$$\beta = \begin{cases} -1 & 0 < \phi \leq \frac{\pi}{2} \\ +1 & \frac{\pi}{2} < \phi \leq \pi \\ -1 & \pi < \phi \leq \frac{3\pi}{2} \\ +1 & \frac{3\pi}{2} < \phi \leq 2\pi \end{cases} \quad \text{for } 0.8 < \frac{\omega d}{V} \leq 2.5 \quad (6.10b)$$

$$\beta = \begin{cases} +1 & 0 < \phi \leq \frac{\pi}{2} \\ \frac{\pi}{\mu} - 1 & \frac{\pi}{2} < \phi \leq \pi \\ \frac{\pi}{\mu} + 1 & \pi < \phi \leq \frac{3\pi}{2} \\ \frac{2\pi}{\mu} - 1 & \frac{3\pi}{2} < \phi \leq 2\pi \end{cases} \quad \text{for } \frac{\omega d}{V} > 2.5 \quad (6.11c)$$

6.3.4. Numerical Illustration

The procedure explained above is applied to simulate an accelerogram at a distance of 100 m from the original record taken from MSK station of the August 17, 1999 Kocaeli earthquake. This event had a 7.5 moment magnitude and hypocentral distance at MSK station is 92.14 km. The recorded ground motion has a sampling frequency of 200 Hz. Herein, one component is used.

The initial reference time history is shown in Figure 6.2. This time history is modified to obtain ground motion consistent with the target spectrum demonstrated in Figure 6.3 using the algorithm described in Figure 6.1.

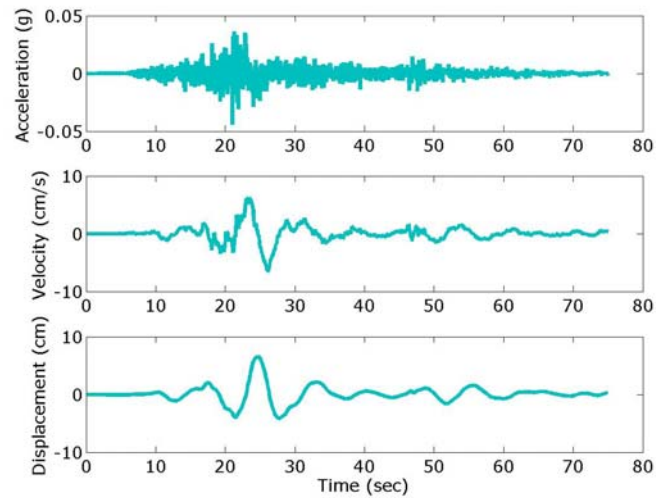


Figure 6.2. The August 17, 1999 Kocaeli earthquake recorded at MSK station:
Acceleration (g), velocity (cm/s) and displacement (cm)

The aforementioned program, RspMatch2005, is applied to generate response-spectrum compatible earthquake ground motion. Comparison of target response spectrum and simulated response spectrum is illustrated in Figure 6.3. It is seen that the five per cent damping response spectra for the simulated ground motion appear to be in good agreement with the target spectrum.

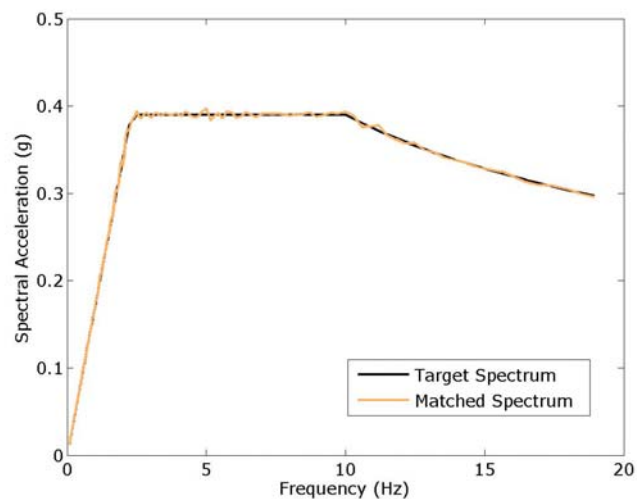


Figure 6.3. Comparison of target spectrum and the matched response spectrum

The generated time histories compatible with prescribed target spectrum are displayed in Figure 6.4. The results are consistent with the initial time histories shown in Figure 6.2.

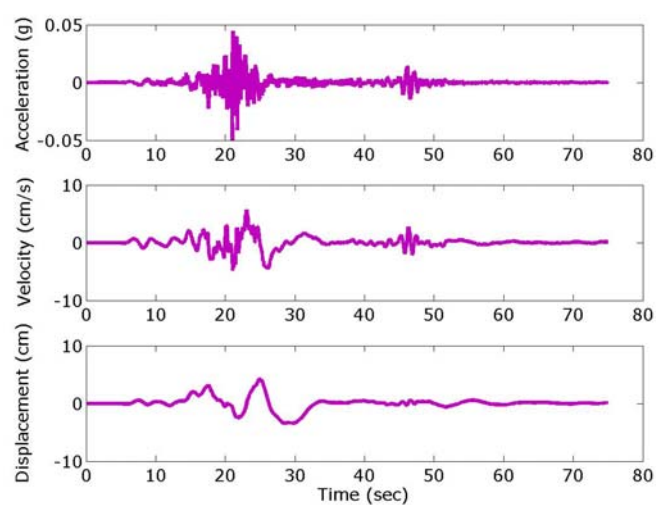


Figure 6.4. Target spectrum compatible time histories: Acceleration (g), velocity (cm/s) and displacement (cm)

The spectrum compatible time histories are used to generate earthquake ground motion that have coherency values consistent with the prescribed coherency function. The method stated above for the simulation of spatially correlated ground motion conditioned by the spectrum compatible time history is applied. The spectrum compatible acceleration is subdivided into a sequence of time windows to represent its temporal variation. An autoregressive (AR) model was used to establish the target power spectrum for each time window. A stochastic harmonic model was used to idealize the ground motion as a stationary random process, which was expanded for each window into a set of discrete frequency components. The statistical dependence of the ground motion at a second station was introduced by means of an exponentially decaying model.

The acceleration time history demonstrated in Figure 6.4 is subdivided into 17 windows with a power of 2 in length. Both the power and phase spectra were determined for each window expressed in Equation (6.4) and (6.5), respectively.

The exponentially decaying coherency model described in Chapter 5.4.2 and expressed in Equation (6.8) was employed as coherency phase stated in Equation (6.7). The computed power spectra, phase spectra, and coherency phase is used to generate coherency model compatible earthquake ground motion (Equation (6.6)). The decay of coherency function with increasing frequency for different separation distances between stations is displayed in Figure 6.5.

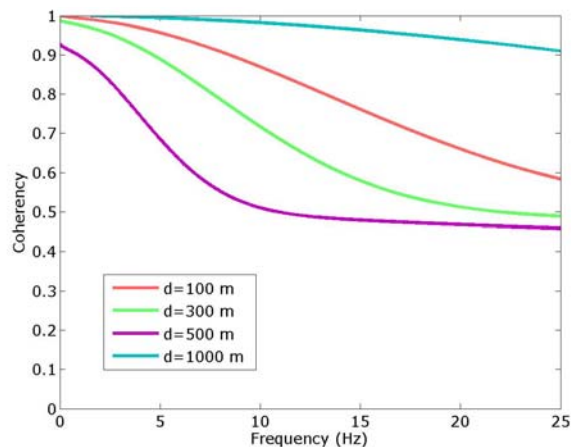


Figure 6.5. Decay of coherencies with respect to frequency for different separation distances

Acceleration, velocity, and displacement time histories of initial reference station are compared with the acceleration, velocity, and displacement time histories of station at a distance of 100 m from reference point. It is observed that the general appearance of the time histories of the simulated accelerations, velocities, and displacements shown at the left column in Figure 6.6, Figure 6.7, Figure 6.8, respectively; conforms to the known record. The differences between the simulated and initial ground motion named relative time history are displayed in Figure 6.6 for acceleration; in Figure 6.7 for velocity; and in Figure 6.8 for displacement time history.

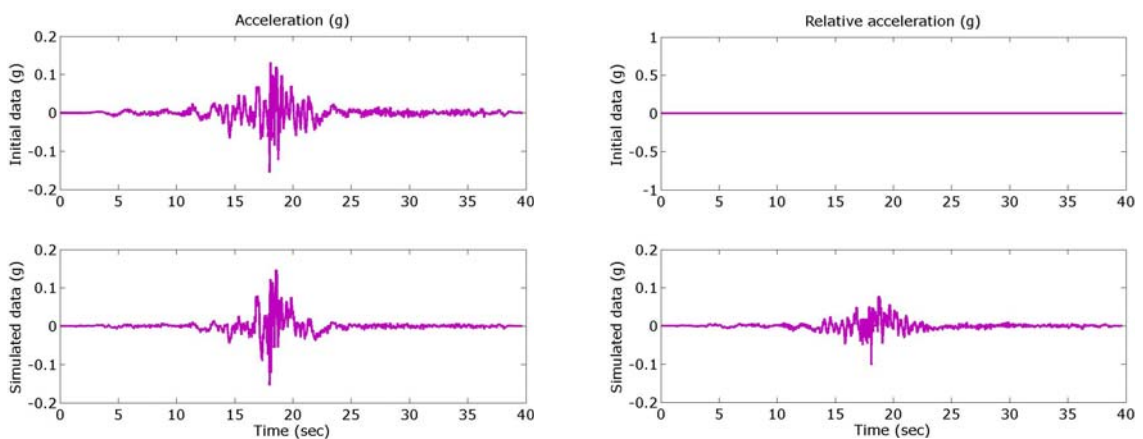


Figure 6.6. Acceleration time history of reference station and simulated data at $d=100$ m at the left column. Relative acceleration time history with respect to reference station at the right column

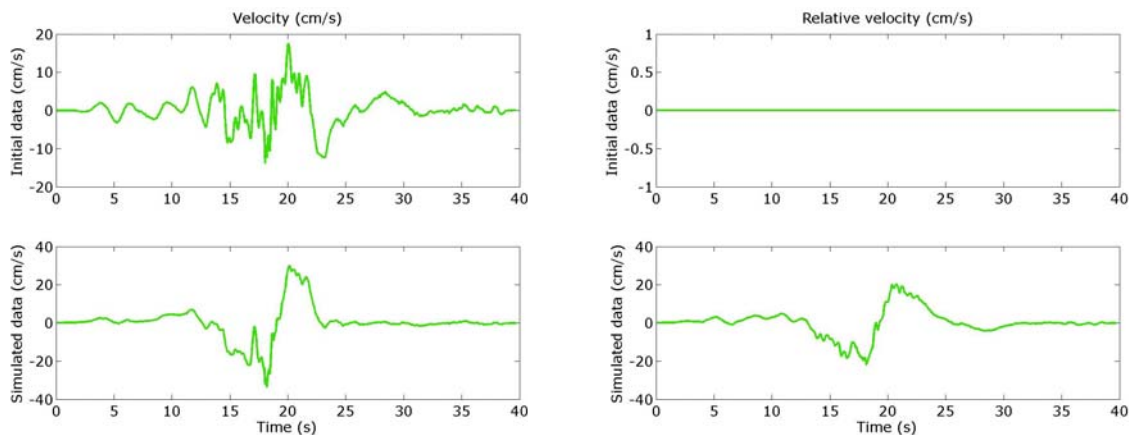


Figure 6.7. Velocity time history of reference station and simulated data at $d=100$ m at the left column. Relative velocity time history with respect to reference station at the right column

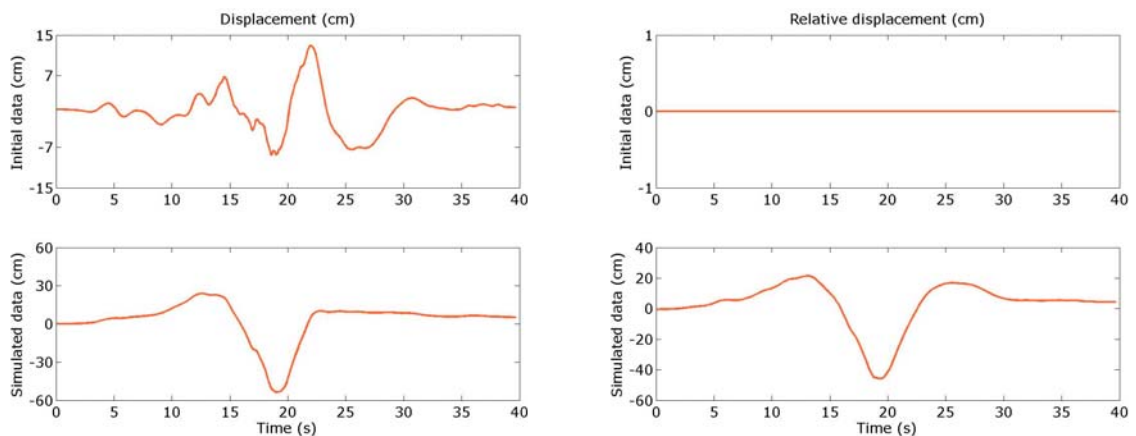


Figure 6.8. Displacement time history of reference station and simulated data at $d=100$ m at the left column. Relative displacement time history with respect to reference station at the right column

The frequency contents of the simulated data to that of reference data are compared. The Fourier amplitude spectra of the simulated acceleration and the Fourier amplitude spectrum of the known ground accelerations are plotted at the left hand side of Figure 6.9. The Fourier amplitudes of the reference data compare favorably to those of the simulated motion. The target spectrum and the matched spectrum computed as a result of generation of target response spectrum compatible ground motion in Figure 6.3 are compared with spectral amplitudes of simulated data at the right column of Figure 6.9.

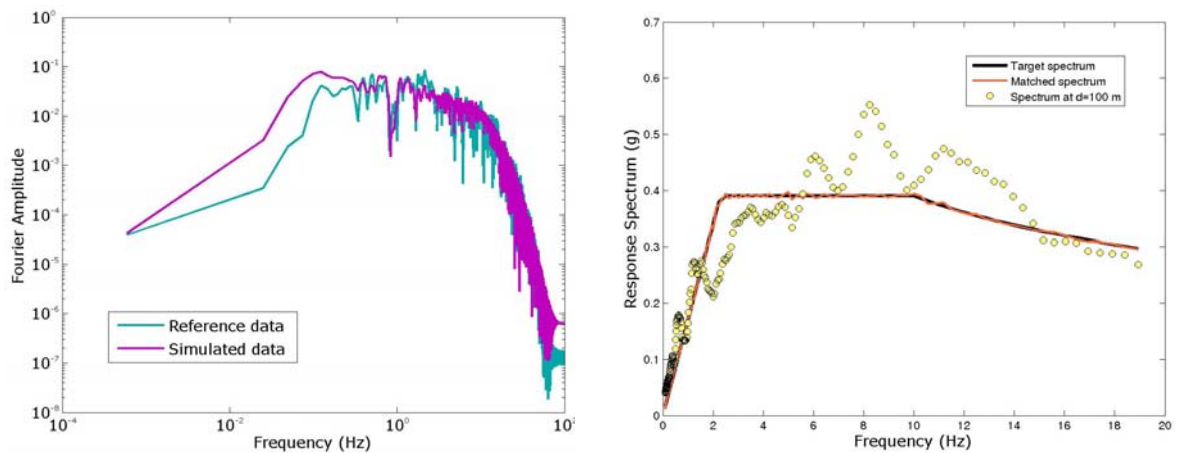


Figure 6.9. Comparison of Fourier amplitude of reference station and simulated data at $d=100$ m at the left column. Comparison of target, spectrum at reference station and spectrum at $d=100$ m at the right column

The coherency values are computed by using reference data and simulated data for the point had a distance of 100 m from that reference point. The target coherency spectrum for increasing frequency at a 100 m separation distance plotted in Figure 6.10 calculated by Equation (6.8). The computed coherencies using reference and simulated data are compared with target coherency spectrum. It is shown that the computed coherency values are in good agreement with that of the target coherency model.

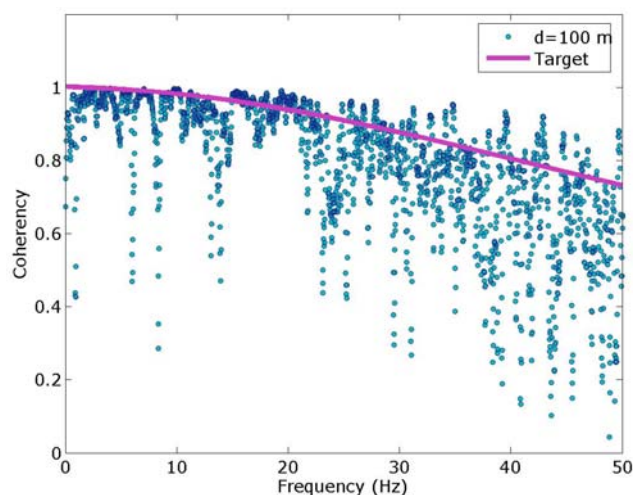


Figure 6.10. Comparison of target coherency spectrum and coherency values computed by simulated ground motion at $d=100$ m

Consequently, a procedure is applied herein to generate earthquake ground motion, compatible with response spectrum for a given target response spectrum, using a method proposed by Hancock *et al.* (2006) and that have coherency values consistent with prescribed coherency model generated for Istanbul, using a model derived by Shama (2007). The overall profile of the results of simulated data compare favorably to those of the initial data.

It must be cautioned that the results are preliminary to generate the target response spectrum and coherency spectrum compatible ground motion. This work forms the skeleton of an automated system to uniformly simulate the ground motion consistent with response and coherency spectrum at the stations distributed linearly or an extended area

7. CONCLUSIONS AND RECOMENDATIONS

The spatial variation of earthquake ground motion can occur as a consequence of source properties, wave propagation through different earth strata, soil media and topographic features and serves to quantify the amplitude and phase differences of ground motion over distance or area. The spatial variability has an important effect on the response of linear lifelines such as bridges, pipelines, communication systems, and should preferably be accounted for in their design. For complex long structures and for the evaluation of the nonlinear seismic response, the deterministic solution is essential with the effect of the spatial variation of the seismic event included in terms of multiple-support excitation.

Alternatively, the generation of estimated maps of shaking after an earthquake provides an important seismological tool to guide emergency response. Estimation of the statistical variation of ground motion between stations is important in characterizing the uncertainty inbuilt in the interpolations necessary to produce these maps. Hence, the statistical properties of the spatial variability in terms of separation distance between the stations over extended areas have been studied by the researchers.

In this thesis, extensive analyses of recorded time histories at selected seismic dense ground motion recording arrays are carried out to understand the spatial variation of earthquake ground motion. The aim is to evaluate and improve existing spatial variation quantification relationships by studying the data available from different networks. In addition, the possibility of employing functional forms for the modeling of spatial variation of ground motion is investigated. A methodology for the assessment of strong ground motion distribution in urban context is developed. This methodology for the interpolation of measured ground motion of discrete array stations to be used in the bias adjustment of the theoretical shake map assessments with the empirical ground motion measurements is a natural follow-up of the investigations. Finally, spatially incoherent earthquake ground motion is simulated.

The earthquakes recorded by Istanbul Earthquake Rapid Response and Early Warning System (IERREWS) are used for the development of the methodology to estimate

the ground parameters over a distance or an area. Methodology is presented for estimating peak ground accelerations, at an arbitrary set of closely-spaced points, compatible with known or prescribed peak ground acceleration at other locations. Additionally, the statistical spatial variation with respect to separation distance is utilized. The estimation of the statistical variation of ground motion between stations is important in characterizing the aforementioned uncertainty. Hence, standard deviations of the logarithmic differences of the ground motion parameters computed from data recorded by IERREWS and the Norwegian Seismic Array (NORSAR) are considered for the quantification of the statistical variability of earthquake ground motion. The data recorded by NORSAR are used representing the shorter distances for the estimation of statistical spatial variation.

Subsequently, the ground-surface strains are used to analyze the spatial variation of the Düzce Basin. A procedure, termed Domain Reduction Method (DRM) is utilized to estimate ground strains, concerning the seismic source, wave propagation, local site effects.

The general properties of coherency function and the coherency estimation procedure based on conventional spectral analysis are studied using data from Istanbul Earthquake Rapid Response System. During the calculation of the coherency values, a code is generated. For the validation of this code, data from Strong Motion Array in Taiwan, Phase (1) (SMART -1) array is used. Location and the configuration of the arrays are illustrated and properties of corresponding events are explained.

Semi-empirical and empirical coherency models are reviewed. Regression procedure for the evaluation of coherency model for Istanbul is explained. In conclusion, a new coherency model is developed.

Finally, the concept of the simulation of target spectrum and coherency function compatible spatially variable ground motion is described. The software for the generation of ground motion related to the prescribed target spectrum is explained primarily, and then the method used for the simulation of spatially variable ground motion consistent with a coherency function is stated in details. The simulation scheme based on target response

spectrum and coherency function is applied by using MSK station record triggered during the Kocaeli earthquake.

The conclusions can be summarized as follows:

- a. The estimated peak ground accelerations at Istanbul Rapid Response stations using the proposed method based on modified kriging method are compared with peak ground accelerations computed from observed data recorded at the same stations. It is seen that the method is appropriate, since the residuals between the estimated and observed PGA are small enough.
- b. The estimated and observed values are compared with the values generated by Akkar and Bommer (2007) equations for each Rapid Response station considering the properties of each earthquake. Akkar and Bommer (2007) equation gives extremely high results for the earthquakes with small magnitude. The reason is that the equation generated from the earthquakes with magnitudes ranging from 5.0 to 7.6. Generally, the results obtained by the proposed method and \pm one geometric standard deviation are in good agreement with the observed values.
- c. The estimation of peak ground acceleration is done for four cases: using observed PGA with no site and distance correction, using observed PGA corrected w.r.t. distance, using observed PGA corrected w.r.t. site class, and using observed PGA corrected w.r.t. distance and site class. The residuals for the case of PGA corrected w.r.t. site class are smaller than the residual for the other cases.
- d. The proposed method is used to compute PGA at the phantom stations. The computed PGA values are compared with the values computed by RRMap (Rapid Response Mapping Application) software based on the spline interpolation. Especially, for the smallest PGA values for each earthquake, PGA obtained by modified kriging method are much compatible with PGA obtained by observed data than PGA obtained by RRMap.

- e. The statistical property of the spatial variation of strong ground motion is examined in terms of the logarithmic standard deviation of peak ground acceleration and of pseudo spectral velocity. The logarithmic standard deviations of PGA differences are compared with Boore (1997) and Evans (2005), and those of PSV differences are compared with Boore *et al.* (1993) and Evans (2005). PGA values are gradually with the separation distance. The results of PSV match well with Boore (1997) and Evans (2005), despite the different magnitude ranges. This comparison may indicate that there is no a significant dependence on earthquake magnitude (Abrahamson *et al.* 1992). The coefficients of Boore (1997) equation for the estimation of the spatial variability in terms of logarithmic standard deviation of PGA differences recalculated for data recorded by IERREWS. The gap for the short station separation distances of IERREWS is filled by the station separation distances of SPITS array.
- f. Analyzing the spatial intraevent variability based on statistical properties of PGA for NORSAR data resulted that the mean value slightly decreases as the logarithm of the station separation increases. As a next step, the increase of the standard deviation with respect to station separation is recognized, as expected.
- g. The spatial variation of peak ground displacement, velocities and accelerations and strains for the longitudinal and vertical directions in Düzce Basin has a smooth variation with horizontal distance. These strong motion parameters increase with the depth of basin.
- h. The derived empirical coherency function in terms of frequency and separation distance correlates well with the observed data recorded by IERRS. The residuals show that the proposed coherency function is appropriate. The model can be used for the assessment and simulation of spatially variable ground motion.
- i. A procedure is applied to generate earthquake ground motion, compatible with response spectrum for a given target response spectrum, using a method proposed by Hancock *et al.* (2006) and that have coherency values consistent with prescribed coherency model generated for Istanbul, using a model derived by Shama (2007).

The overall profile of the results of simulated data compare favorably to those of the initial data.

- j. It must be cautioned that the results of the simulation scheme are preliminary to generate the target response spectrum and coherency spectrum compatible ground motion. This work forms the skeleton of an automated system to uniformly simulate the ground motion consistent with response and coherency spectrum at the stations distributed linearly or an extended area.

A large number of studies confirmed that the effect of the spatially variable ground motion on the response of the extended structures such as long bridges, pipelines, communication systems during an earthquake is essential. In this sense, the application of the spatial variation of the earthquake ground motion on the response of long structures, that could be Marmaray rail tube tunnel, would be studied, as a future study.

REFERENCES

- Abrahamson, N. A., 1985, *Estimation of Seismic Wave Coherency and Rupture Velocity Using the SMART-1 Strong Motion Array Recordings*, EERC Report No. EERC/UCB/85-02, Earthquake Engineering Research Center, University of California.
- Abrahamson, N. A., 1988, "Statistical Properties of Peak Ground Accelerations Recorded by the Smart 1 Array", *Bulletin of the Seismological Society of America*, Vol. 78, pp. 26-41.
- Abrahamson, N. A., 1992, "Generation of Spatially Incoherent Strong Motion Time Histories", *Proceedings of Tenth World Conference on Earthquake Engineering*, Madrid, Spain.
- Abrahamson N. A., 1993, "Spatial Variation of Multiple Support Inputs", *Proceedings of the First U.S. Seminar on Seismic Evaluation and Retrofit of Steel Bridges*, San Francisco.
- Abrahamson, N. A., J. F. Schneider and J. C. Stepp, 1990, "Spatial Variation of Strong Ground Motion for Use in Soil-Structure Interaction Analyses", *Proceedings of Fourth U.S. National Conference on Earthquake Engineering*, Palm Springs, California.
- Abrahamson, N. A., J. F. Schneider and J. C. Stepp, 1991, "Empirical Spatial Coherency Functions for Applications to Soil-Structure Interaction Analyses", *Earthquake Spectra*, Vol. 7, pp. 1-27.
- Abrahamson, N. A., J. F. Schneider and J. C. Stepp, 1992, "The Spatial Variation of Earthquake Ground Motion and Effect of Local Site Conditions", *Proceedings of Tenth World Conference on Earthquake Engineering*, Madrid, Spain.

- Abrahamson, N. A. and D. Sykora, 1993, "Variations of Ground Motions Across Individual Sites", *Proceedings of the Fourth DOE Natural Phenomena Hazards Mitigation Conference*, pp. 9192-9198, Atlanta, Georgia.
- Akkar, S. and J. J. Bommer, 2007, "Prediction of Elastic Displacement Response Spectra in Europe and the Middle East", *Earthquake Engineering Structural Dynamics*, Vol. 36, No. 10, pp. 1275–1301.
- Bi, K. and H. Hao, 2003, "Simulation of Spatially Varying Ground Motions with Non-Uniform Intensities and Frequency Content", *Earthquake Engineering in Australia Conference Ballarat*, Australia.
- Bielak, J., K. Loukakis, Y. Hisada and C. Yoshimura, 2003, "Domain Reduction Method for Three-Dimensional Earthquake Modeling in Localized Regions. Part I: Theory" *Bulletin of the Seismological Society of America*, Vol. 93, No. 2, pp. 817-824.
- Birgören, G., H. Sekiguchi and K. Irikura, 2004, "Rupture Model of the 1999 Düzce, Turkey, Earthquake Deduced from High and Low Frequency Strong Motion Data," *Geophysical Research Letters*, Vol. 31, L05610, doi:10.1029/2003GL019194.
- Bogdanoff, J. L., J. E. Goldberg and A. J. Schiff, 1965, "The Effect of Ground Transmission Time on the Response of Long Structures", *Bulletin of the Seismological Society of America*, Vol. 55, pp. 627-640.
- Bohling, G., 2005, *Kriging*, Kansas Geological Survey, C&PE 940.
- Boissieres, H. P. and E. H. Vanmarcke, 1995, "Estimation of Lags for a Seismograph Array: Wave Propagation and Composite Correlation", *Soil Dynamics and Earthquake Engineering*, Vol. 14, pp. 5-22.
- Bommer, J. J. and H. Crowley, 2006, "The Influence of Ground Motion Variability in Earthquake Loss Modelling", *Bulletin of Earthquake Engineering*, Vol. 4, No. 3, pp. 231-248.

- Boore, D. M., 1997, "Estimates of Average Spectral Amplitudes at FOAKE Sites, Appendix C in An Evaluation of Methodology for Seismic Qualification of Equipment, Cable Trays, and Ducts in ALWR Plants by Use of Experience Data", in K. K. Bandyopadhyay, D. D. Kana, R. P. Kennedy and A. J. Schiff (editors), *U.S. Nuclear Regulatory Commission*, NUREG/CR-6464 and Brookhaven National Lab BNL-NUREG- 52500, C-1-C-69.
- Boore, D. M., W. B. Joyner and T. E. Fumal, 1993, *Estimation of Response Spectra and Peak Accelerations from Western North American Earthquakes: An Interim Report*, U.S.G.S. Open File Report, 93-509, pp. 72.
- Boore, D. M. and W. B. Joyner, 1997, "Site Amplifications for Generic Rock Sites", *Bulletin of the Seismological Society of America*, Vol. 87, pp. 327–341.
- Box, G. E., G. M. Jenkins and G. C. Reinsel, 1994, *Time Series Analysis Forecasting and Control*, 3rd ed., Englewood Cliffs, Prentice Hall, New Jersey.
- Conte, J. P., K. S. Pister and S. A. Mahin, 1992, "Non-Stationary ARMA Modeling of Seismic Ground Motions", *Soil Dynamics and Earthquake Engineering*, Vol. 11, pp. 411-426.
- Das, S and V. K. Gupta, 2008, "Wavelet-Based Simulation of Spectrum-Compatible Aftershock Accelerograms", *Earthquake Engineering and Structural Dynamics*, Vol. 37, pp. 1333-1348.
- Der Kiureghian, A., 1996, "A Coherency Model for Spatially Varying Ground Motions", *Earthquake Engineering and Structural Dynamics*; Vol. 25, pp.99-111.
- Ellis, G. W. and A. S. Cakmak, 1991, "Time Series Modeling of Strong Ground Motion from Multiple Event Earthquakes" *Soil Dynamics and Earthquake Engineering*, Vol. 10, pp. 42-54.

- Erdik, M., N. Aydinoğlu, Y. Fahjan, K. Sesetyan, M. Demircioğlu, B. Siyahi, E. Durukal, C. Özbey, Y. Biro, H. Akman and O. Yüzügüllü, 2003a, "Earthquake Risk Assessment for Istanbul Metropolitan Area", *Earthquake Engineering and Engineering Vibration*, Vol. 2, No. 1, pp. 21-23.
- Erdik, M., Y. Fahjan, O. Ozel, H. Alcik, A. Mert and M. Gul, 2003b, "Istanbul Earthquake Rapid Response and the Early Warning System", *Bulletin of Earthquake Engineering*, Vol. 1, No. 1, pp. 157-163.
- Erdik, M., 2006, "Urban Earthquake Rapid Response and Early Warning Systems", *First European Conference on Earthquake Engineering and Seismology (a joint event of the 13th ECEE & 30th General Assembly of the ESC)*, Keynote lecture 4, Geneva, Switzerland.
- Evans, J. R., 2005, "Spatial Variance of Strong Shaking in the Parkfield M_w 6.0 Earthquake of 28 September 2004", *Cosmos Annual Meeting*, Westin Hotel, Millbrae, California.
- Evans, J. R., R. H. Hamstra, Jr. P. Spudich, C. Kündig, P. Camina, and J. A. Rogers, 2003, *TREMOR: A Wireless, MEMS Accelerograph for Dense Arrays*, U.S.G.S. Open File Report 03-159.
- Faccioli, E., F. Maggio, R. Paolucci, A. Quarteroni, 1997, "2D and 3D Elastic Wave Propagation by a Pseudo-Spectral Domain Decomposition Method", *Journal of Seismology*, Vol. 1, pp. 237-251.
- Faccioli, E., R. Paolucci and V. Pessina, 2002, "Engineering Assessment of Seismic Hazard and Long Period Ground Motions at Bolu Viaduct Site Following the November 1999 Earthquake" *Journal of Seismology*, Vol. 6, pp. 307-327.
- Faccioli, E., M. Vanini, R. Paolucci, M. Stupazzini, 2005, "Comment on: Domain Reduction Method for Three-Dimensional Earthquake Modelling in Localized Regions, Part I: Theory by J. Bielak, K. Loukakis, Y. Hisada, C. Yoshimura, and Part

- II: Verification and applications, by C. Yoshimura, J. Bielak, Y. Hisada, A. Fernández”, *Bulletin of the Seismological Society of America*, Vol. 95, No. 2, 763-769.
- Fenton, G. A. and E. H. Vanmarcke, 1990, “Simulations of Random Fields via Local Average Subdivision”, *Journal of Engineering Mechanics*, Vol. 116, pp. 1733-1749.
- Field, H. E. and S. E. Hough, 1997, “The Variability of PSV Response Spectra across a Dense Array Developed During the Northridge Aftershock Sequence”, *Earthquake Spectra*, Vol. 13, No. 2, pp. 243-257.
- Gasparini, D. A., E. H. Vanmarcke, 1976, *Simulated Earthquake Motions Compatible with Prescribed Response Spectra*, Report no. 2, Cambridge (MA): Department of Civil Engineering, MIT.
- Gurley, K. and A. Kareem A, 1994, “On the Analysis and Simulation of Random Processes Utilizing Higher Order Spectra and Wavelet Transforms”, *Proceedings of Second International Conference on Computational Stochastic Mechanics*, Athens, Greece.
- Hancock, J, J. J. Bommer, P. J. Stafford, 2008, “Numbers of Scaled and Matched Accelerograms Required for Inelastic Dynamic Analyses”, *Earthquake Engineering and Structural Dynamics*, Vol. 37, pp. 1585-1607.
- Hao, H., C. S. Oliveira and J. Penzien, 1989, “Multiple-Station Ground Motion Processing and Simulation based on SMART-1 Array Data”, *Nuclear Engineering Design*, Vol. 111, pp. 293-310.
- Harada, T., 1984, “Probabilistic Modeling of Spatial Variation of Strong Earthquake Ground Displacement”, *Proceedings of Eighth World Conference on Earthquake Engineering*, San Francisco, pp. 605–612.

- Harichandran, R. S., 1988, "Local Spatial Variation of Earthquake Ground Motion", in J. L. Von Thun (editor), *Earthquake Engineering and Soil Dynamics II - Recent Advances in Ground-Motion Evaluation*, American Society of Civil Engineers, New York, pp. 203-217.
- Harichandran, R. S., 1991. "Estimating the Spatial Variation of Earthquake Ground Motion from Dense Array Recordings", *Structural Safety*, Vol. 10, pp. 219-233.
- Harichandran, R. S., and E. Vanmarcke, 1986, "Stochastic Variation of Earthquake Ground Motion in Space and Time", *Journal of Engineering Mechanics, ASCE*, Vol. 112, No. 2, pp. 154-174.
- Harmandar, E., E. Durukal, M. Erdik and O. Özel 2006a, "Spatial Variation Strong Ground Motion in Istanbul: Preliminary Results based on Data from the Istanbul Earthquake Rapid Response System", *European Geosciences Union (EGU) General Assembly*, Vienna, Austria.
- Harmandar, E., E. Durukal, M. Erdik and O. Ozel, 2006b, "Spatial Variation of Strong Ground Motion in Istanbul", *First European Conference on Earthquake Engineering and Sesimology*, Geneva.
- Hisada, Y. and J. Bielak, 2003, "A Theoretical Method for Computing Near Fault Ground Motion in a Layered Half-Spaces Considering Static Offset Due to Surface Faulting, with a Physical Interpretation of Fling Step and Rupture Directivity", *Bulletin of the Seismological Society of America*, Vol. 93, No. 3, pp. 1154-1168.
- Hoshiya, M., 1994, "Conditional Simulation of Stochastic Field", in G. I. Schueller, M. Shinozuka, and J. T. P. Yao (editors), *Structural Safety and Reliability*, Balkema, Rotterdam.
- Hoshiya, M., 1995. "Kriging and Conditional Simulation of Gaussian Field." *Journal of Engineering Mechanics*, ASCE, Vol. 121 (No. 2), 181-186.

- Hoshiya, M., and O. Marugama, 1994, "Stochastic Interpolation of Earthquake Wave Propagation", in G. I. Schueller, M. Shinozuka, and J. T. P. Yao (editors), *Structural Safety and Reliability*, Balkema, Rotterdam.
- Jenkins, G. M. and D. G. Watts, 1968, *Spectral Analysis and Its Application*, Holden-Day, San Francisco.
- Journel, A. G. and C. J. Huijbregts, 1978, *Mining Geostatistics*, Academic Press, London, England.
- Joyner, W. B. and D. M. Boore, 1981, "Peak Horizontal Acceleration and Velocity From Strong-Motion Records Including Records from the 1979 Imperial Valley, California, Earthquake", *Bulletin of the Seismological Society of America*, Vol. 71, pp. 2011-2038.
- Kameda, H. and H. Morikawa, 1992, "An Interpolating Stochastic Process for Simulation of Conditional Random Fields", *Probabilistic Engineering Mechanics*, Vol. 7, No. 4, pp. 243-254.
- Kameda, H. and H. Morikawa, 1994, "Conditioned Stochastic Processes for Conditional Random Fields", *Journal of Engineering Mechanics, ASCE*, Vol. 120, No. 4, pp. 855-875.
- Katafygiotis, L. S. , A. Zerva, D. Pachakis, 1999a, "Simulation of Homogenous and Partially Isotropic Random Fields", *Proceedings of International Conference on Applications of Statistics and Probability*, Sydney, Australia.
- Katafygiotis, L. S., A. Zerva, D. Pachakis, 1999b, "An Efficient Approach for the Simulation of Spatially Variable Motions for the Seismic Response of Lifelines", *Proceedings of the Thirteenth Conference on Engineering Mechanics, ASCE*, Baltimore, Maryland, USA.

- Kawakami, H. and H. Mogi, 2003, "Analyzing Spatial Intraevent Variability of Peak Ground Accelerations as a Function Of Separation Distance", *Bulletin of the Seismological Society of America*, Vol. 93, pp. 1079-1090.
- Krige, D. G., 1966, "Two-Dimensional Weighted Moving Average Trend Surfaces for Ore Valuation", *Journal of the South African Institute of Mining and Metallurgy*, Vol. 66, pp. 13-38.
- Kudo, K., T. Kanno, H. Okada, O. Özel, M. Erdik, T. Sasatani, S. Higashi, M. Takahashi and K. Yoshida, 2002, "Site-Specific Issues for Strong Ground Motions During the Kocaeli, Turkey, Earthquake of 17 August 1999, as Inferred From Array Observations of Microtremors and Aftershocks", *Bulletin of the Seismological Society of America*, Vol. 92, No. 1, pp. 448-465.
- Kværna, T., 1990, "Sources of Short-Term Fluctuations in the Seismic Noise Level at NORESS", *Physics of the Earth and Planetary Interiors*, Vol. 63, pp. 269-276.
- Laouami, N. and P. Labbe, 2001, "Analytical Approach for Evaluation of the Seismic Ground Motion Coherency Function", *Soil Dynamics and Earthquake Engineering*, Vol. 21, No. 8, pp. 727-33.
- Li, Y. and A. Kareem, 1997, "Simulation of Multivariate Nonstationary Random Processes: Hybrid DFT and Digital Filtering Approach", *Journal of Engineering Mechanics, ASCE*, Vol. 123, pp. 1302-1310.
- Lilhanand, K. and W. S. Tseng, 1988, "Development and Application of Realistic Earthquake Time Histories Compatible with Multiple-Damping Design Spectra", *Proceedings of Ninth World Conference on Earthquake Engineering*, Vol. 2, pp. 819-829, Tokyo- Kyoto.
- Loh, C. H., J. Penzien and Y. B. Tsai, 1982, "Engineering Analysis of SMART-1 Array Accelerograms", *Earthquake Engineering Structural Dynamics*, Vol. 10, pp. 575-591.

- Loh, C. H., 1985, "Analysis of the Spatial Variation of Seismic Waves and Ground Movements from SMART-1 Array Data", *Earthquake Engineering and Structural Dynamics*, Vol. 13, pp. 561–581.
- Loh, C. H. and Y. T. Yeh, 1988, "Spatial Variation and Stochastic Modeling of Seismic Differential Ground Movement", *Earthquake Engineering and Structural Dynamics*, Vol. 16, pp. 583–596.
- Loh, C. H. and S. G. Lin, 1990, "Directionality and Simulation in Spatial Variation of Seismic Waves", *Engineering Structures*, Vol. 12, pp. 134–143.
- Luco, J. E. and H. L. Wong, 1986, "Response of a Rigid Foundation to a Spatially Random Ground Motion", *Earthquake Engineering and Structural Dynamics*, Vol. 14, pp. 891-908.
- Maggio, F., L. Massidda, J. Sabadell and G. Siddi, 2001, *A Parallel Spectral Element Method for Applications to Computational Mechanics*, Internal Report, CRS4-TECH-REP-01/103, CRS4, Italy.
- Marple, S. L., 1987, *Digital Spectral Analysis with Applications*, Prentice-Hall, New Jersey.
- Matsushima, Y., 1977, "Stochastic Response of Structure due to Spatially Variant Earthquake Excitations", *Proceedings of Sixth World Conference on Earthquake Engineering*, Vol. II, 1077-1082, Sarita Prakashan, Meerut, India.
- McLaughlin, K. L., 1983, *Spatial Coherency of Seismic Waveforms*, Ph.D. Dissertation, University of California, Berkeley.
- Mignolet, M. P. and P. D. Spanos, 1992, "Simulation of Homogeneous Two-Dimensional Random Fields: Part I—AR and ARMA Models", *Journal of Applied Mechanics*, Vol. 59, pp. 260–269.

- Mykkeltveit, S., J. Fyen, F. Ringdal and T. Kværna, 1990, "Spatial Characteristics of the Noress Noise Field and Implications for Array Detection Processing", *Physics of the Earth and Planetary Interiors*, Vol. 63, pp. 277-283.
- Naeim, F. and M. Lew, 1995, "On the Use of Design Spectrum Compatible Time Histories", *Earthquake Spectra*, Vol. 11, No. 1, pp. 111-127.
- Novak, M. and A. Hindy, 1979, "Seismic Response of Buried Pipelines", *Proceedings of Third Canadian Conference on Earthquake Engineering*, Montreal Canada.
- Novak, M., 1987, "Discussion on Stochastic Variation of Earthquake Ground Motion in Space And Time by R. S. Harichandran and E. H. Vanmarcke", *Journal of the Engineering Mechanics Division*, Vol. 113, pp. 1267-1270.
- Ohsaki, Y., 1979, "On the Significance of the Phase Content in Earthquake Ground Motions", *Earthquake Engineering and Structural Dynamics*, Vol. 7, pp. 427-39.
- Oliveira, C. S., H. Hao and J. Penzien, 1991, "Ground Motion Modeling for Multiple-Input Structural Analysis", *Structural Safety*, Vol. 10, pp. 79-93.
- Porter, K. A., "An Overview of PEER's Performance-based Earthquake Engineering Methodology", *Proceeding of Nineth International Conference on Applications of Statistics and Probability in Civil Engineering*, San Francisco, California.
- Priestley, M. B., 1981, *Spectral Analysis and Time Series*, Elsevier Academic Press, London.
- Ramadan, O. and M. Novak, 1993a, *Coherency Functions for Spatially Correlated Seismic Ground Motions*, Geotechnical Research Center Report No. GEOT-9-93, University of Western Ontario, London, Canada.
- Ramadan, O. and M. Novak, 1993b, "Simulation of Spatially Incoherent Random Ground Motions", *Journal of Engineering Mechanics*, Vol. 119, pp. 997-1016.

- Ramadan, O. and M. Novak, 1994, "Simulation of Multidimensional Anisotropic Ground Motions", *Journal of Engineering Mechanics*, Vol. 120, pp. 1773–1785.
- Rice, S. O., 1944, "Mathematical Analysis of Random Noise", *Bell System Technical Journal*, Vol. 23, No. 3, pp. 282–332.
- Ringdal, F., 1997, "Study of Low-Magnitude Seismic Events Near the Novaya Zemlya Nuclear Test Site", *Bulletin of the Seismological Society of America*, Vol. 87, No. 6, pp. 1563 - 1575.
- Ringdal, F., 2005, *Semi-annual Technical Summary (1 July-31 December 2004)*, NORSAR scientific report no.1-2005, Kjeller.
- Rizzo, P. C., D. E. Shaw, and S. J. Jarecki, 1975, "Development of Real/Synthetic Time Histories to Match Smooth Design Spectra", *Nuclear Engineering and Design*, Vol. 32, pp. 148-155.
- Sandi, H., 1970, "Conventional Seismic Forces Corresponding to Non-Synchronous Ground Motion", *Proceeding of Third European Symposium on Earthquake Engineering*, Sofia, Bulgaria.
- Scandella, L., 2007, *Numerical Evaluation of Transient Ground Strains for the Seismic Response Analysis of Underground Structures*, Ph. D Dissertation, Politecnico di Milano.
- Scandella, L, E. Harmandar, E. Faccioli, R. Paolucci, E. Durukal and M. Erdik, 2007, "Numerical Evaluation of Earthquake Induced Ground Strains: The case of Düzce", *Proceedings of the Fourth International Conference on Earthquake Geotechnical Engineering*, Thessaloniki, Greece, 25-28 June, Paper 1214.
- Schneider, J. F., N. A. Abrahamson, P. G. Somerville and J. C. Stepp, 1990, "Spatial Variability of Ground Motion from EPRI's Dense Accelerograph Array at Parkfield,

- California”, *Proceedings of Fourth U. S. National Conf. on Earthquake Engineering*, EERI, Palm Springs, pp. 375-384.
- Shama, A., 2007. “Simplified Procedure for Simulating Spatially Correlated Earthquake Ground Motions”, *Engineering Structures*, Vol. 29, pp. 248-258.
- Shin, T. C., Y. B. Tsai, Y. T. Yeh, C. C. Liu and Y. M. Wu, 2003, “Strong-Motion Instrumentation Programs in Taiwan”, in W. H. K. Lee, H. Kanamori, P. C. Jennings and C. Kisslinger (editors), *International Handbook of Earthquake and Engineering Seismology*, Part B, pp. 1057-1062, Academic Press, San Diego, California.
- Shinozuka, M., 1971, “Simulation of Multivariate and Multidimensional Random Processes”, *Journal of Acoustic Society of America*, Vol. 49, pp. 357–367.
- Shinozuka, M., 1972, “Monte Carlo Solution of Structural Dynamics”, *Computers and Structures*, Vol. 2, pp. 855–874.
- Shinozuka, M. and G. Deodatis, 1991, “Simulation of Stochastic Processes by Spectral Representation”, *Applied Mechanics Review*, Vol. 44, pp. 191–204.
- Shinozuka, M. and R. Zhang, 1996, "Equivalence between Kriging and CPDF Method for Conditional Simulation", *Journal of Engineering Mechanics, ACSE*, Vol. 122, No. 6, pp. 530-538.
- Shrikhande, M. and V. K. Gupta, 1996, “Synthesizing Ensembles of Spatially Correlated Accelerograms”, *Journal of Engineering Mechanics, ASCE*, Vol. 124, pp. 1185–1192.
- Silva, W. J. and K. Lee, 1987, *WES RASCAL Code for Synthesizing Earthquake Ground Motions, State-of-the-art for Assessing Earthquake Hazards in the United States, Report 2.4*, Miscellaneous Paper S-73-1, U.S. Army Corps of Engineers, Vicksburg, Mississippi.

- Smith, S. W., E. Ehrenberg and E. N. Hernandez, 1982, “Analysis of the El Centro Differential Array for the 1979 Imperial Valley Earthquake”, *Bulletin of Seismological Society of America*, Vol. 72, pp. 237–258.
- Somerville, P. G., J. P. McLaren and C. K. Saikia, 1988, “Site-Specific Estimation of Spatial Incoherence of Strong Ground Motion”, in *Earthquake Engineering and Soil Dynamics II, Recent Advances in Ground Motion Evaluation*, Geotechnical Special Publication, No. 20, ASCE, New York.
- Song, S. G., A. Pitarka and P. Somerville, 2009, “Exploring Spatial Coherence between Earthquake Source Parameters”, *Bulletin of the Seismological Society of America*, Vol. 99; No. 4, pp. 2564-2571.
- Songtao, L., 2006, *Physical Characterization of Seismic Ground Motion Spatial Variation and Conditional Simulation for Performance-Based Design*, Ph. D. Dissertation, Drexel University.
- Spanos, P. D. and M. P. Mignolet, 1992, “Simulation of Homogeneous Two-Dimensional Random Fields: Part II—MA and ARMA Models”, *Journal of Applied Mechanics*, Vol. 59, pp. 270–277.
- Spanos, P. D. and B. A. Zeldin, 1996, “Efficient Iterative ARMA Approximation of Multivariate Random Processes for Structural Dynamics Application”, *Earthquake Engineering and Structural Dynamics*; Vol. 25, pp. 497-507.
- Spudich, P., 1994, *Recent Seismological Insights in to the Spatial Variation of Earthquake Ground Motions*, New Developments in Earthquake Ground Motion Estimation and Implications for Engineering Design Practice, ATC 35-1.
- Stewart, J. P., S. J. Chiou, J. D. Bray, R. W. Graves, P. Somerville and N. A. Abrahamson, 2001, *Ground Motion Evaluation Procedures for Performance-Based Design*, Pacific Earthquake Engineering Research Center Report No. PEER 2001/09.

- Stupazzini, M., 2004, *A Spectral Element Approach for 3D Dynamic Soil-Structure Interaction Problems*, Ph. D. Dissertation, Milan University of Technology.
- Stoica, P. and R. Moses, 1997, *Introduction to Spectral Analysis*, Prentice Hall, New Jersey.
- Tseng, W. S., K. Lilhanand and M. S. Yang, 1993, "Generation of Multiple-Station Response-spectrum-and-coherency-compatible Earthquake Ground Motions for Engineering Applications", *Proceedings of Twelfth Structural Mechanics in Reactor Technology*, Stuttgart, Germany; Paper No. K01=3:13-19.
- Vanmarcke, E. and G. Fenton, 1991, "Conditioned Simulation of Local Fields of Earthquake Ground Motion", *Structural Safety*, Vol. 10, pp. 247-264.
- Vanmarcke, E. H., E. Heredia-Zavoni and G. A: Fenton, 1993, "Conditional Simulation of Spatially Correlated Earthquake Ground Motion", *Journal of Engineering Mechanics, ASCE*, Vol. 119, No. 11, pp. 2333-2352.
- Vernon, F., J. Fletcher, L. Carroll, A. Chave and E. Sembera, 1991, "Coherence of Seismic Body Waves as Measured by a Small Aperture Array", *Journal of Geophysical Research*, Vol. 96, pp. 11981-11996.
- Wang, J., A. Carr, N. Cooke and P. Moss, 2003, "A Simple Method for Stochastic Dispersion of Earthquake Waves", *Proceedings of Pacific Conference in Earthquake Engineering*, Paper no: 51, Christchurch, New Zealand.
- Yagi, Y. and M. Kikuchi, 2000, "Source Rupture Process of the Kocaeli, Turkey, Earthquake of August 17, 1999, Obtained by Joint Inversion of Near-Field Data and Teleseismic Data", *Geophysical Research Letters*, Vol. 27, pp. 1969-1972.
- Zeldin, B. A. and P. D. Spanos, 1996, "Random Field Representation and Synthesis Using Wavelet bases", *Journal of Applied Mechanics, ASME*, Vol. 63, pp. 946-952.

- Zendagui, D. and M. K. Berrah, 2002, "Spatial Variation of Seismic Motion Induced by Propagation of Body Waves", *Soil Dynamics and Earthquake Engineering*, Vol. 22, pp. 805–811.
- Zerva, A., 1992, "Seismic Ground Motion Simulations from a Class of Spatial Variability Models", *Earthquake Engineering and Structural Dynamics*, Vol. 21, pp. 351–61.
- Zerva, A., 2009, *Spatial Variation of Seismic Ground Motions*, CRS Press, New York.
- Zerva, A. and T. Harada, 1997, "Effect of Surface Layer Stochasticity on Seismic Ground Motion Coherence and Strain Estimates", *Soil Dynamics and Earthquake Engineering*, Vol. 16, pp. 445-457.
- Zerva, A. and O. Zhang, 1997, "Correlation Patterns in Characteristics of Spatially Variable Seismic Ground Motions", *Earthquake Engineering and Structural Dynamics*, Vol. 26, pp. 19–39.
- Zerva, A. and L. S. Katafygiotis, 2000, "Selection of Simulation Scheme for the Nonlinear Seismic Response of Spatial Structures", *Proceedings of Fourth International Colloquium on Computation of Shell and Spatial Structures*, Chania, Greece.
- Zerva, A., and V. Zervas, 2002, "Spatial Variation of Seismic Ground Motions: An Overview", *Applied Mechanics Review*, Vol. 55, No. 3, pp. 271-297.